RC. 807

Progress on Seismic Zonation in the San Francisco Bay Region

GEOLOGICAL SURVEY CIRCULAR 807

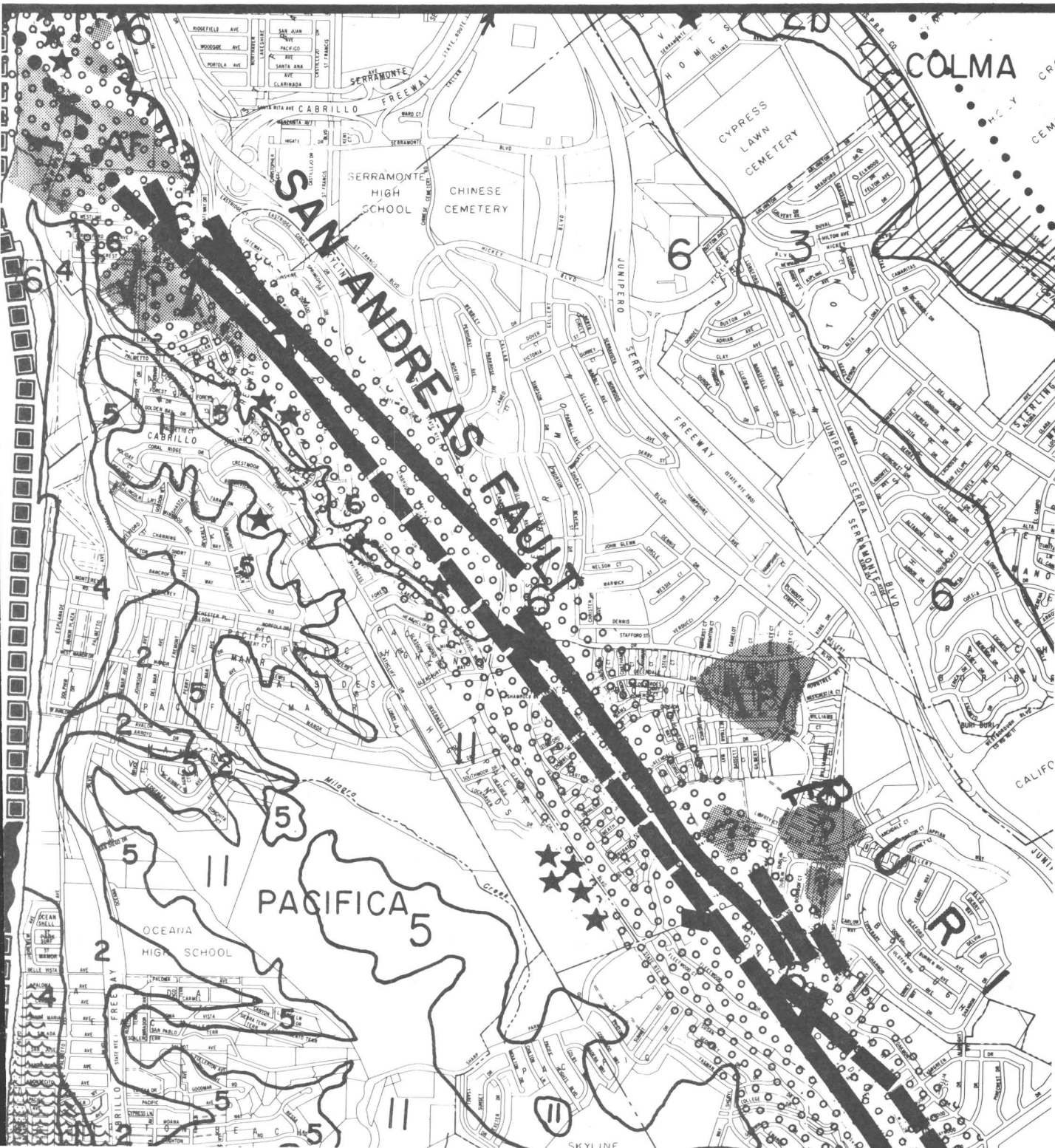

Progress on Seismic Zonation in the San Francisco Bay Region

E. E. Brabb, Editor

GEOLOGICAL SURVEY CIRCULAR 807

1979

United States Department of the Interior

CECIL D. ANDRUS, *Secretary*

Geological Survey

H. William Menard, *Director*

Free on application to Branch of Distribution, U.S. Geological Survey, 1200 South Eads Street, Arlington, VA 22202

CONTENTS, ILLUSTRATIONS, AND TABLES

FOREWORD

EARTHQUAKE HAZARD REDUCTION PROGRAM

This report represents another step in the evolution of methods for reducing the hazards of earthquakes. The great Alaska earthquake of 1964 triggered an awareness among public officials of the seriousness of the earthquake hazard to many of the Nation's major cities. If the effects of the Alaska earthquake are used as a gage, it is clear that when a major earthquake hits California cities such as Los Angeles or San Francisco, casualties could be in the tens of thousands and damage could be in the tens of billions of dollars.

After the Alaska earthquake, the U.S. Geological Survey began to focus its diverse earth-science capabilities more specifically toward the goal of reducing earthquake hazards. The possible effectiveness of land-use planning to avoid the most serious hazards began to be recognized as a supplement to the common practice of incorporating earthquake-resistant designs into structures. For decades geologists had known, for example, that structures built astride the San Andreas fault were in jeopardy, but only in a few places had the fault been delineated in sufficient detail to serve as a guide to community officials and developers. Even if the fault data had been available, standard procedures were inadequate for translating the data into land-use plans or actions. Indeed, land-use planning was, and still is, in an early phase of evolution in the United States. No national land-use policy has been adopted.

In order to satisfy some of the most urgent needs for basic data, several projects were started after the Alaska earthquake. The entire 1,400-km (868-mi) length of the San Andreas fault was mapped for the first time on the best available topographic base maps. Nets of closely spaced seismic instruments were installed at experimental field laboratories along part of the San Andreas fault to study the basic mechanisms of earthquakes and the patterns of energy radiation and attenuation as earthquake waves pass through different types of rocks and soil. New laboratory studies were initiated to explore the physical principles of earthquakes. Research demonstrated the feasibility of earthquake prediction and of earthquake control and modification.

The science of earthquakes is complex, requiring data and research in seismology, geology, soil mechanics, geophysics, hydrology, and engineering. Nevertheless, if earthquake hazards are to be reduced, earth-science data must be translated from scientific and technical language into a form that can be used effectively in the decisionmaking process.

THE SAN FRANCISCO BAY REGION ENVIRONMENT AND RESOURCES PLANNING STUDY

Out of this recognition of the need to use earth-science information in regional planning and decisionmaking came an experimental program--the San Francisco Bay Region Environment and Resources Planning Study. The study, begun in 1970 and completed in 1975, was jointly supported by the U.S. Geological Survey, Department of the Interior, and the Office of Policy Development and Research, Department of Housing and Urban Development. The Association of Bay Area Governments participated in the study and provided a liaison and communication link with other regional planning agencies and with county and local governments.

Although the study focused on the nine-county 19,000 km^2 San Francisco Bay region, it related to a difficult issue that is of national concern--how best to accommodate orderly development and growth while conserving our natural resource base, insuring public health and safety, and minimizing degradation of our natural and manmade environment. The issue, however, can only be approached if we understand the natural characteristics of the land, the processes that shape it, its resource potential, and its natural hazards. These subjects are chiefly within the domain of the earth sciences: geology, geophysics, hydrology, and the soil sciences. Appropriate earth-science information, if available, can be rationally applied in guiding growth and development, but the existence of the information does not assure its effective use in the day-to-day decisions that shape development. Planners, elected officials, and the public rarely have the training or experience needed to recognize the significance of basic earth-science information, and many of the conventional methods of communicating earth-science information are ill suited to the needs of that particular group of users.

The study was intended to aid the planning and decisionmaking community by (1) identifying important problems that are rooted in the earth sciences and related to growth and development in the bay region, (2) providing the earth-science information that is needed to solve these problems, (3) interpreting and publishing findings in forms understandable to and usable by nonscientists, (4) establishing new avenues of communication between scientists and users, and (5) exploring alternate ways of applying earth-science information in planning and decisionmaking.

The study produced more than 100 reports and maps. These cover a wide range of topics: reduction of flood and earthquake hazards, unstable slopes, engineering characteristics of hillside and lowland areas, mineral and water resources management, solid and liquid waste disposal, erosion and sedimentation problems, bay water circulation patterns, and others. The methods used in the study and the results it has produced have elicited broad interest and a wide range of applications from planners, government officials, industry, universities, and the general public.

SEISMIC ZONATION

The skills and knowledge developed during the Earthquake Hazard Reduction Program and the San Francisco Bay Region Environment and Resources Planning Study were focused in 1972 on an analysis of the state-of-the-art for assessing potential earthquake effects on a regional scale for purposes of seismic zonation. The analysis was done by a group of 16 earth scientists representing several different disciplines and organizational units within the U.S. Geological Survey. The preliminary results of these studies were presented at the First International Conference on Microzonation, Seattle, Washington, in November, 1972, and were published in 1975 as U.S. Geological Survey Professional Paper 941-A. This report provided the earth-science basis for a comprehensive approach to reducing earthquake hazards in large areas such as the San Francisco Bay region. The report included an analysis of the direct effects of earthquakes, such as fault displacement and ground shaking as well as indirect effects of landsliding and liquefaction. To illustrate the analysis, an earthquake of magnitude 6.5 was assumed for the San Andreas fault, and the various effects were predicted on a profile through the southern San Francisco Bay region.

Since 1975, the composition of the core group within the U.S. Geological Survey concerned with seismic zonation has evolved to include seismologists and engineers concerned with probabilistic approaches to earthquake damage, a planner to facilitate the information transfer from scientists and engineers to city, county, and regional planning staffs charged with the responsibility for implementing earthquake hazard reduction measures, and representatives from the Association of Bay Area Governments, who are working on economic risk, transportation, and land capability maps for the San Francisco Bay region. The progress of this group was reported at the Second International Conference on Microzonation held in San Francisco in November, 1978; the papers in this report are taken verbatim from the Proceedings of the Conference.

The entire Proceedings, consisting of 3 volumes and 1132 pages of reports, can be purchased for $65 by writing to: Dr. Mehmet A. Sherif, Microzonation Conference Chairman, 132 More Hall FX-10, University of Washington, Seattle, Washington 98195.

PROGRESS ON SEISMIC ZONATION IN THE SAN FRANCISCO BAY REGION

INTRODUCTION AND SUMMARY

by

Earl E. Brabb and Roger D. Borcherdt

Studies by 16 researchers in various earth-science and engineering disciplines were summarized at the First International Conference on Microzonation in 1972. These reports, published in expanded form as U.S. Geological Survey Professional Paper 941-A, established that seismic zonation of the San Francisco Bay region was feasible and showed the necessity for a multidisciplinary approach to the problem. The reports emphasized methodologies for constructing seismic zonation maps from earth-science data that were currently available on a regional scale. The maps showed maximum earthquake intensity, active faults, geologic units, qualitative ground response, liquefaction susceptibility, landslide susceptibility, and areas of potential tsunami inundation. These maps served to delineate areas with potential earthquake problems, identify the problem, and indicate its possible severity.

These basic tools and a number of other products developed as part of a cooperative project between the U.S. Geological Survey and the Department of Housing and Urban Development have been utilized by most of the 91 cities and all of the counties in the San Francisco Bay region. They have also been used in the preparation of seismic safety, public safety, conservation, and open-space elements of general plans together with ordinance administration policy and environmental impact statements. They are the basic building blocks for derivative maps prepared by the Association of Bay Area Governments for regional planning, such as the appropriate location for toxic waste disposal, industrial development, population concentration, and transportation. This wide application of the products has resulted in a significantly increased demand for new and improved earth-science data that can be used for development of policies for earthquake hazard reduction.

Since the initial study, a number of new data have been collected and a number of new approaches have been developed concerning communication of these data to the planning communities. The following set of papers discusses some of these new results in detail. Some of the highlights are as follows:

Discovery of three new potentially active fault systems;

Mapping of all faults with Quaternary displacement in northern San Francisco Bay region at scales of 1:125,000 and 1:24,000;

Seismic and geologic logging of 59 drill holes in southern San Francisco Bay region to develop a data base for improved regional ground motion predictions;

Development of new Methods utilizing synthetic seismograms to improve quantitative ground motion predictions;

Mapping liquefaction susceptibility of Santa Cruz County at a scale of 1:62,500 using new techniques;

Development of new techniques for mapping regional slope stability during earthquakes; and

Development of improved methods for estimating earthquake-induced damage to buildings on a regional scale.

The need for new and improved data in all metropolitan areas of high seismic risk is becoming increasingly apparent. The recent Earthquake Hazards Reduction Act of 1977 (P.L. 95-124) calls for the identification, evaluation and characterization of seismic hazards in all areas of high or moderate risk and the development of means to coordinate information about seismic risk with land-use policy decisions. Some of the methods and policies developed in the San Francisco Bay region will be directly applicable to other areas of the United States; however, where earthquake problems and basic data sets are different, additional methods and policies will be needed.

NEOTECTONIC FRAMEWORK OF CENTRAL COASTAL CALIFORNIA AND ITS IMPLICATIONS TO MICROZONATION OF THE SAN FRANCISCO BAY REGION

by

Darrell G. Herd

ABSTRACT

Microzonation of the San Francisco Bay region must consider future earthquakes on several major northwest-trending faults. Principal among these, the San Andreas fault zone extends through the central Coast Ranges to San Francisco, and then north along the Pacific coastline. Paralleling it offshore to the west is the San Gregorio-Hosgri fault system, which joins with the San Andreas near San Francisco. At Hollister, the Hayward-Lake Mountain fault system branches eastward from the San Andreas, extending north beyond Eureka. The Calaveras-Sunol, Concord, and Green Valley faults form a line that splays from the Hayward-Lake Mountain fault system near San Jose. East of San Francisco, the San Joaquin fault zone bounds the east flank of the Coast Ranges.

Large earthquakes ($M \geq 7$) are credible on several fault zones in the San Francisco Bay area and have a basic recurrence of tens to hundreds of years on a few.

INTRODUCTION

Microzonation of the San Francisco Bay region for seismic shaking must consider future earthquakes that likely will occur along several predominantly northwest-trending faults. The San Francisco Bay region lies astride the San Andreas fault zone at its intersection with two other major fault systems. These faults, which constitute the neotectonic framework of central coastal California, have been repeatedly active throughout the Quaternary Period (last 1.8 m.y.).

Most historic California earthquakes have originated along such recently active faults (1, 2). An assessment of the length, character, and rate of displacement along them, with reference to historic worldwide seismicity, can be used to estimate the magnitude and frequency of large earthquakes expectable in the San Francisco Bay area.

NEOTECTONIC FRAMEWORK

Recently active faults. The San Francisco Bay region (fig. 1) is cut by several major northwest-trending right-slip faults. These faults, which have been active in both historic (Table 1) and geologically recent time, sliver coastal California into narrow crustal blocks. Principal among these faults, the San Andreas fault zone extends from southern California through the central Coast Ranges of San Francisco. From there north, the San Andreas skirts the Pacific coastline to near Cape Mendocino (see fig. 3), where the fault zone intersects the Mendocino fracture zone. The San Andreas is paralleled offshore to the west by the San Gregorio-Hosgri fault system (3), which begins west of Point Conception and joins the San

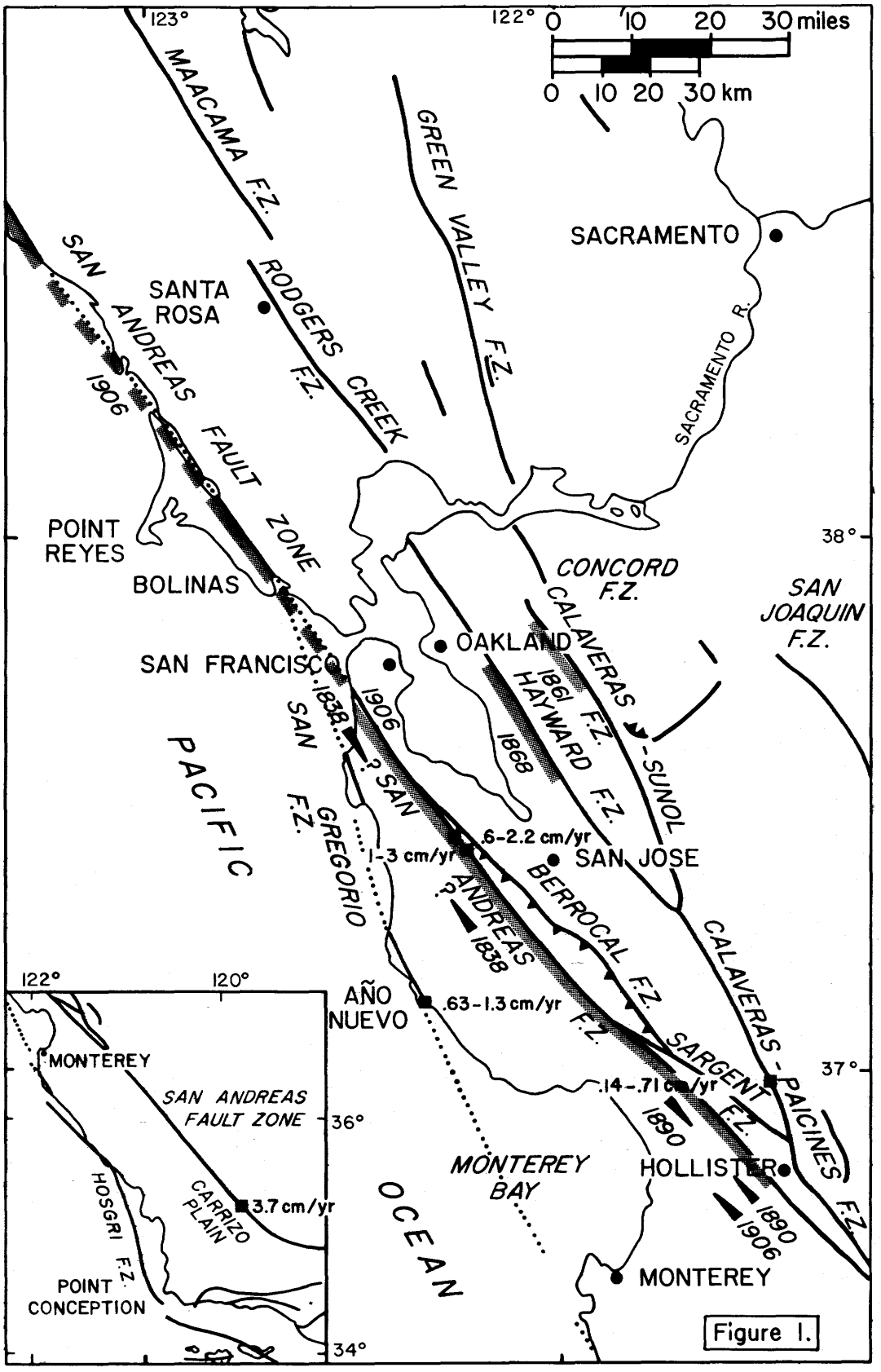

Figure 1.--Principal recently active faults in San Francisco Bay region, showing zones of surface rupture associated with historic earthquakes (Table 1). Squares denote locally determined rates of geologic offset.

Andreas just west of San Francisco. Approximately 120 km southeast of San Francisco a second system of faults, the Hayward-Lake Mountain (4), branches eastward from the San Andreas fault zone at Hollister. This line of large en echelon, recently active right-slip fault zones parallels the San Andreas northward, passing east of Cape Mendocino. The fault system extends beyond Eureka onto the continental shelf southwest of Crescent City. A much shorter line of three faults, the Calaveras-Sunol, Concord, and Green Valley, splays from the Hayward-Lake Mountain fault system near San Jose. To the south, the Sargent fault zone joins the Calaveras-Paicines fault zone and the San Andreas (5).

Southwest of San Jose, an imbricate system of thrust faults (collectively referred to here as the Berrocal fault zone) abuts the northeast side of the San Andreas fault zone (5). East of San Francisco, the San Joaquin fault zone bounds the east flank of the Coast Ranges. The zone is predominantly normal in character (east side down), with local reverse faults.

Faulting and plate tectonics. The northward movement of the Pacific plate relative to North America (fig. 3) is manifested in coastal California as slip along the San Andreas fault zone and the subsidiary faults. The relative rate of movement across the plate boundary is not uniform and is difficult to measure because the area is slivered by intersecting and branching fault systems. One of the crustal slivers, the Humboldt plate (4), moves independently of the Pacific and North American plates. This small plate, bounded on the east by the Hayward-Lake Mountain fault system and on the west by the San Andreas, converges northwestward with the Gorda plate. Near San Jose, the Humboldt plate locally overrides and is crushed by the Pacific plate (along the Berrocal thrust faults). The crustal extension at the east side of the Coast Ranges (evidenced by normal faulting along the San Joaquin fault zone) may be due to the northwestward movement of the Humboldt plate away from the North American plate.

Fault slip. Movement on the recently active faults in the San Francisco Bay region occurs catastrophically in seismic slip events (as much as 5 m of right-lateral displacement was measured (2) across the San Andreas fault after the 1906 earthquake) as well as gradually by fault creep.

An average of 3.7 cm/yr of long-term slip (determined from the right-lateral offset of a 3,000-year-old stream channel (6) in the Carrizo Plain) occurs along the San Andreas fault zone south of Hollister (fig. 1, inset).

Table 1.--Historic surface fault displacements associated with earthquakes in the San Francisco Bay region (2)

Date	Fault	Rupture length	Magnitude
Late June, 1838	San Andreas	Unknown	
July 3, 1861	Calaveras-Sunol	Unknown	
October 22, 1868	Hayward	>30 km	7±1/2 (estimated)
April 24, 1890	San Andreas	>10 km?	
April 18, 1906	San Andreas	∿430 km	8.3

Surface faulting has previously been reported (2) for the June 10, 1836 earthquake on the Hayward fault zone. However, re-examination of the original newspaper accounts (referenced in 7) does not support such an interpretation. The described earth fissures were probably due to ground shaking and slope failure rather than faulting.

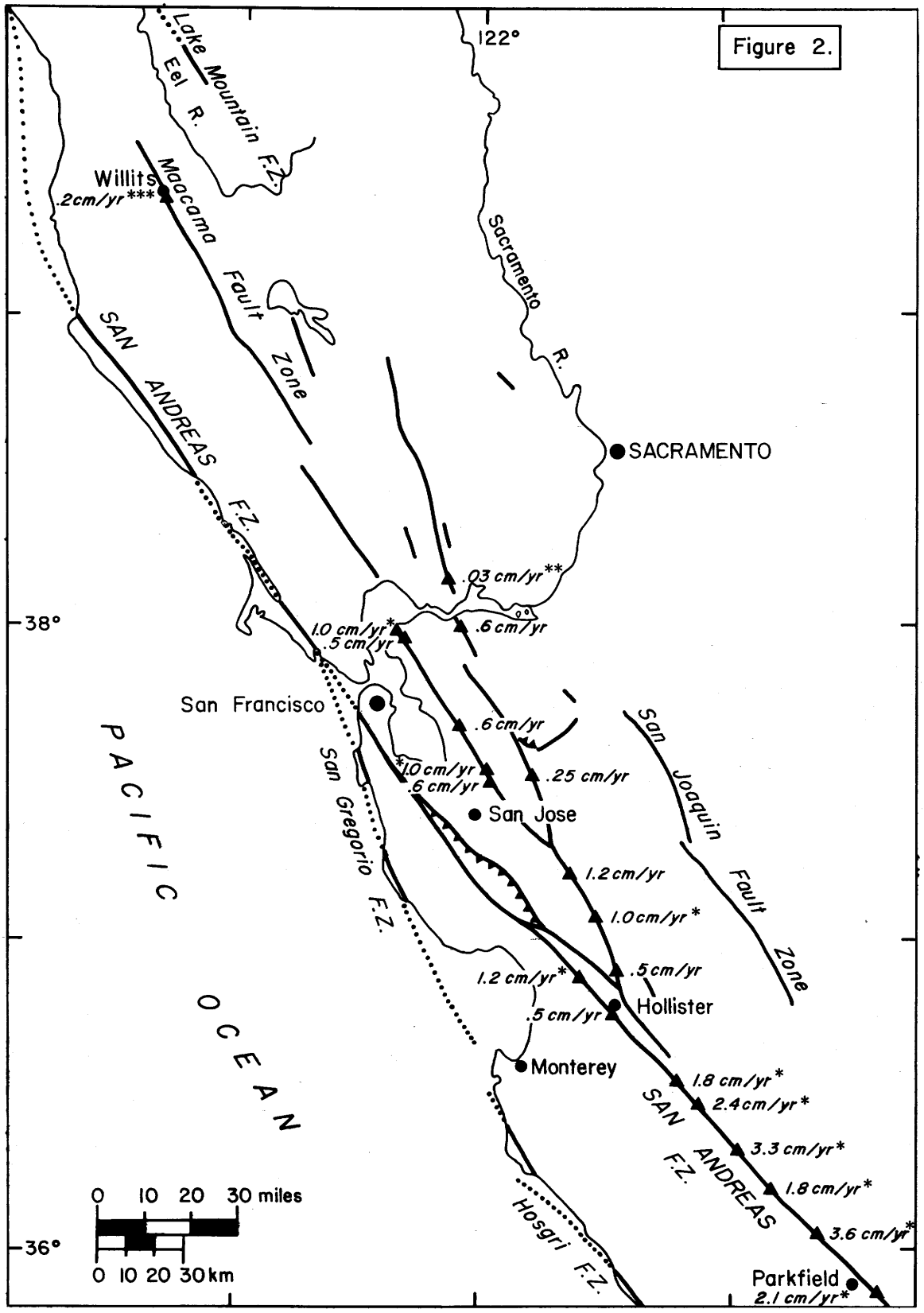

Figure 2.--Documented creep on faults in central coastal California. Data marked by * are from R. O. Burford (8), ** from Frizzell and Brown (9), *** from Harsh and others (10). Other data from Wesson and others (2).

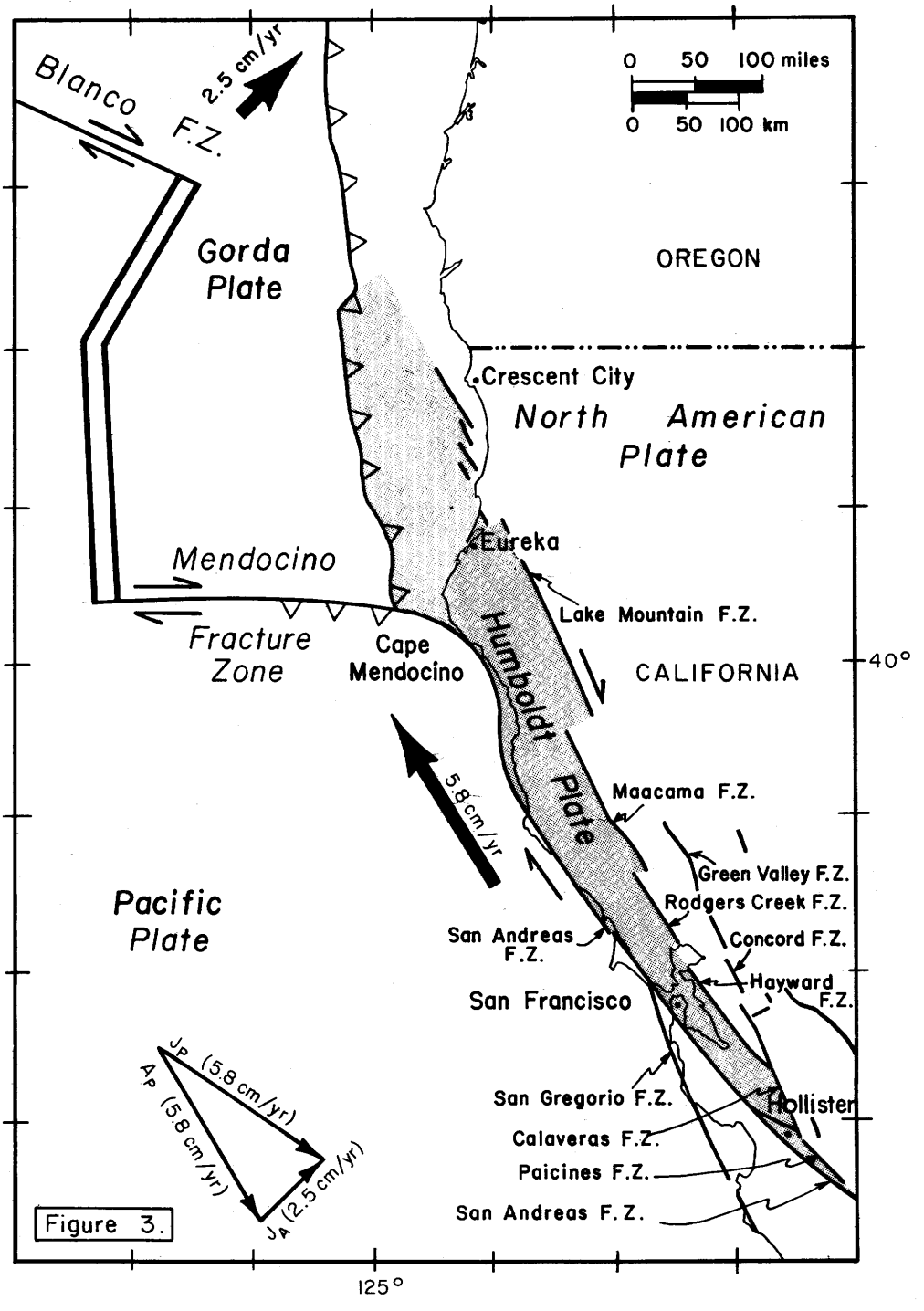

Figure 3.--Map showing plate tectonics of coastal northern California and Oregon (4). Recently active faults of coastal California are represented. Large black arrows show movement of Pacific and Gorda plates relative to the North American plate deduced from vector diagram in bottom center. Motion of the North American plate with respect to the Pacific plate (Ap) is assumed to be 5.8 cm/yr parallel to the San Andreas fault zone. Motion of the Gorda plate with respect to the Pacific plate (Jp) is assumed to be 5.8 cm/yr parallel to the Blanco fracture zone. The resultant motion of the Gorda plate with respect to the North American plate (Ja) is a compression in a north-northeast direction of 2.5 cm/yr.

Part of the displacement (currently as much as 3.6 cm/yr) occurs locally as creep (fig. 2). North of Hollister, near San Francisco (fig. 1), only 2 cm/yr of long-term slip has been documented along the San Andreas fault zone, 0.6-2.2 cm/yr in displaced Pliocene (1.8-5.0 m.y.) rocks (11), and 1-3 cm/yr in offset deposits 1-3 m.y. old (12).

Most of the 1.7 cm/yr of slip that is not carried northward along the San Andreas beyond Hollister is apparently transferred to the Calaveras-Paicines fault zone, which branches from the San Andreas just south of Hollister (fig. 1). Although the actual long-term rate of slip along the Calaveras-Paicines fault zone is not known (a minimum of 0.14-0.71 cm/yr slip has been determined (13) from offset 3.5-m.y.-old volcanic rocks north of Hollister, fig. 1), the long-term rate is maybe at least 1.2 cm/yr and more probably about 1.5 cm/yr. Southeast of San Jose (fig. 2), 1.0-1.2 cm/yr of creep has been documented on the Paicines-Calaveras fault zone. The rate of creep along the Calaveras-Paicines fault zone, like the San Andreas south of Hollister, is presumably equal to or less than the long-term slip rate (the difference being made up in catastrophic seismic slip events).

Slip along the Calaveras-Paicines fault zone is apportioned at San Jose between the Hayward-Lake Mountain fault system and the Calaveras-Sunol--Concord--Green Valley fault system (fig. 1). Although no geologic rates of offset have been locally determined along either fault system, the measurement of 0.6 cm/yr of creep on both the Hayward and Concord fault zones at about the same latitude suggests that the 1.5 cm/yr (?) of slip along the Calaveras-Paicines is equally divided between the two. A marked diminution in long-term slip rate northward along the respective fault systems is suggested by only 0.2 cm/yr of creep along the Maacama fault zone at Willits (fig. 2), and 0.03 cm/yr of creep on the Green Valley fault zone.

About 1 cm/yr (0.63-1.3 cm/yr) of movement for the last 200,000 years has been measured (14) across the San Gregorio fault zone at Año Nuevo (fig. 1). This amount of slip is added to the San Andreas fault zone west of San Francisco, apparently increasing the long-term slip rate along the San Andreas north of Bolinas to about 3.0 cm/yr.

"BASIC" EARTHQUAKE RECURRENCE

Curves of Wallace's (15) "basic" earthquake recurrence can be determined for earthquakes of different magnitude at given points on faults in the San Francisco Bay area if (a) the rate of displacement on the fault is known; (b) the slip rate is constant; (c) all the long-term offset or slip on the fault was the cumulative effect of sudden slips accompanying earthquakes, interspersed with periods of elastic strain build-up; and (d) all earthquakes are assumed to be of the same size. These curves (fig. 4) can be generated for the Hayward, Calaveras-Sunol, Calaveras-Paicines, and San Gregorio fault zones, and parts of the San Andreas (for which average geologic slip rates can be approximated) by the formula

$$R_M = \frac{D}{S}$$

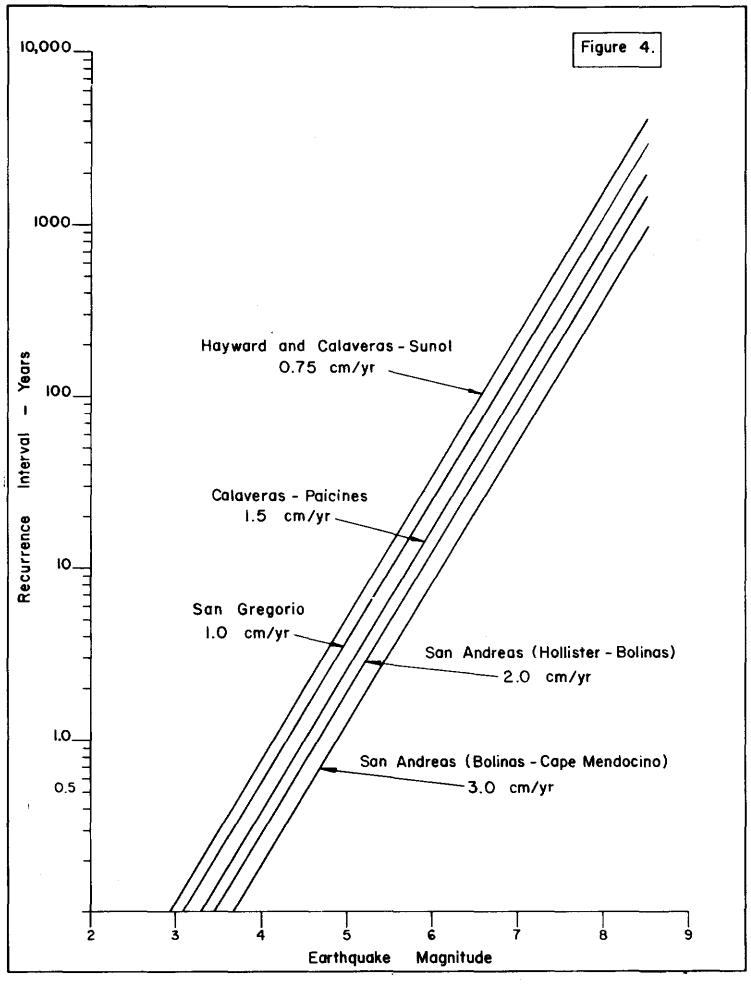

Figure 4.--Basic recurrence intervals (15) at a given point on fault zones in the San Francisco Bay region, assuming average displacement rates indicated. The earthquake magnitudes have been calculated from the empirical relation of Slemmons (17) $M = 6.717 + 1.214 \log_{10} (D)$, where M is magnitude and D is displacement in meters ($n = 30$, $r^2 = 0.408$, $s = 0.639$).

---

where R_M = recurrence interval, at a point on the fault of an earthquake of magnitude M,

D = most probable surface displacement associated with an earthquake of magnitude M, determined from a linear regression of earthquake magnitude on surface displacement from data on historical magnitude and surface rupture, and

S = long-term strain rate.

The curves suggest that large earthquakes ($M \geq 7$) have a "basic" recurrence of tens to hundreds of years on the faults. However, the curves are only a first approximation of estimated earthquake recurrence since the energy released during earthquakes of other magnitudes is not deducted. Moreover, the effect of fault creep, which may be considered a noncatastrophic mode of fault slip and thus an inhibiting factor in the accumulation of elastic strain and the generation of earthquakes, is not considered.

"MOST PROBABLE" EARTHQUAKE MAGNITUDES

Estimates of the "most probable" earthquake magnitudes that can be expected along faults in the San Francisco Bay area if one-half the total fault length ruptured (Table 2) can be used to calculate ground response for microzonation. These estimates, which have commonly been called "maximum credible" or "maximum expectable" earthquake magnitudes (16), are made from linear regressions of earthquake magnitude on length of surface rupture using historical earthquake magnitudes and lengths of surface ruptures (17, 18, 19).

The earthquake magnitudes estimated in Table 2 imply that $M \geq 6$ earthquakes are credible on most principal fault zones in the San Francisco Bay area. The values differ from those previously determined for faults in the Bay area (2) because they are based on newly mapped fault lengths, and because they are not calculated from regressions of fault length on earthquake magnitude (18).

Table 2.--Most probable magnitudes of earthquakes that would be expected, provided that rupture of one-half the total length of faults or fault segments in the San Francisco Bay region occurred.

Fault zone	Character of motion	Length (L) km	Most probable magnitude 1/2 L
San Andreas			
Hollister - Cape Mendocino	Right-slip	430	7.8
Hollister - Bolinas	do	160	7.2
Bolinas - Cape Mendocino	do	270	7.5
Paicines-Calaveras	do	100	6.9
Hayward	do	90	6.9
Rodgers Creek	do	50	6.5
Maacama	do	140	7.1
Calaveras-Sunol	do	70	6.7
Concord	do	20	6.0
Green Valley	do	90	6.9
San Gregorio	do	140	7.1
San Joaquin	Predominantly normal	120	7.3
Sargent	Right-slip	60	6.6
Berrocal	Thrsut	60	7.4

The magnitudes are calculated using the empirical relations of Slemmons (17): $M = 0.597 + 1.351 \log_{10} (L)$ for strike-slip faults ($n = 31$, $r^2 = 0.601$, $s = 0.694$); $M = 1.845 + 1.151 \log_{10} (L)$ for normal faults ($n = 18$, $r^2 = 0.331$, $s = 0.521$); and $M = 4.145 + 0.717 \log_{10} (L)$ for reverse faults ($n = 9$, $r^2 = 0.869$, $s = 0.167$), where M is magnitude and L is fault length in meters.

REFERENCES CITED

1. Allen, C. R., St. Amand, P., Richter, C. F., and Nordquist, J. M., 1965, Relationship between seismicity and geologic structure in the southern California region: Bulletin of the Seismological Society of America, v. 55, no. 4, p. 753-797.

2. Wesson, R. L., Helley, E. J., Lajoie, K. R., and Wentworth, C. M., 1975, Faults and future earthquakes, in Borcherdt, R. D., ed., Studies for seismic zonation of the San Francisco Bay region: U.S. Geological Survey Professional Paper 941-A, p. A5-A30.

3. Graham, S. A., and Dickinson, W. R., 1978, Evidence for 115 kilometers of right slip on the San Gregorio-Hosgri fault trend: Science, v. 199, no. 4325, p. 179-181.

4. Herd, D. G., 1978, An intracontinental plate boundary east of Cape Mendocino, California: Geology, in press.

5. McLaughlin, R. J., 1974, the Sargent-Berrocal fault zone and its relation to the San Andreas fault system in the southern San Francisco Bay region and Santa Clara Valley, California: Journal of Research of the U.S. Geological Survey, v. 2, no. 5, p. 593-598.

6. Hall, N. T., and Sieh, K. E., 1977, Late Holocene rate of slip on the San Andreas fault in the northern Carrizo Plain, San Luis Obispo County, California (abst.): Geological Society of America Abstracts with Programs, v. 9, no. 4, p. 428-429.

7. Louderback, G. D., 1947, Central California earthquakes of the 1830's: Seismological Society of America Bulletin, v. 37, p. 33-74.

8. Savage, J. C., and Burford, R. O., 1973, Geodetic determination of relative plate motion in central California: Journal of Geophysical Research, v. 78, no. 5, p. 832-845.

9. Frizzell, V. A., Jr., and Brown, R. D., Jr., 1976, Map showing recently active breaks along the Green Valley fault, Napa and Solano Counties, California: U.S. Geological Survey Miscellaneous Field Studies Map MF-743, scale 1:24,000.

10. Harsh, P. W., Pampeyan, E. H., and Coakley, J. M., 1978, Slip on the Willits fault, California (abst.): Seismological Society of America Earthquake Notes, v. 49, no. 1, p. 22.

11. Addicott, W. A., 1969, Late Pliocene mollusks from San Francisco Peninsula, California, and their paleogeographic significance: Proceedings of the California Academy of Sciences, Fourth Series, v. 37, no. 3, p. 57-93.

12. Cummings, J. C., 1968, The Santa Clara Formation and possible post-Pliocene slip on the San Andreas fault in central California, in Dickinson, W. R., and Grantz, Arthur, eds., Proceedings of conference on geologic problems of San Andreas fault system: Stanford University Publications in the Geological Sciences, v. 11, p. 191-207.

13. Nakata, J. K., 1977, Distribution and petrology of the Anderson-Coyote Reservoir volcanic rocks: San Jose State University, California, Master of Science Thesis, 105 p.

14. Weber, G. E., and Lajoie, K. R., 1977, Late Pleistocene and Holocene tectonics of the San Gregorio fault zone between Moss Beach and Point Año Nuevo, San Mateo County, California (abst.): Geological Society of America Abstracts with Programs, v. 9, no. 4, p. 524.

15. Wallace, R. E., 1970, Earthquake recurrence intervals on the San Andreas fault: Geological Society of America Bulletin, v. 81, p. 2875-2890.

16. Wesson, R. L., Page, R. A., Boore, D. M., and Yerkes, R. F., 1974, Expectable earthquakes in the Van Norman Reservoirs area: U.S. Geological Survey Circular 691-B, 9 p.

17. Slemmons, D. B., 1977, State-of-the-art for assessing earthquake hazards in the United States: U.S. Army Engineer Waterways Experiment Station Miscellaneous Paper S-73-1, Report 6, var. pag.

18. Mark, R. K., 1977, Application of linear statistical models of earthquake magnitude versus fault length in estimating maximum expectable earthquakes: Geology, v. 5, p. 464-466.

19. Mark, R. K., and Bonilla, M. G., 1977, Regression analysis of earthquake magnitude and surface fault length using the 1970 data of Bonilla and Buchanan: U.S. Geological Survey Open-file Report 77-614, 8 p.

PROGRESS ON GROUND MOTION PREDICTIONS FOR THE SAN FRANCISCO BAY REGION, CALIFORNIA

by

Roger D. Borcherdt , James F. Gibbs , and Thomas E. Fumal

ABSTRACT

The amount of damage in the San Francisco Bay region from the 1906 earthquake depended strongly on the geologic character of the ground. This dependence indicates the need for seismic zonation maps of the region to outline areas where special earthquake resistant design is necessary to reduce losses from future earthquakes.

Current research is directed at defining methodologies for improved quantitative estimates of ground response on a regional scale. This research includes determination of seismic and geologic logs in 59 drill holes to a depth of 30 meters.

Relations derived between site amplifications (Amp), 1906 earthquake intensity increments (δI), and shear-wave velocity are, respectively,

$$\text{Amp} = -11.4 \log (\text{S-vel, m/s}) + 33.6$$

and

$$\delta I = -0.0027 (\text{S-vel, m/s}) + 2.25$$

Geotechnical parameters such as texture, standard penetration, and depth, for sediments, and fracture spacing and hardness, for rocks, show strong correlations with seismic velocities and provide a useful means of defining 13 units with distinct seismic characteristics. Utilizing the preceding empirical relations, quantitative estimates of ground response at 59 sites, recently developed numerical models, and the classification of seismically distinct units on the basis of geotechnical parameters, improved quantitative estimates of variations in ground shaking can be provided on a regional scale for seismic zonation of the San Francisco Bay region. In addition, the seismic velocity relations permit extrapolation of these data to other regions.

Introduction

The most widespread earthquake damage is generally due to ground shaking and is strongly dependent on the geologic character of the ground. After the 1906 earthquake, Lawson (12) reported evidence for increased damage due to geologic conditions in 18 California communities. This strong dependence of damage on the geological character of the ground defined a strong need for predictions of regional ground motion that can

be used for economical earthquake-resistant design. This paper describes a new data base for developing a methodology to prepare predictions of regional ground motion that account for variations in geologic conditions.

The problem of predicting regional ground motion is quite distinct from that of predicting for specific sites. For specific sites (for example, siting of a nuclear power plant or a high-rise structure), detailed geologic and seismic data are available. As a result, recently developed numerical modeling procedures can be used to predict reasonably detailed time histories of ground motion. However, such detailed seismic and geologic information is not available on a regional basis, and predictions must necessarily be more generalized.

Previous Work on Regional Problem

At the time of the First International Conference on Microzonation, Borcherdt, et al., (5) reported on data available for regional ground motion predictions in the San Francisco Bay region. These data included observed 1906 earthquake intensities, recordings of the 1957 earthquake, comparative measurements at 99 sites of ground shaking generated by nuclear explosions, and high-strain laboratory measurements of dynamic soil properties.

Comparative measurements of ground shaking generated by the nuclear explosions and the 1957 earthquake showed that a significant and consistent difference in the response to shaking exists between different geologic units in the San Francisco Bay region (Borcherdt, 1). Comparison of the measured amplifications with the high quality 1906 intensity data showed that an increase in amplification corresponds to an increase in intensity. This correlation suggested that sites at equal distance from the fault with large observed amplifications may also be sites of relatively high intensity in future earthquakes. These data together with available geologic information were used to predict the maximum intensity that sites in the San Francisco Bay region might sustain from large earthquakes on either the San Andreas fault or the Hayward fault (Borcherdt, Gibbs, and Lajoie, 4). (See Fig. 1 for map).

The intensity map delineates general areas susceptible to problems from earthquakes in the San Francisco Bay region, and, when properly interpreted, it provides a preliminary form of seismic zonation. The map has been used in the required Seismic Safety Elements of several bay region communities and for development of general land-use policies designed to reduce earthquake losses. The map does not provide quantitative estimates of ground shaking nor does it predict the nature and areal extent of such problems as surface faulting or liquefaction. It does delineate many potentially hazardous areas and provides a qualitative estimate of the overall hazard from shaking on a regional scale. In addition to their use for the maximum predicted intensity maps, the data available in the San Francisco Bay region were considered adequate to prepare a map showing that the expected effects of amplified ground shaking would be least on bedrock, intermediate on alluvium, and greatest on bay mud (Borcherdt et al., 2). However, the data were not considered adequate to prepare more quantitative maps depicting such parameters as peak acceleration, velocity and displacement. Such predictions require not only detailed models of the earthquake source and the seismic wave transmission path, but also detailed knowledge of the geometry and configuration of near-surface geologic deposits.

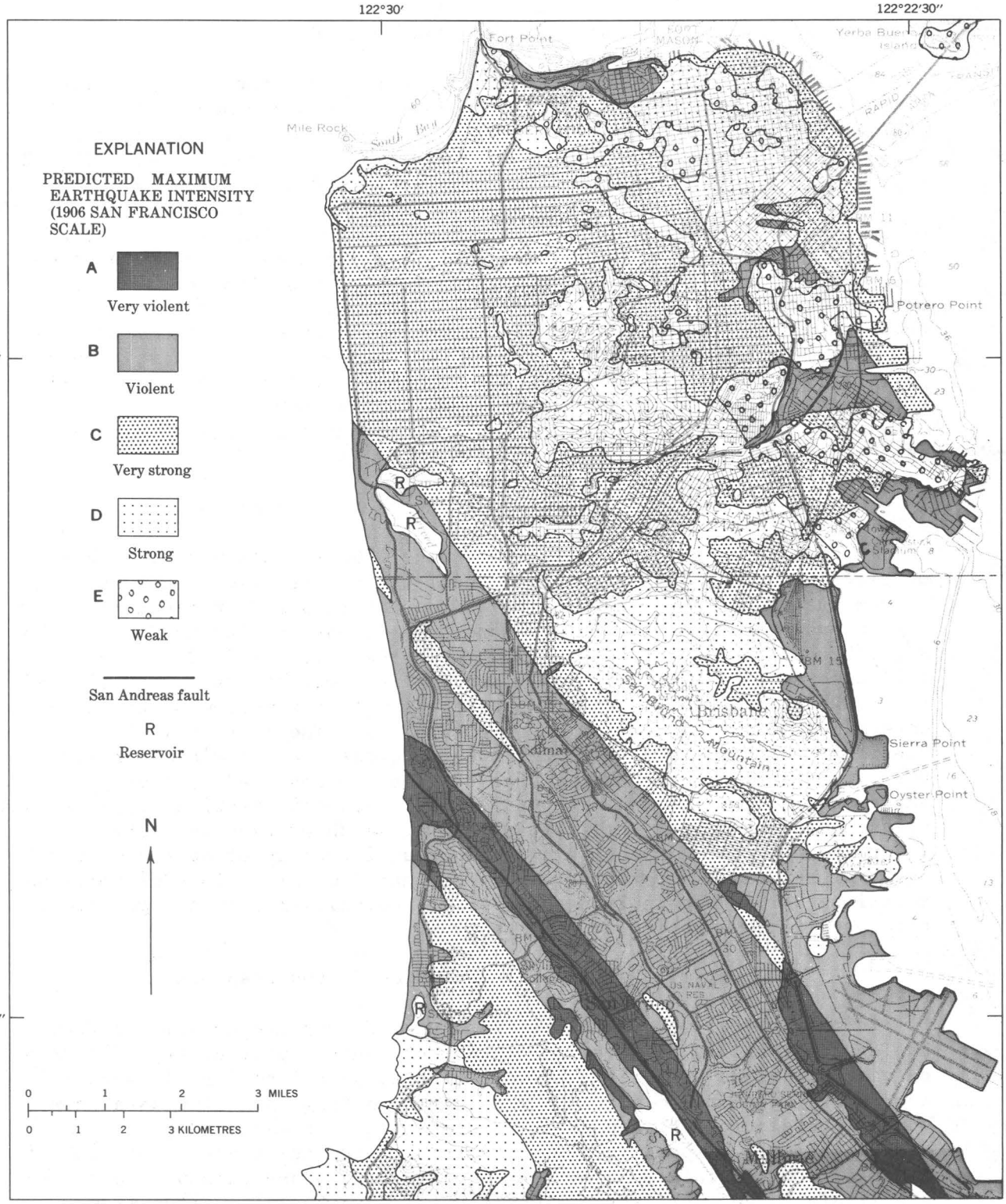

Figure 1.-Maximum earthquake intensities predicted for San Francisco (map is excerpt from Borcherdt, Gibbs, and Lajoie, 4). Each value is maximum of those predicted assuming a large earthquake on San Andreas or Hayward fault. Intensity values are predicted from empirical relations based on only good intensity data for the 1906 earthquake together with a generalized geologic map compiled by K. R. Lajoie (written comm., 1974). Letters A-E indicate grades of San Francisco intensity scale.

New Data Base for Regional Problem

To develop an improved data base for more quantitative predictions of ground motion on a regional scale, a program was undertaken by the U.S. Geological Survey to determine detailed seismic and geologic logs for a large number of sites in all major geologic units in the San Francisco Bay region. To date, seismic velocity logs of P- and S- waves, together with geologic logs, have been determined for 59 sites in drill holes to a depth of 30 meters (Fig. 2) (Gibbs et al., 7, 8, 9, 10). Seismic velocities (Fig. 3) were measured at 2.5-meter intervals using an in-hole technique developed by Kobayashi (11) and Warrick (13). (See Gibbs et al., 7, for detailed description of technique). Interpretive geologic logs were compiled for each hole using field data, including descriptions of three to six samples taken at lithologic contacts and at points where changes in physical properties were indicated (see Fumal, 6, for details). Drill hole sites were selected on the basis of available high-quality 1906 intensity data, measured ground response from nuclear explosions, and detailed geologic mapping.

Seismic Velocity vs. Intensity Increments

To compare seismic velocities with the 1906 intensity data, the effect of distance on the observed 1906 intensities was removed by computing increments in observed intensity with respect to a mean attenuation curve for intensities observed on the Franciscan Formation (Borcherdt and Gibbs, 3). Those intensity increments, based on the better 1906 data and collected at sites for which no ground failure was observed, are plotted as a function of average shear wave velocity to the bottom of the hole determined at the corresponding site (Fig. 4). The plot shows considerable scatter in the data, but a decrease in seismic shear wave velocity clearly corresponding to a decrease in observed intensity increment. The relations without regard to geologic setting suggests that sites equidistant from the fault with average shear wave velocities of about 250 m/s could expect to experience an intensity of approximately 2 units higher than sites with velocities near 1000 m/s. In addition, the relations helps to establish that seismic velocity may be a significant parameter for evaluating seismic hazards.

Seismic Velocity vs. Measured Ground Response

To compare seismic velocities with ground response determined from nuclear explosions, the average of the horizontal spectral amplification curves (Borcherdt and Gibbs, 3) were plotted as a function of average shear wave velocity to the bottom of the hole (Fig. 5). The data show a strong correlation between shear wave velocity and measured amplification. In particular, at sites with average shear velocities of 250 m/s, low-strain ground motions over the frequency band 0.5 to 2.5 Hz are likely to be about seven times greater than those at sites with velocities near 900 m/s.

The data from drill holes more than 100 m from the site of the measured amplification show considerably more scatter, and this scatter suggests that amplification effects are very localized and that care is required in extrapolating site-specific measurements to a regional scale.

The data suggest that the seismic shear wave velocity of the upper 30

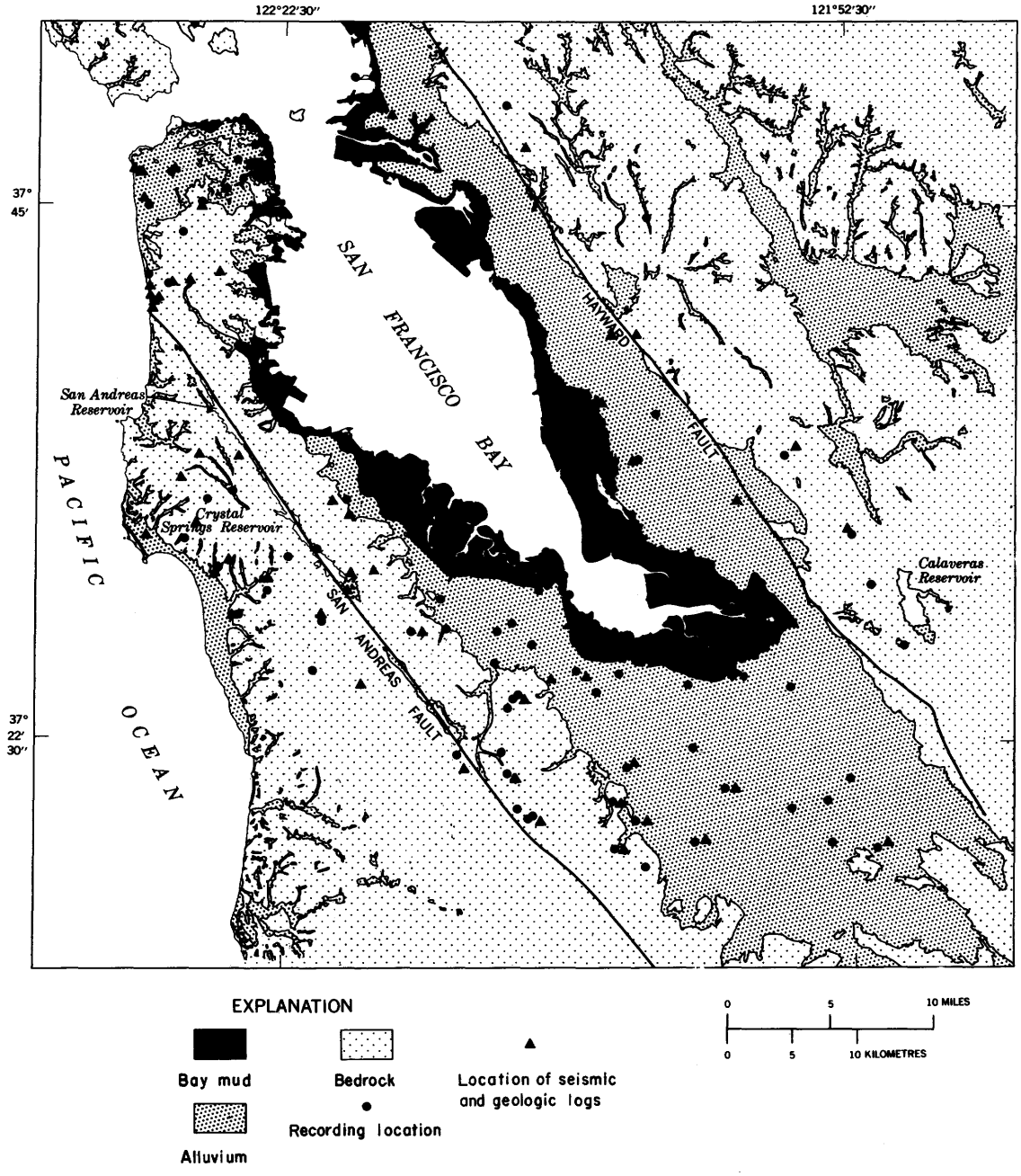

Figure 2.-Distribution of generalized geologic units, locations where seismic and geologic logs have been compiled in drill holes to 30 m depth, and locations where ground response has been measured from a nuclear source.

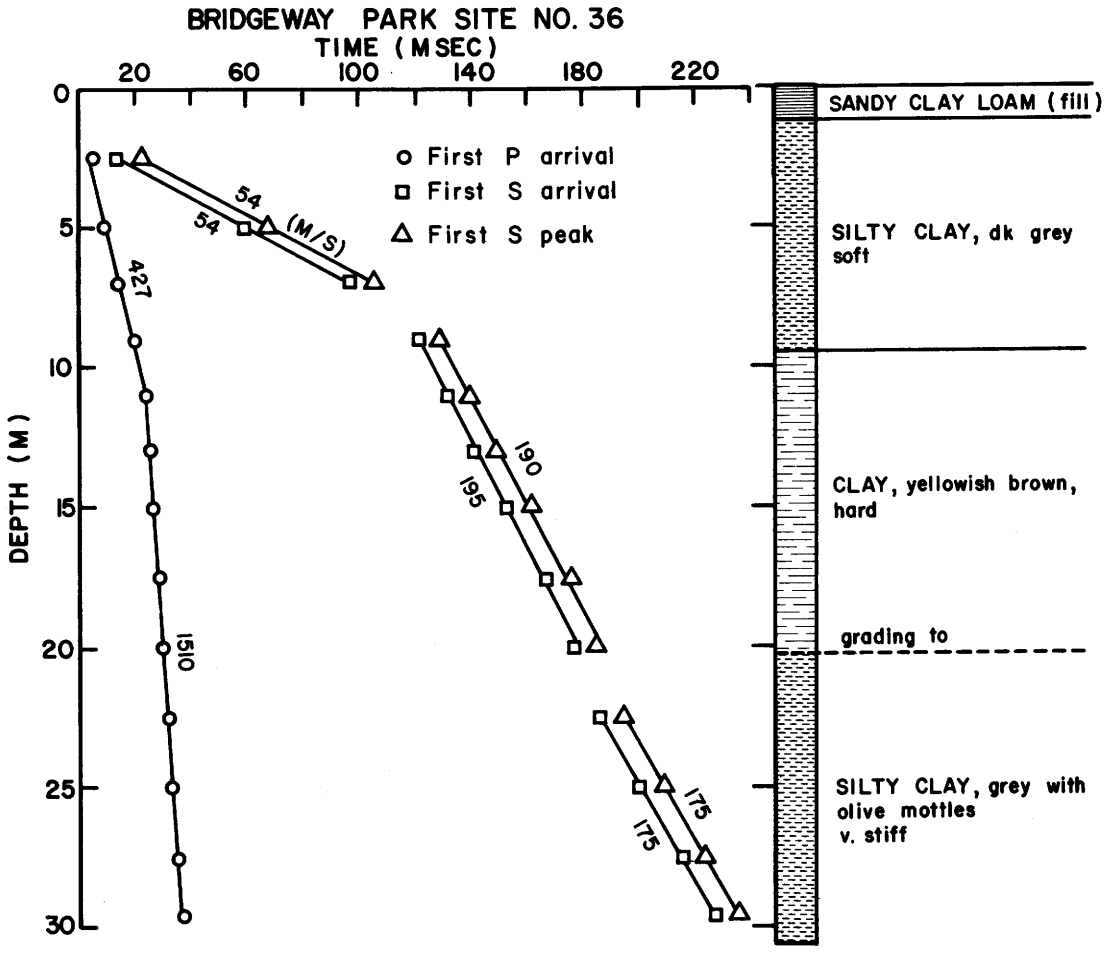

Figure 3.-Example of traveltime curves for P and S waves and simplified geologic log. Two picks are shown for the S-wave group--first S arrival and first S peak.

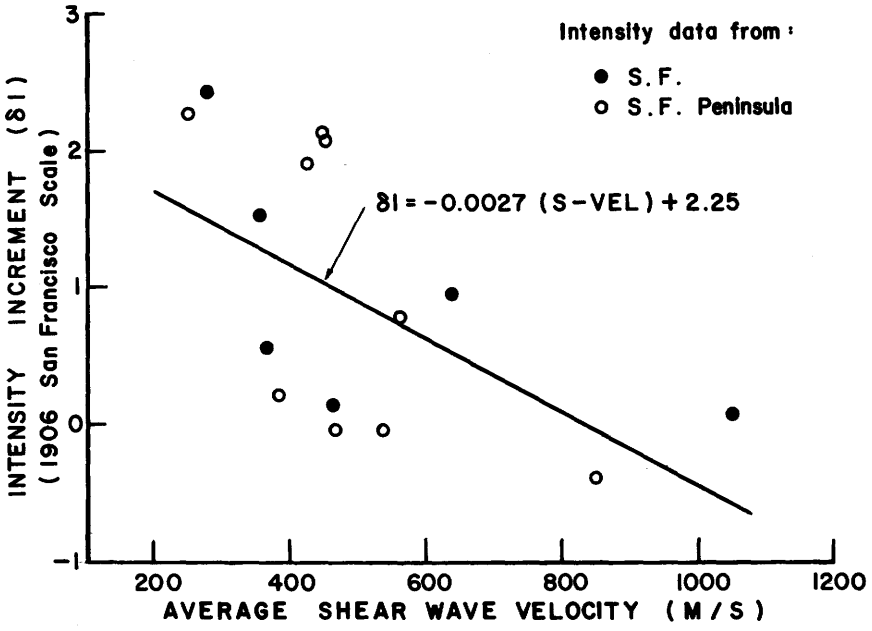

Figure 4.-Intensity increment (δI) determined from data of 1906 San Francisco Earthquake vs. shear wave velocity averaged from surface to approximately 30 m depth. Dots are observed data using San Francisco intensity scale and circles are data using Rossi-Forel scale. Intensity increments are expressed in terms of the San Francisco intensity scale converting the letters A-E to 4-0, respectively. Observed data expressed in Rossi-Forel scale were converted to San Francisco scale using X→A, IX→B, VIII-IX→C, VII-VIII→D, and VI-VII→E.

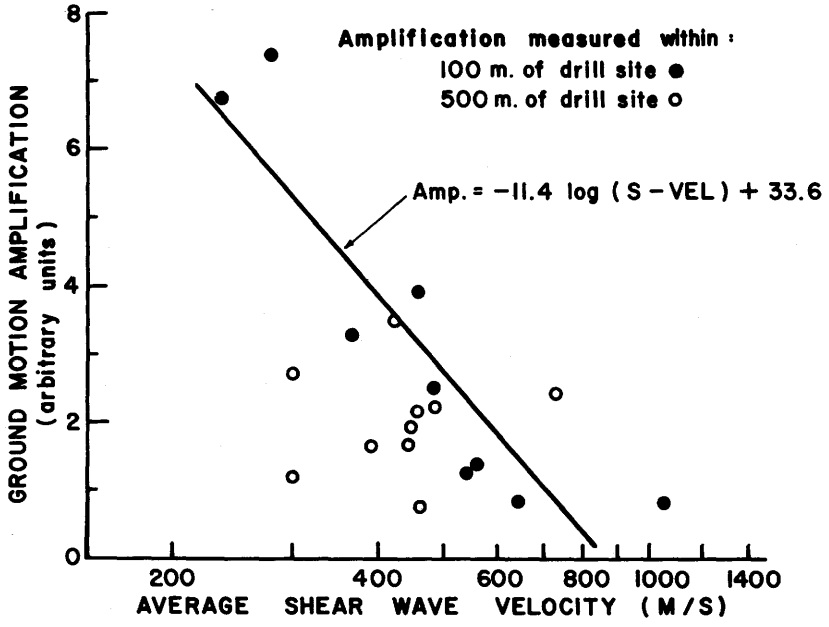

Figure 5.-Amplification (Amp.) as determined from recordings of ground motion generated by nuclear explosions vs. shear wave velocity averaged from surface to approximately 30 m depth. Dots represent ground motion amplification measured within 100 m; and circles, within 500 m of drill site.

meters of a surficial deposit plays a significant role in changing the anticipated characteristics of seismic waves in certain frequency bands.

Geologic and Physical Properties of Seismically Distinct Units

Preparation of regional ground response maps requires utilization of data available on a regional scale. In most urban areas this data base is limited to standard geologic mapping. Most such maps, however, are compiled for purposes of inferring geologic history and are not immediately applicable to preparing special-purpose interpretive maps. Mapped units commonly contain materials with a wide range of physical properties and seismic characteristics.

In order to adapt the geologic data base for purposes of regional seismic zonation, a detailed study was undertaken to investigate correlations between geologic and physical descriptions of the various units and seismic velocities (Fumal, 6). The study identified a suite of physical properties of geologic materials that can be used to identify seismically distinct units and can be readily determined in the field and thus incorporated in geologic mapping schemes.

Seismic wave velocities were measured in each of the geologic map units in the San Francisco Bay region. The range of seismic velocities for a given unit is dependent on the variety of materials included in the unit, which is largely a function of the age of the deposit. Each of the Holocene map units shows a distinct and relatively narrow range of shear wave velocity. Older sedimentary deposits and bedrock materials show relatively wide and overlapping velocity ranges. For these materials, age has been an important factor in defining geologic units. Differences in age, however, frequently do not correlate with significant variation in the physical properties that affect seismic velocities.

For the unconsolidated to semiconsolidated sedimentary units, texture or relative grain size distribution was found to have the most significant effect on seismic shear wave velocity. On the basis of texture alone, the unconsolidated sedimentary deposits in the San Francisco Bay region can be divided into four categories: (1) clay and silty clay, (2) sandy clay and silt loam, (3) sand, (4) and gravel. Utilizing standard penetration resistance measurements (SPR), the clay and silty clay unit and the sand unit each can be subdivided into two additional units. Each unit identified according to physical properties is clearly identifiable seismically (lower abscissa Fig. 6, Table 1) with the exception of the sand unit, which was classified separately because it is easily distinguishable in the field and because its compaction varies over a broad range. Each of the units identified according to texture and SPR is also easily recognized in the field and should be readily differentiated in areas that have existing geologic maps.

For the bedrock materials in the San Francisco Bay region, fracture spacing was found to have the most significant effect on seismic shear wave velocity for various rock types. Hardness has the second largest effect and lithology can be used to distinguish between hard sedimentary and igneous rocks like the sedimentary units, each bedrock unit identified according to physical properties is seismically distinct (lower abscissa, Fig. 7; Table 1). The seismically distinct bedrock units can not be so easily mapped as the unconsolidated sediments because fracture spacing

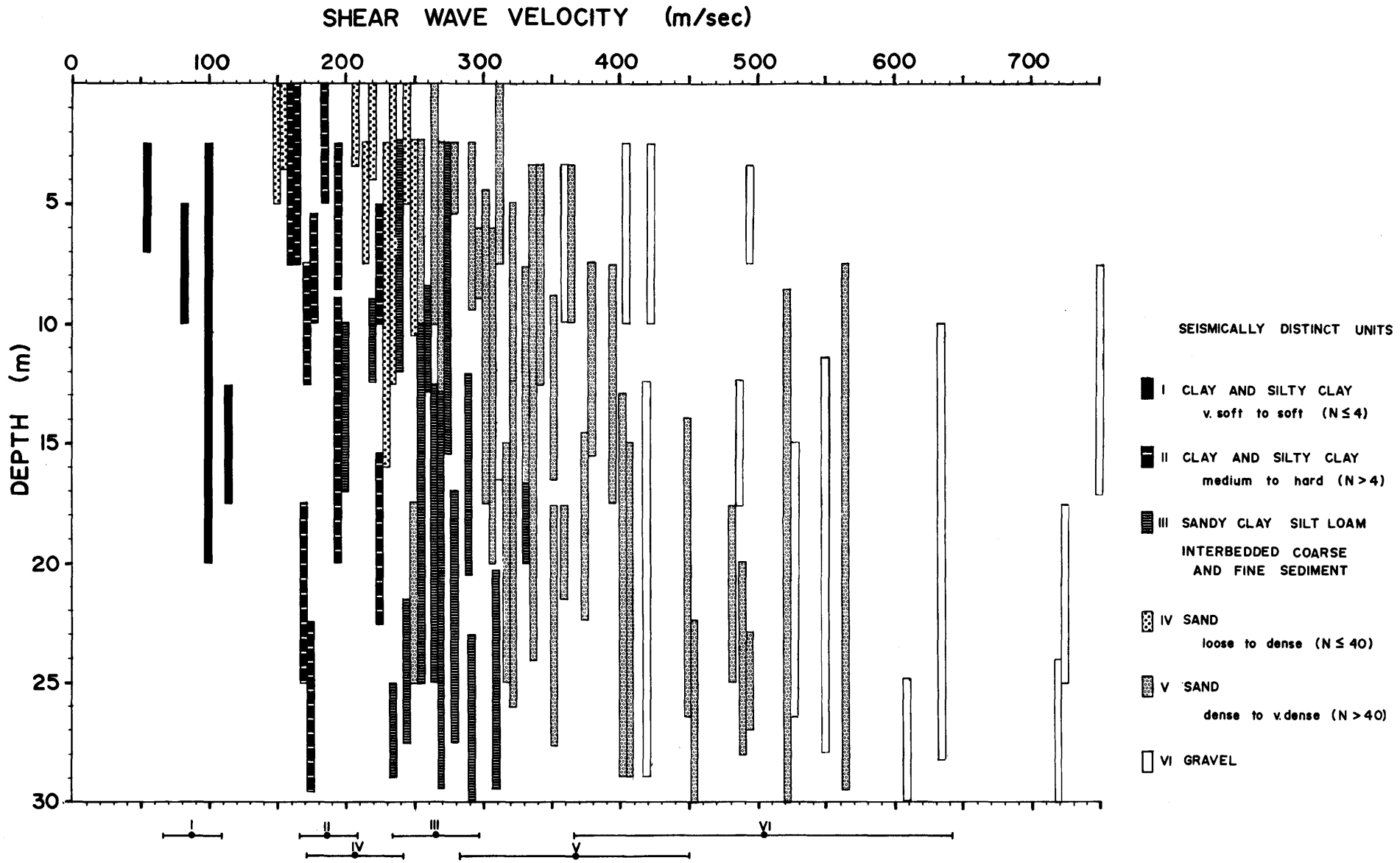

Figure 6.-Shear wave velocity for various depth intervals determined in drill holes for unconsolidated to semiconsolidated sedimentary deposits. Seismically distinct units are classified according to the physical properties of texture or relative grain size and standard penetration resistance. Means and standard deviations for each unit are shown along lower abscissa by dots and error bars, respectively.

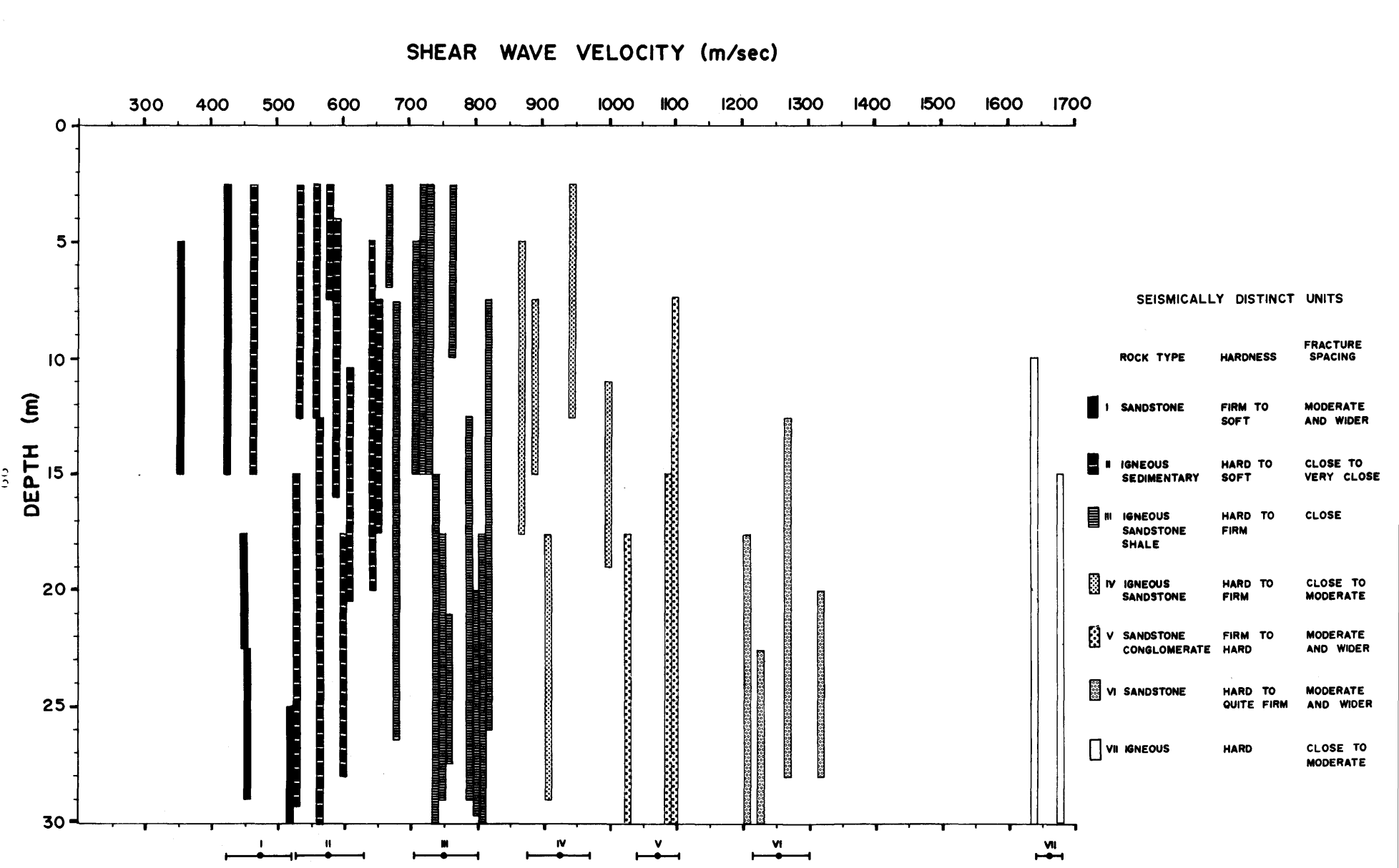

Figure 7.-Shear wave velocity for various depth intervals determined in drill holes for bedrock materials. Seismically distinct units are classified according to the physical properties of fracture spacing, hardness, and lithology. Means and standard deviations for each unit are shown along lower abscissa by dots and error bars, respectively.

TABLE I

SHEAR WAVE VELOCITIES IN GEOLOGIC MATERIALS

Distinct Seismic Units	Physical Properties	Shear Wave Vel. (m/s) Mean	Std. Dev.	Amp. (Pred.)	Intensity Increment (Pred.)
	Sedimentary Deposits				
I	Clay-Silty Clay very soft-soft ($N \leq 4$)	88	22	11.43	2.01
II	Clay-Silty Clay medium-hard ($N \geq 4$)	186	22	7.73	1.75
III	Sandy Clay-Silt Loam Interbedded Coarse and Fine Sediment	265	32	5.97	1.53
IV	Sand loose to dense ($N \leq 40$)	206	36	7.22	1.69
V	Sand dense to very dense ($N \geq 40$)	366	84	4.38	1.26
VI	Gravel	504	138	2.79	.89

Distinct Seismic Units	Physical Properties Rock Type	Hardness	Fracture Spacing	Shear Wave Vel. (m/s) Mean	Std. Dev.	Amp. (Pred.)	Intensity Increment (Pred.)
			Bedrock Materials				
I	Sand-stone	Firm to Soft	Moderate and wider	470	48	3.14	0.98
II	Igneous Sedi-mentary	Hard to Soft	Close to very close	577	51	2.12	.69
III	Igneous Sands-stone Shale	Hard to Firm	Close	751	46	.82	.22
IV	Igneous Sandstone	Hard to Firm	Close to Moderate	923	48	-.20	-.24
V	Sandstone Conglom-erate	Firm to Hard	Moderate and wider	1073	31	-.95	-.65
VI	Sandstone	Hard to quite firm	Moderate and wider	1257	42	—	—
VII	Igneous	Hard	Close to	1660	20	—	—

and hardness vary widely within many map units. For purposes of mapping regional ground response, however, subdivision of the bedrock materials is not so important, and fewer subdivisions may be adequate for many areas.

Methodology for Regional Maps

Regional maps depicting expected variations in ground response must be based on data available on a regional scale. Geologic and physical property data can be readily tied to more quantitative estimates of ground response such as amplifications and intensity increments utilizing seismic velocity data.

Intensity increments and amplifications are predicted for 11 of the 13 units in the San Francisco Bay region using relations in figures 4 and 5 (Table 1). Both the intensity increments and amplifications predicted are easily distinguishable for the various units and show that a considerable geographic variation can be expected in ground response to earthquake generated shaking. These predictions, together with appropriate bedrock attenuation curves from a potential earthquake source, provide a technique for developing a preliminary but improved regional ground motion map for the San Francisco Bay region. To prepare ground response maps for other areas where similar intensity and amplification data are not available, measurement of seismic velocities in a relatively few seismically distinct units would permit extrapolation of the San Francisco data. A program is currently under way to compare data in the San Francisco and Los Angeles regions.

REFERENCES

1. Borcherdt, R.D. (1970), Effects of local geology on ground motion near San Francisco Bay, Bull. Seis. Soc. Am., v. 60, pp. 29-61.

2. Borcherdt, R.D. (Editor) (1975), Studies for seismic zonation of the San Francisco Bay region, U.S. Geological Survey Professional Paper 941-A.

3. Borcherdt, R.D. and Gibbs, J.F. (1976), Effects of local geological conditions in the San Francisco Bay region on ground motions and the intensities of the 1906 earthquake, Bull. Seis. Soc. Am., v. 66, pp. 467-500.

4. Borcherdt, R.D., Gibbs, J.F. and Lajoie, K.R. (1975), Prediction of maximum earthquake intensity in the San Francisco Bay region, California, for large earthquakes on the San Andreas and Hayward faults, U.S. Geological Survey, MF 709.

5. Borcherdt, R.D., Joyner, W.B., Nichols, D.R., Chen, A.T.F., Warrick, R. E., and Gibbs, J. (1972), Ground motion predictions, abs., Proceedings of the international conference on microzonation, p. 862, Seattle, WA.

6. Fumal, T.E. (1978), Correlations between seismic wave velocities and physical properties of near-surface geologic materials in the southern San Francisco Bay region, U.S. Geological Survey, Open-file report (in progress).

7. Gibbs, J.F., Fumal, T.E. and Borcherdt, R.D. (1975), In-situ measurements of seismic velocities at twelve locations in the San Francisco Bay region, U.S. Geological Survey, Open-file report 75-564.

8. Gibbs, J.F., Fumal, T.E. and Borcherdt, R.D. (1976), In-situ measurements of seismic velocities in the San Francisco Bay region...Part II, U.S. Geological Survey, Open-file report 76-731.

9. Gibbs, J.F., Fumal, T.E., and Borcherdt, R.D. (1978), In-situ measurements of seismic velocities at 59 locations in the San Francisco Bay region, abs., 73rd Annual Meeting, Seis. Soc. of Am., Sparks, Nv.

10. Gibbs, J.F., Fumal, T.E., Borcherdt, R.D. and Roth, E.F. (1977), in-situ measurements of seismic velocities in the San Francisco Bay region...Part III, U.S. Geological Survey, Open-file report 77-850.

11. Kobayaski, N. (1959), A method of determining the underground structure by means of SH waves, Zisin, ser. 2, v. 12, pp. 19-24.

12. Lawson, A.C. (Chairman) (1908), The California earthquake of April 18, 1906, report of the state earthquake commission, Carnegie Inst. Washington, p. 160-253.

13. Warrick, R.E. (1974), Seismic investigation of a San Francisco Bay mud site, Bull. Seism. Soc. Am., v. 64, pp. 375-385.

A METHODOLOGY FOR PREDICTING GROUND MOTION AT SPECIFIC SITES

Ralph J. Archuleta , William B. Joyner and David M. Boore[1]

ABSTRACT

An important development in current research on earthquake ground motion is the synthesis of ground motion records based on the physics of a propagating fracture. Different techniques are used for generating synthetic records depending upon the frequency range of interest. For frequencies below about 1-2 Hertz we used a finite element method to simulate a propagating fracture; for higher frequencies we used a stochastic dislocation model. With the finite element method we have been able to simulate a dynamic earthquake in a fully three-dimensional geometry. We compute the ground motion from two hypothetical earthquakes that differ only in their shear stress distribution with depth. On the free surface we have contoured the maximum particle velocity. From such contours one could approximate the areas most likely to suffer damage during an earthquake. We have also used the fault slip generated by a propagating stress relaxation as input for the stochastic model. Acceleration is computed using a statistical source model in which the amplitude of the dislocation-time function varies randomly along the fault while the shape of the function and the rupture velocity are constant.

INTRODUCTION

One of the fundamental assumptions for any microzonation plan is that one can realistically estimate the ground motion resulting from an earthquake. We are developing methods for computing complete time histories of earthquake ground motion from physical models of the source and propagation path. We expect that the time histories will be useful, not only in the detailed dynamic analysis of structures, but also in estimating ground motion parameters, e.g., peak particle velocity and peak particle acceleration, for microzonation purposes.

A major difficulty in making estimates of the ground motion in the near field is that the frequencies of interest range from d.c. to tens of hertz. In order to span this wide range of frequencies we have modeled the earthquake source by using a three-dimensional, finite element model of a propagating stress relaxation (1) in combination with a stochastic propagating dislocation (2). The finite element provides estimates of the dislocation time history (2). In addition the finite element method

---

[1] Professor of Geophysics, Stanford University, Stanford, CA. 94305.

provides estimates of particle displacement and particle velocity while the stochastic dislocation gives some estimate of the particle acceleration. The finite element method has been used successfully to model real ground motion data from the 1966 Parkfield earthquake (3). In this paper we illustrate the method by applying it to two hypothetical earthquakes: the first has a shear prestress distribution that is uniform over the width of the fault; the second has a prestress distribution that varies with depth, Figure 1. A comparison illustrates the influence of one of the important aspects of the earthquake source model.

METHODS

To simulate an earthquake in a prestressed medium we use the method of Archuleta and Frazier (1) that allows the fracture to nucleate at a hypocenter and spread with a prescribed rupture velocity over a given finite-sized fault area embedded within a halfspace. As the fracture spreads, it relaxes the stress enclosed by its rupture front. This model was based on the generally accepted elastic rebound hypothesis (4) as the mechanism for shallow, tectonic earthquakes. This method is fully three-dimensional and the rupture surface may or may not intersect the traction-free surface of the halfspace. Driven by the stress relaxation the medium adjusts to the new stress state. The particle displacement and particle velocity can be computed everywhere including the rupture surface and the free surface.

To demonstrate that their numerical method correctly simulated the physics of a propagating stress relaxation, Archuleta and Frazier (1) compared their numerically computed dislocations for a circular fault in a full space with the dislocations analytically determined by Kostrov (5) for a continuously expanding circular stress relaxation. Until the arrival of edge effects due to the finiteness of the fault in the numerical method, the numerical and analytical dislocations showed exceptional agreement including the square root behavior of the dislocation at the arrival of the rupture front.

As an example of using such an earthquake model, together with the response of a layered medium, Archuleta and Day (3) have computed synthetic seismograms to compare with those recorded during the 1966 Parkfield earthquake at Stations 2, 5, 8 and 12 which were about .8, 3.4, 9.1, and 14 km off the fault, respectively. A comparison of displacement time histories for Station 5 in the Cholame-Shandon array is shown in Figure 2. One can see that the match between components is close. The phases could probably be made to match better by adjusting the rupture velocity. The other stations showed similar agreements between synthetic and recorded displacements.

The frequency resolution of waves propagated using the finite element method depends critically on the number of nodal points per wavelength (6). Thus the finite element (and finite difference) methods

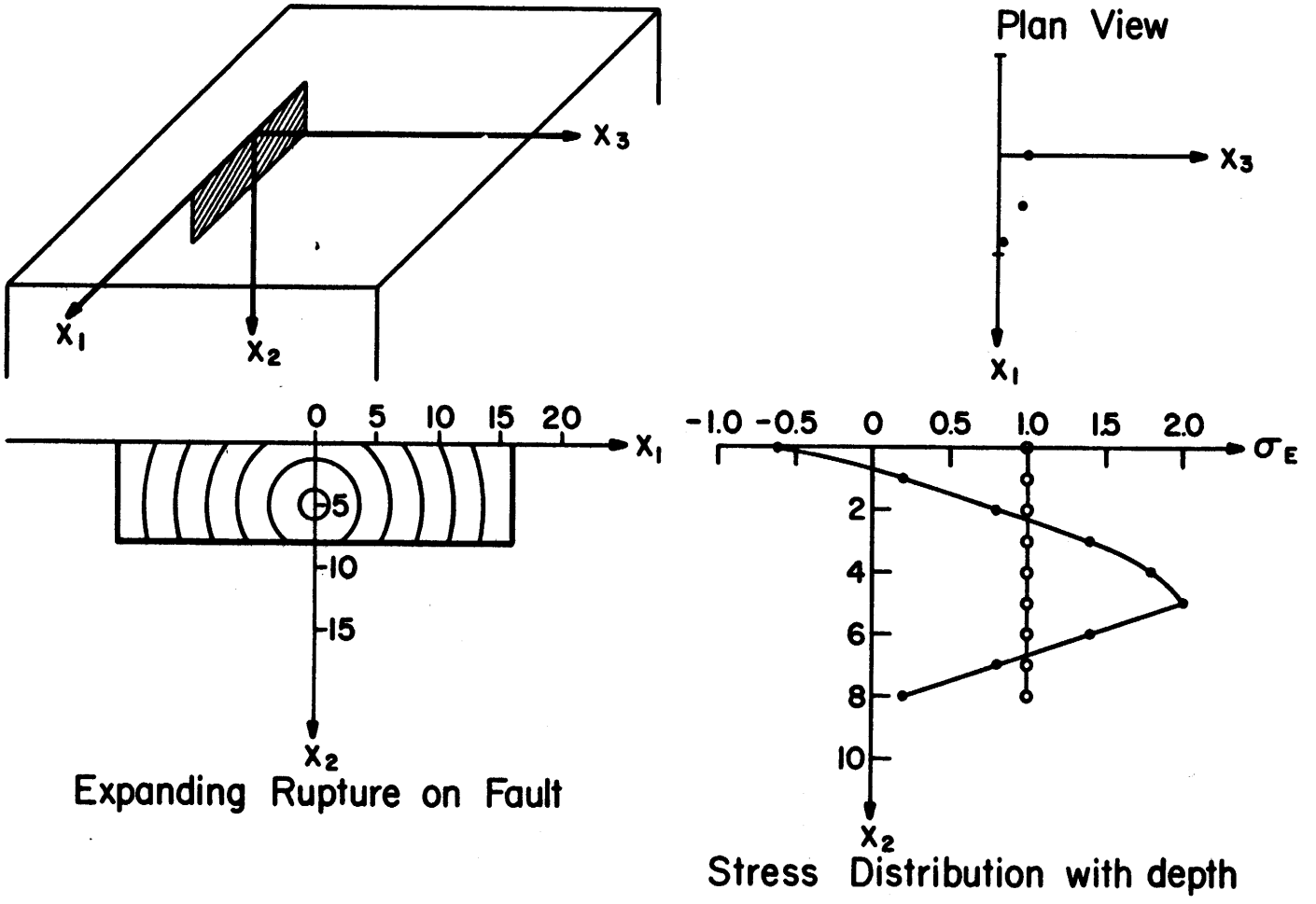

Figure 1. Schematic of fault, rupture surface and stress distribution.

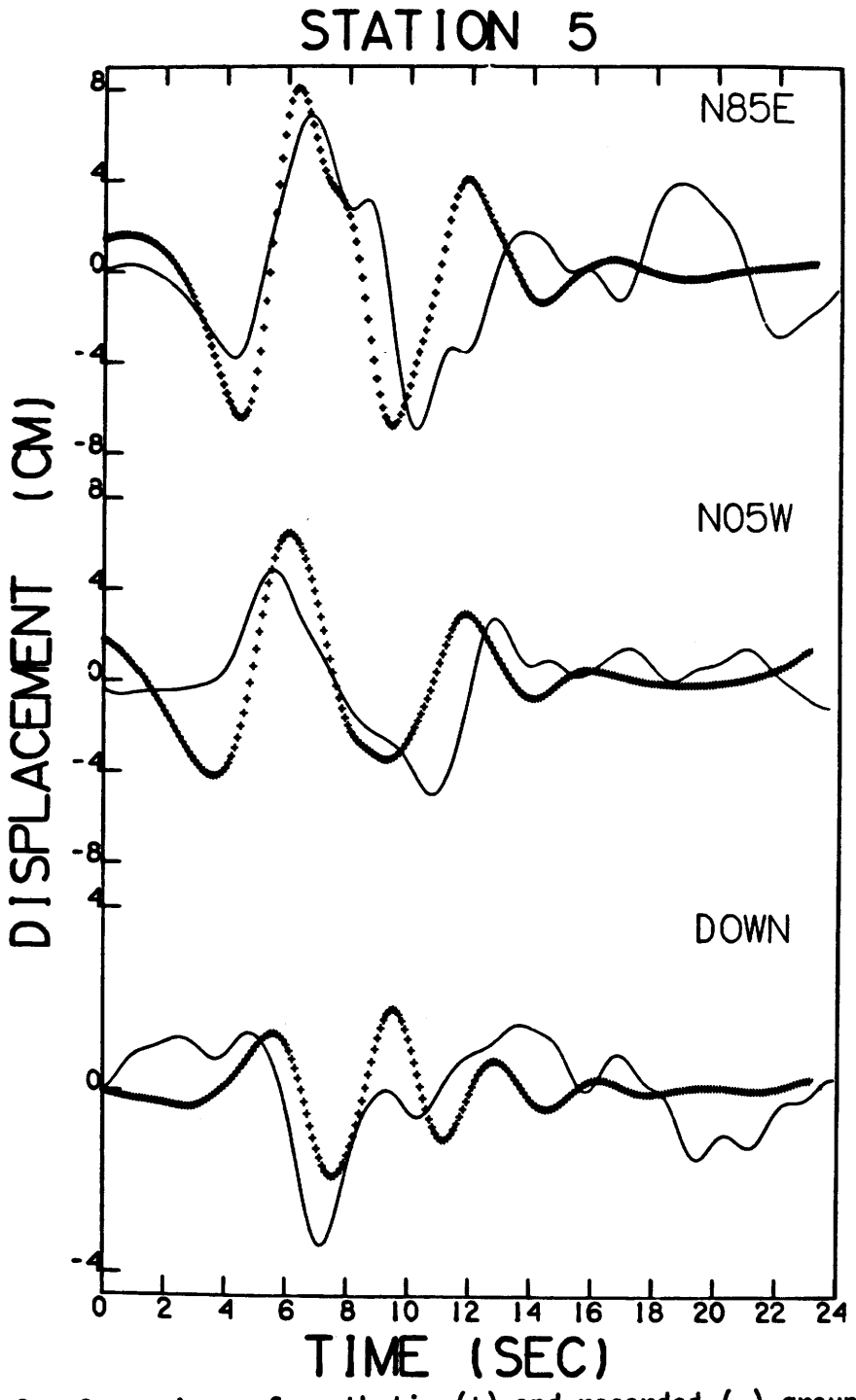

Figure 2. Comparison of synthetic (+) and recorded (-) ground motion of the 1966 Parkfield earthquake.

cannot economically resolve the high frequencies found in acceleration records. It can also be argued that on a scale of several hundred meters which corresponds to wavelengths associated with a 10 Hertz wave that we neither know the spatial variation of stress on the fault nor the inhomogeneities of the medium. Thus we have chosen to estimate the high frequencies from a propagating stochastic dislocation along a line at a fixed depth. A representative dislocation function is selected from the dislocations computed using the finite element stress relaxation. The dislocation is propagated with the same velocity from the same hypocenter. However, the amplitude of the dislocation is allowed to vary randomly about a mean value calculated from the stress relaxation model. The width of the fault is taken into account by assigning the dislocation function a weighting factor related to the width used in the stress relaxation problem.

EARTHQUAKE MODEL

We will model a strike-slip earthquake that occurs on a vertical fault that is 32 km in length and 8 km in width. The plane of the fault intersects the traction free surface of a homogeneous, isotropic, linearly elastic halfspace. The halfspace is characterized by a compressional wave speed (α) 6.0 km/sec, shear wave speed (β) 3.5 km/sec and density of 2.7 x 10^3 kg/m^3. To designate the spatial positions we use a Cartesian coordinate system X_1, X_2, X_3 with the origin at the midpoint of the strike of the fault at the traction free surface, Figure 1. Components of motion referred to as parallel, vertical and transverse are the components in the X_1, X_2, X_3 directions, respectively. The fracture nucleates at (0., 5., 0.) and spreads radially over the fault surface with a rupture velocity of $.9\beta$, Figure 1. As the fracture spreads it relaxes the σ_{31} component of stress.

We consider two different shear prestress distributions on the fault as a function of depth (σ_{31} (X_2)); however both shear stress distributions have the same average value. We also assume that the sliding friction stress does not vary with depth. The shear prestress does not vary along the strike of the fault. The parameter σ_E is the magnitude of the difference between the tractions on the fault before the fracture nucleates and the tractions on the fault during sliding. Because the sliding friction stress is uniform, σ_E varies with depth exactly as does the prestress. The amplitude of the particle motion scales directly with σ_E (7).

RESULTS

To illustrate the particle motion on the fault we show in Figure 3 time histories of particle velocity for points starting at the hypocenter and progressively moving toward the end of the fault on a line of constant depth. An important feature for microzonation is that the amplitude of the particle velocity increases in the direction of rupture propagation.

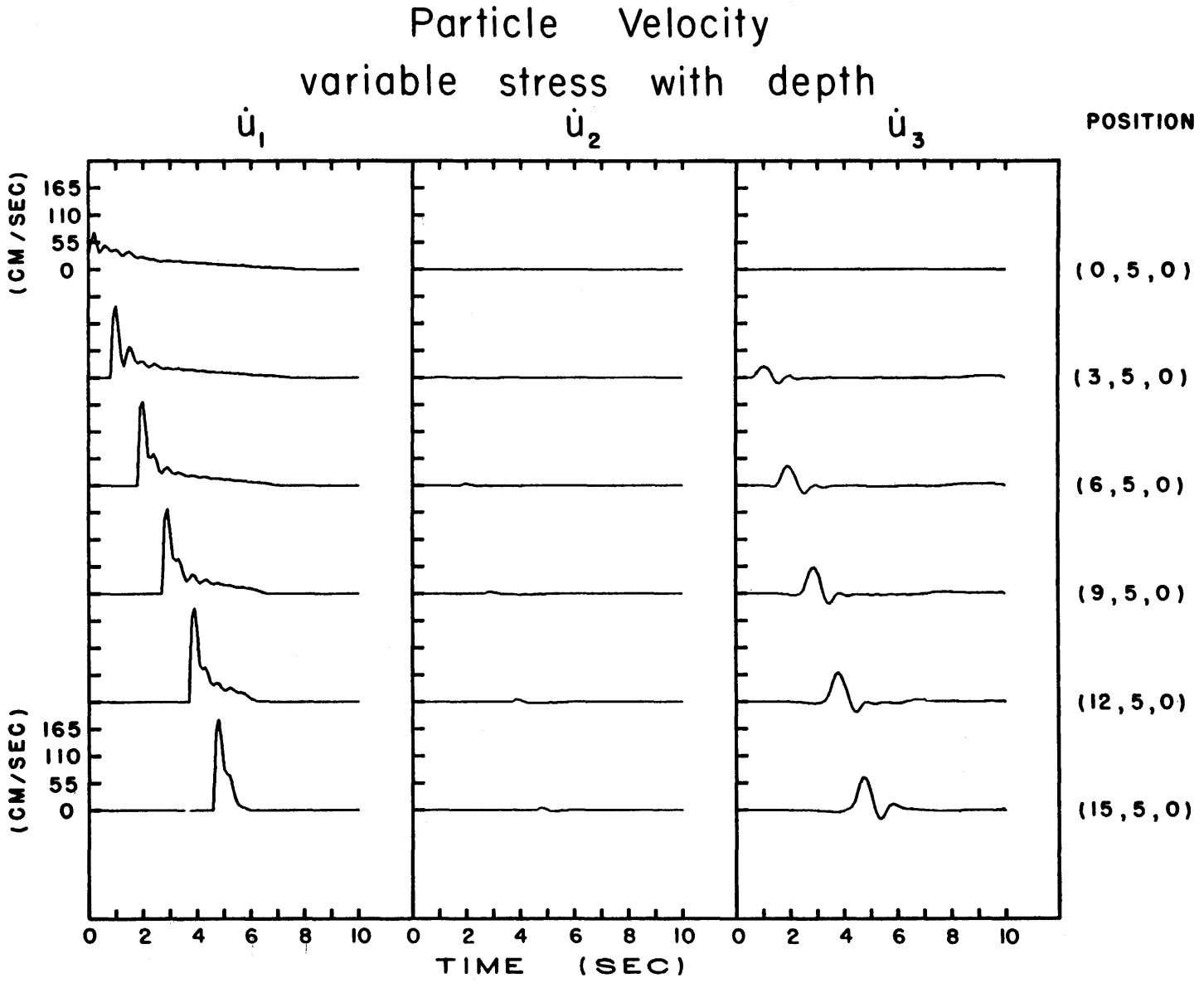

Figure 3. Particle velocity time histories on the fault surface.

As pointed out by Archuleta and Frazier (1) this focusing of energy is a combination of both the directivity associated with a moving source (8) and the buildup of stresses on the fault ahead of a subsonic rupture. This focusing can be an important consideration in microzonation because the largest amplitude ground shaking depends not only on the stress but also the rupture velocity and its direction of propagation. It should be mentioned that if the rupture nucleates at depth and propagates towards the free surface, the particle velocity will increase in amplitude as it approaches the free surface. The free surface has the additional effect of nearly doubling the amplitude of the particle velocity should the rupture front break through the surface (1).

To see how the earth's surface might respond to an earthquake we have plotted contours of maximum horizontal particle velocity in Figure 4 for the cases of uniform stress with depth and variable stress with depth. Maximum horizontal particle velocity is calculated by first taking the absolute value of the vector sum of the parallel and transverse components of particle velocity for each node on the free surface for every time step of the computation. The maximum value attained during the entire process is then contoured using a linear interpolation between adjacent nodes. Depending on what information is considered important other variables such as peak displacement or maxima of individual components of particle velocity could be contoured.

In order to provide numerical estimates of the peak horizontal particle velocity we have assumed an average value for σ_E of 55 bars for both stress distributions. σ_E can underestimate the static stress drop by about 20 to 25 percent (1) due to the inertial effects of a dynamic rupture (9). With σ_E of 55 bars, $\mu = 3.3 \times 10^5$ bars, $\alpha = 6$ km/sec and $\beta = S$ 3.5 km/sec the contours are drawn at 0.9 m/sec, 0.8 m/sec, etc. One can see that in the case of variable stress with depth the areas near the ends of the fault have the highest values; whereas if the stress were uniform over the entire fault, the distribution of horizontal particle velocity is nearly uniform along the entire strike of the fault with a gradual flaring of the contours near the ends. It should be pointed out that the maximum values of horizontal particle velocity anywhere on the free surface were 1.0 m/sec and 1.9 m/sec for the variable stress and uniform stress, respectively. Thus the contour of 0.9 m/sec for a uniform prestress not only encloses a larger area but also encloses larger values of peak horizontal particle velocity. Although the uniform stress produces larger values near the fault and over a larger area, the differences in the contours between the uniform and variable stress cases decreases with distance from the fault. At a distance of approximately one fault depth the contours are almost indistinguishable. Although the finite element propagating stress-relaxation can be used to compute variables such as particle velocity and particle displacement, it is too expensive an approach for computing particle acceleration where the frequencies of interest are around 10 Hertz.

Contours of Maximum Horizontal Particle Velocity
Uniform effective stress (σ_e) Fault 32X8 Hypocenter (0, 5, 0)
α = 6.0 Km/sec β = 3.5 Km/sec ρ = 2.7 Kg/m^3 v = 0.9 β
For σ_e = 55 bars, contours are drawn for 0.9 m/sec, 0.8 m/sec ....

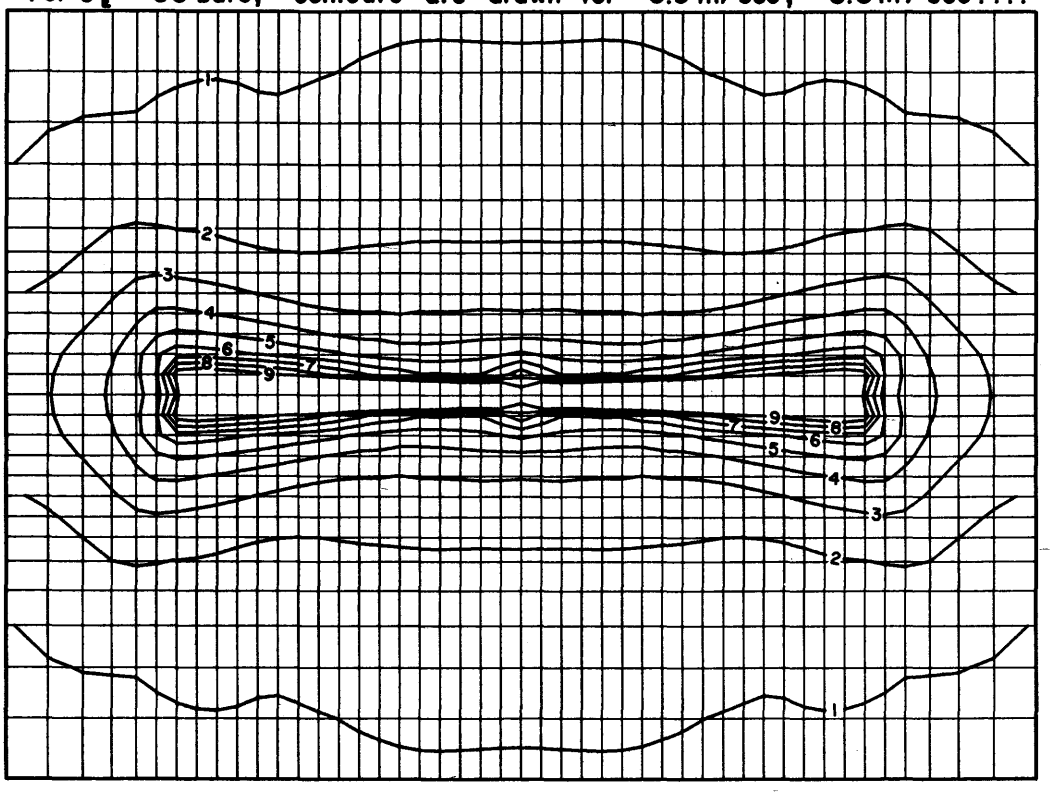

Contours of Maximum Horizontal Particle Velocity
Variable effective stress (σ_e) Fault 32X8 Hypocenter (0, 5, 0)
α = 6.0 Km/sec β = 3.5 Km/sec ρ = 2.7 Kg/m^3 v = 0.9 β
For σ_e = 55 bars, contours are drawn for 0.9 m/sec, 0.8 m/sec ....

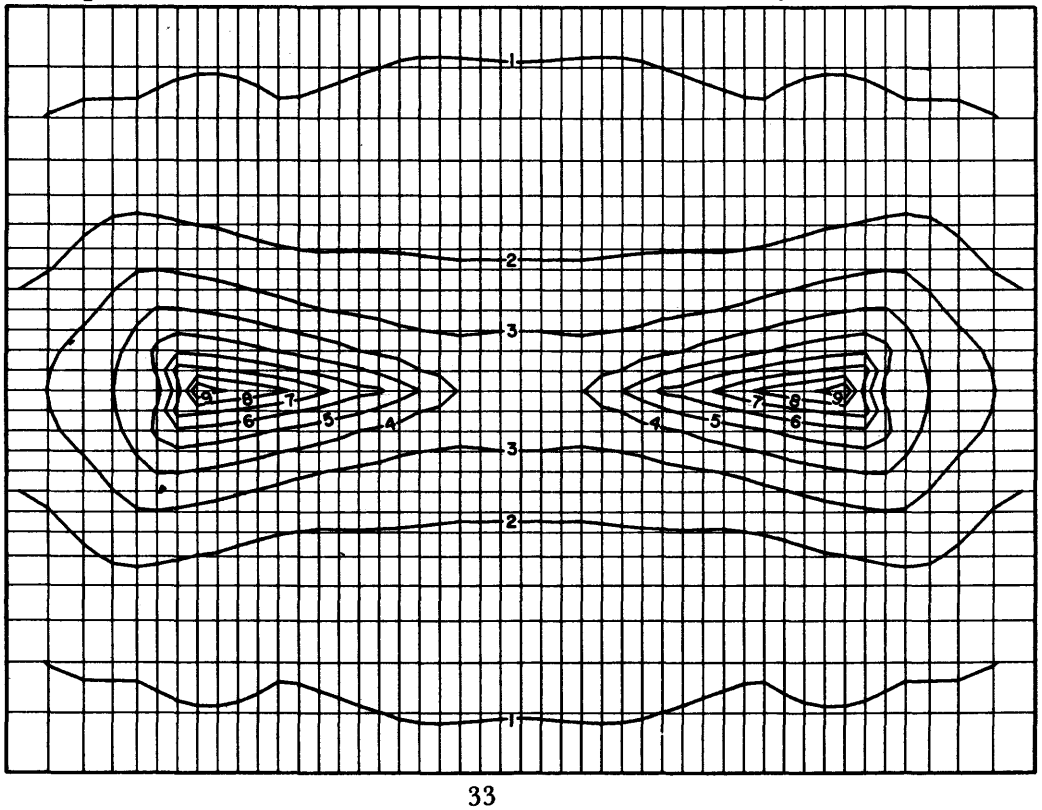

Figure 4. Contours of particle velocity on the free surface.

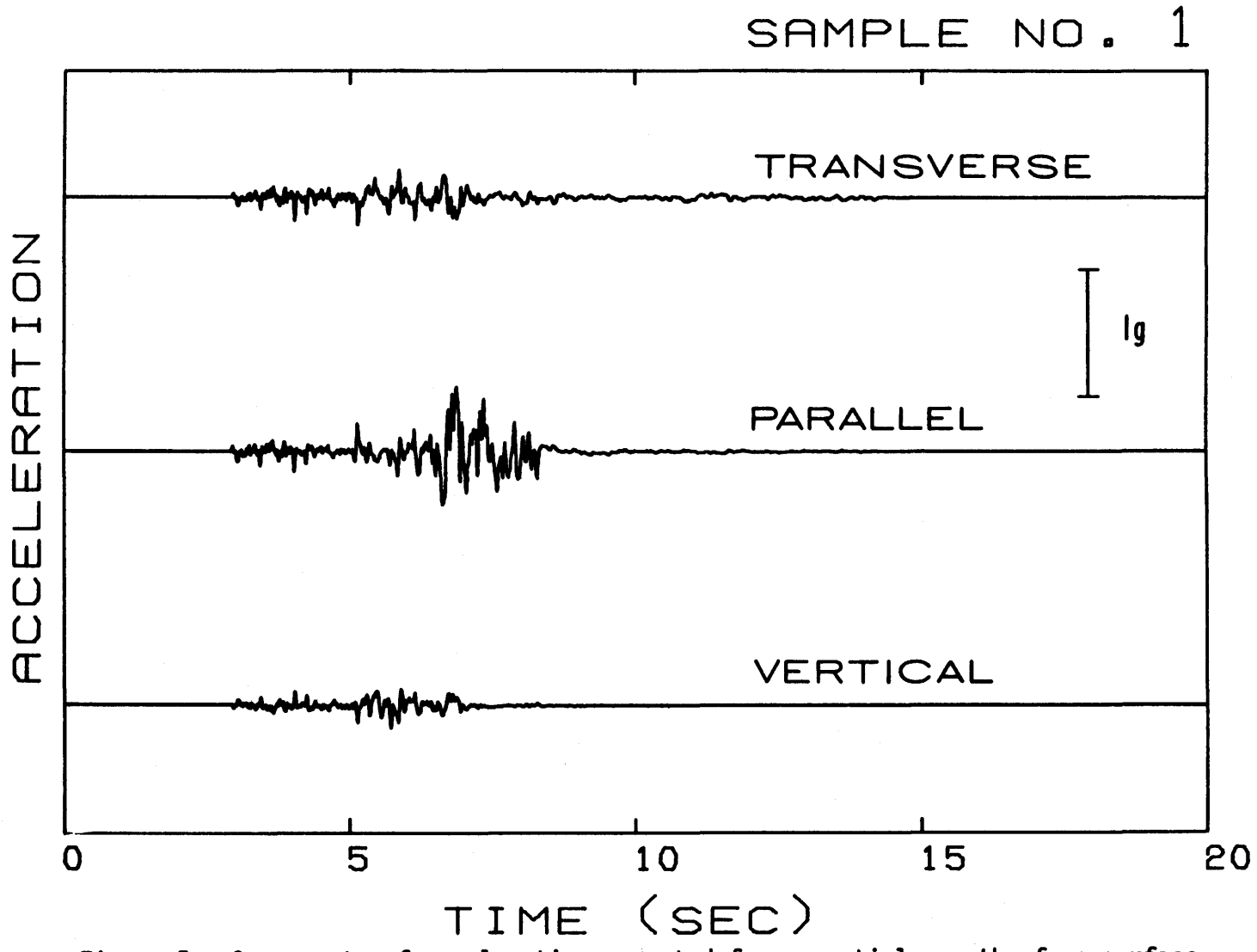

Figure 5. Components of acceleration computed for a particle on the free surface at (14.,0.,10.)

To calculate particle accelerations we have characterized the source as a propagating dislocation along a line at constant depth with the amplitude of the dislocation varying randomly from point to point. The form of the dislocation is derived from the dislocation computed in the stress relaxation problem. Since the method of Joyner and Boore (2) is strictly applicable only for the farfield, the dislocation rate rather than the dislocation is necessary to compute the accelerograms. We have taken the particle velocity function shown in Figure 3 at position (12., 5., 0.) as a representative for the entire faulting process. Using the Green's function for a full space and taking into account the free surface interaction by applying complex plane wave reflection coefficients we have computed accelerograms for the point(14.,0.,10.). A representative of the ensemble of accelerograms based on the stochastic method is shown in Figure 5. The acceleration records have been operated on by both the instrument response of an accelerograph with a natural frequency of 20 Hertz and damping 0.6 critical and by an attenuation operator (10) using a quality factor of 150 for shear values. The peak values of acceleration are 0.52g, 0.22g, and 0.19g, for the parallel, transverse and vertical directions, respectively where $g = 9.8\ m/sec^2$.

The methods of computing ground motion presented in this paper are approximations to our understanding of the earthquake source and the propagation paths. Further refinement of these methods plus the development of new techniques should lead to even better estimates of ground motion near a propagating fracture.

REFERENCES

(1) Archuleta, R. J. and G. A. Frazier (1978). Three-dimensional numerical simulation of dynamic faulting in a halfspace, Bull. Seis. Soc. Am., 68, No. 3, p. 541-572.

(2) Joyner, W. B. and D. M. Boore (1978). A statistical source model for synthetic strong motion seismograms, Earthquake Notes, 49, No. 1, p. 3.

(3) Archuleta, R. J. and S. M. Day (1977). Near-field particle motion resulting from a propagating stress relaxation over a fault embedded within a layered medium, EOS, 58, p. 445.

(4) Reid, H. F., (1910). Mechanics of the Earthquake, in California Earthquake, of April 18, 1906, II: Carnegie Inst., of Washington D. C. (updated in 1969).

(5) Kostrov, B. V. (1964). Self-similar problems of propagation of shear cracks, J. App. Math. Mech. 38, p. 1077-1087.

(6) Day, S. M. (1977). Finite element analysis of seismic scattering problems, Ph.D. Dissertation, University of California, San Diego.

(7) Madariaga, R. (1976). Dynamics of an expanding circular fault, Bull. Seism. Soc. Am. 66, p. 639-666.

(8) Ben-Menahem, A. (1962). Radiation of seismic body waves from a finite source in the Earth, J. Geophys. Res. 67, p. 345-350.

(9) Savage, J. C. and M. D. Wood (1971). The relation between apparent stress and stress drop, Bull. Seism. Soc. Am. 61, p. 1381-1388.

(10) O'Neill, M. E. and D. P. Hill (1978). Frequency-dependent anelasticity and its effect on synthetic seismograms, Earthquake Notes 49, No. 1, p. 54.

Liquefaction Potential Map of San Fernando Valley, California

by

T.L. Youd , J.C. Tinsley , D.M. Perkins , E.J. King
and R.F. Preston

ABSTRACT

Ground failure caused by liquefaction is a primary hazard associated with earthquakes. A first step in avoiding or mitigating this hazard is to recognize where liquefaction is likely to occur. A liquefaction potential map has been compiled for the San Fernando Valley, California, showing areas where conditions may be favorable for the development of liquefaction. The map incorporates assessments of age and type of sedimentary deposits, ground water depth, and expected seismicity into the delineated zones. This map is useful to planners, building officials, engineers, and others responsible for minimizing seismic risk because it points out areas where potential hazards exist and where further investigation, regulation, zoning, or other measures might be required. The map is not sufficient for evaluation of the actual liquefaction potential at an individual site. Site-specific geotechnical investigations are required to make such an assessment.

INTRODUCTION

Ground failures generated by liquefaction have been a major cause of damage during past earthquakes and pose considerable potential for damage and injury during future temblors. For example, during the 1971 San Fernando, California, earthquake, liquefaction-induced ground failures inflicted irreparable damage to several buildings at the San Fernando Valley Juvenile Hall and caused major damage to the partly completed Jensen Water Filtration Plant. Such failures do not occur at random, but rather are limited to certain geologic and hydrologic settings and to certain types of materials. A threshold seismic shaking intensity is also required to generate ground failure. This paper presents an analysis of these factors and their geographical distribution in the San Fernando Valley and a map to show general areas where potential for liquefaction and associated ground failure may exist. Site-specific studies are required to evaluate the potential beneath any specific parcel of land.

The procedure used to develop the liquefaction potential map is a combination of the techniques proposed by Youd and Perkins (9) and Youd and others (8). The technique of Youd and others was used to make a liquefaction potential map for the southern San Francisco Bay area. The procedure used here requires the development of two constituent maps, a liquefaction susceptibility map and a liquefaction opportunity map. The susceptibility map delineates areas where liquefiable materials are most

likely to occur. The opportunity map shows recurrence intervals for earthquake shaking strong enough to generate liquefaction in susceptible materials. These maps are then superimposed to form a liquefaction potential map.

LIQUEFACTION SUSCEPTIBILITY MAP

The liquefaction susceptibility map developed herein incorporates the following factors that affect liquefaction susceptibility: age and type of sedimentary deposits; standard penetration resistance of cohesionless sediments; and depth to perched or other ground water.

Sedimentary Deposits

Analyses of historical occurrences of liquefaction, in general, indicate that the more recently a sediment is deposited, the more likely it is to be susceptible to liquefaction, and that certain types of deposits, such as river channel and flood-plain deposits, are more susceptible to liquefaction than other deposits, such as alluvial fan deposits (9). Grain size distribution and packing also influence susceptibility. Sand and silty sand are the textural classes most likely to be adversely affected. In general, the more loosely the grains are packed, the more susceptible the sediment is to liquefaction. Standard penetration resistance is commonly used by engineers as an index of density of packing; the smaller the penetration resistance, the more likely the sediment will liquefy.

The San Fernando Valley lies in the Transverse Ranges structural province of southern California. The valley is an asymmetric basin filled chiefly with Miocene and younger (less than 20 million years old) sedimentary rocks. The relatively flat surface of the valley is underlain by unconsolidated sediments of middle to late Pleistocene or younger age that are as thick as 650 ft (200 m) (7). The exposed unconsolidated sediments are herein subdivided into three units -- most recent Holocene sediments (R), other Holocene sediments (H), and late Pleistocene deposits (P). The distribution of these units is shown on the map in Fig. 1. The margins of the basin comprise undifferentiated Pliocene to middle Pleistocene deposits (TQ) which include the Saugus and Pacoima Formations of Oakeshott (4), undifferentiated Tertiary sedimentary rocks (T), undifferentiated Mesozoic sedimentary rocks (K), and pre-Tertiary igneous and metamorphic rocks in the mountains mapped collectively as basement complex (BC).

Areas mapped as most recent Holocene sediments are chiefly those known to have been flooded historically, where the most recent deposition is known or presumed to have occurred. The primary data used to delineate the extent of flooding include field notes and unpublished maps prepared by the Los Angeles Flood Control District that show and describe areas inundated during floods in 1934, 1938, 1941, 1943, 1944, 1952, 1954, and 1956. Other data used include comparative photo-interpretive studies of 1928 and 1938, aerial photography at a scale of 1:24,000 or larger. The 1938 photographs were taken three to five months after the major floods of March, 1938. Features on the photographs used to delineate areas of recent deposition or flooding include changes in patterns of distributary channels or alluvial fans, areas where row crops, roads and other cultural features were washed out, areas adjacent to streams that were incised to depths less than 5 ft (1.5 m), and areas characterized topographically by bar and swale channel deposits. We have specifically excluded from the most recent Holocene unit areas that were locally inundated along streets where culverts

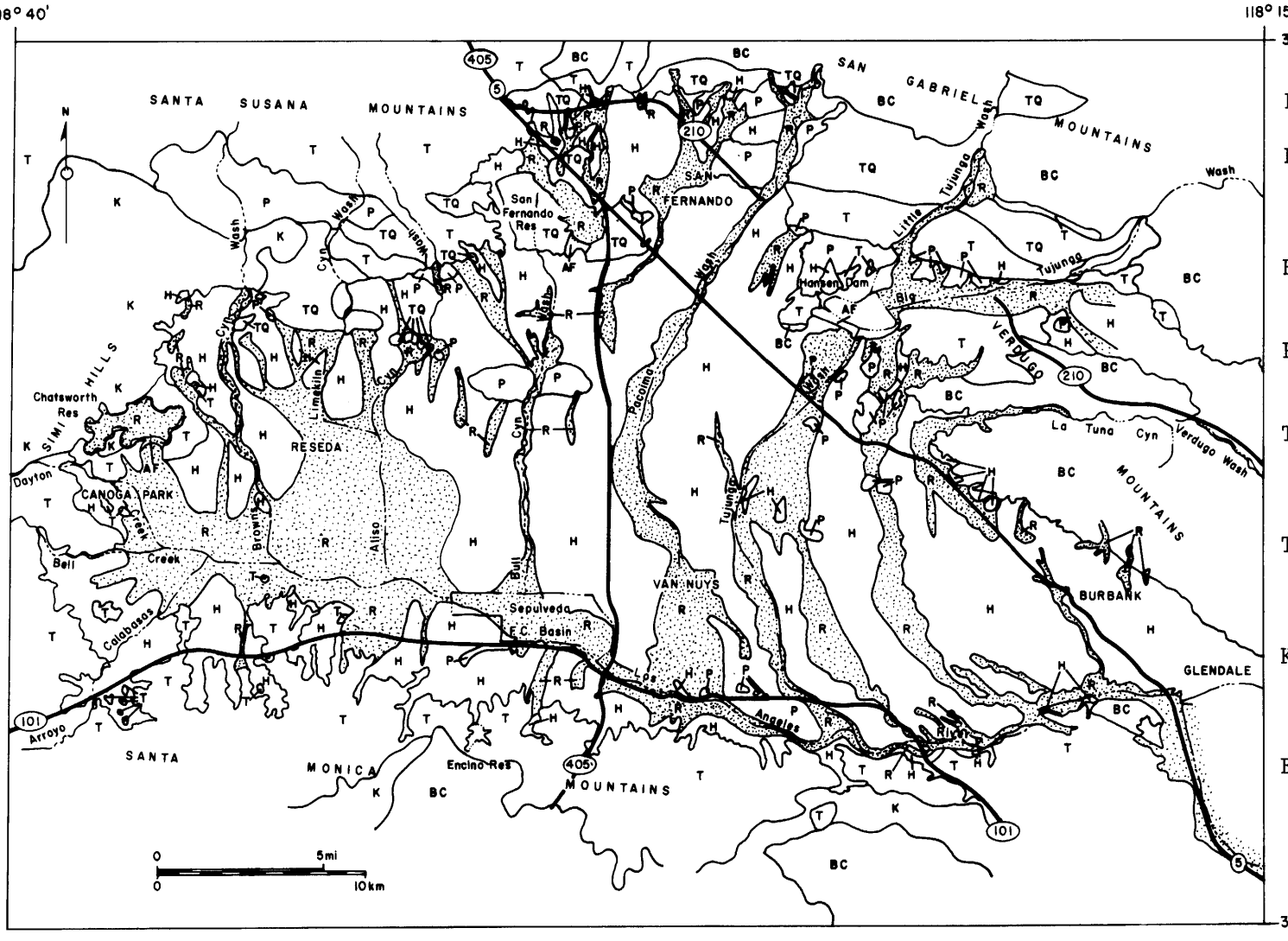

Fig. 1. Map showing distribution of geologic units in the San Fernando Valley, Calif. Bedrock units (T,K,BC, and TQ) from Jennings and Strand (3); R,H,P, and some TQ from J.C. Tinsley (unpub. field data)

plugged and water simply backed up. In all cases, interpretations reflect our efforts to identify and delineate the youngest stages of a very youthful depositional system because these are most likely to contain sediments susceptible to liquefaction.

Areas mapped as other Holocene sediments are differentiated chiefly on the basis of lack of record of recent inundation, a topographic position slightly higher than the most recent Holocene unit and by undeveloped to very weakly developed cumulative pedogenic soil profiles (chiefly entisols, inceptisols, and vertisols) typical of Holocene deposits. Soil maps prepared by the U.S. Bureau of Soils (2), and the U.S. Department of Agriculture (6) were the primary data used to delineate this Holocene unit.

Areas mapped as late Pleistocene deposits were differentiated on the basis of morphology and pedological development. They generally are exposed as topographic benches and terraces near the margins of the valley and on the up-thrown side of thrust faults in the northern part of the valley. They are also characterized by surface soils with textural "B" horizons. Under present climatic conditions, to form such a soil profile requires a period of development that began in Pleistocene time.

By the criteria set out in Youd and Perkins (9), water-saturated, clay-free sediments in the most recent Holocene unit generally are expected to have high susceptibility to liquefaction; clay-free sediments in the other Holocene unit generally would be expected to have moderate susceptibility, and clay-free sediments in the late Pleistocene unit would be expected to have low susceptibility. The qualitative assessments of liquefaction susceptibilities were further verified by comparing them with liquefaction susceptibilities determined from standard penetration data. The evaluation of liquefaction susceptibility from standard penetration data followed the procedure previously used to compile a liquefaction potential map for the southern San Francisco Bay region. Plots were made of standard penetration resistance versus depth for the three youngest (R, H, and P) sedimentary units. Thicknesses of the two Holocene units have been inferred from descriptive logs of boreholes by identifying subsurface features such as, (a) an oxidized clay-rich layer which may indicate an ancient soil horizon that likely formed on the late Pleistocene unit before deposition of the Holocene unit, (b) an abrupt increase in penetration resistance not caused by intersecting a gravel layer, and (c) an estimated maximum thickness of the most recent Holocene unit of about 12 ft (3.6 m), based on rates of vertical acretion.

Using the criteria developed for the southern San Francisco Bay region (8), percentages of penetration data were grouped into high, moderate, and low liquefaction susceptibility categories for each sedimentary unit (Table 1). These categories are based on analyses developed in the simplified procedure for evaluating soil liquefaction potential formulated by Seed and Idriss (5) and analyses used by Youd and others (8) to map the San Francisco Bay area. The high susceptibility category represents saturated sediments that would be likely to liquefy in a nearby moderate (M=6.5) earthquake (energy source within 10 mi or 16 km) or a distant, very large (M=8) earthquake (energy source within about 60 mi or 100 km). The moderate susceptibility category indicates sediments that might liquefy during a nearby large (M=8) earthquake (energy source within 10 mi or 16 km). Low susceptibility indicates sediments that should not liquefy even when shaken by a nearby large earthquake. Assumptions made in deriving these categories are the same as those used in the San Francisco Bay region (8)

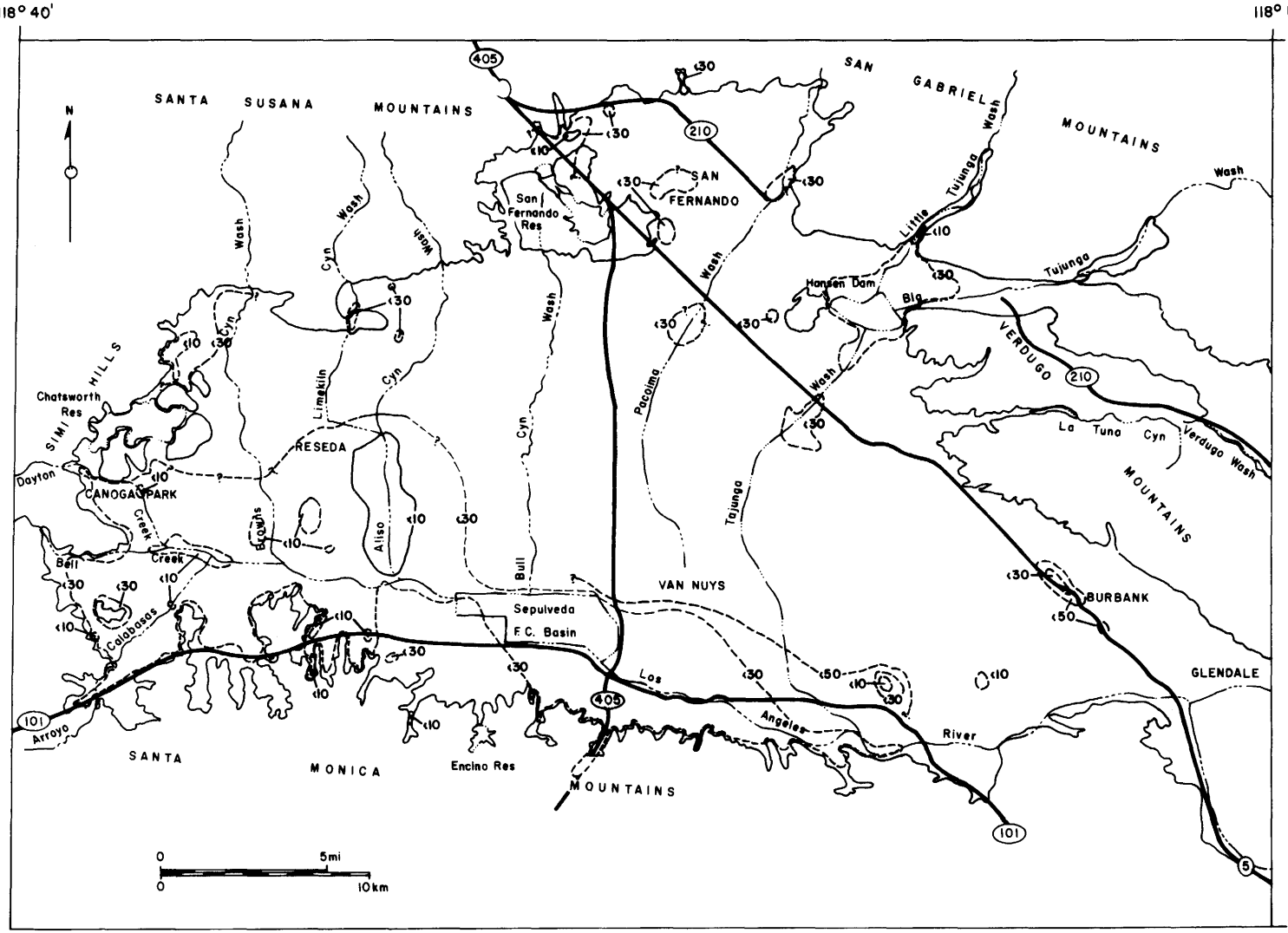

Explanation:

C30

Depth at which ground water was found. Dashed where not tightly constrained; queried where speculative.

Fig. 2. Map showing approximate depth to ground water, including perched ground water, for the San Fernando Valley, California

Table 1.--Evaluation of liquefaction susceptibility in clay-free granular layers from standard penetration data.

Sedimentary unit	Percentage of standard penetration data in susceptibility categories			Number of tests
	High	Moderate	Low	
Most recent Holocene	61	33	6	153
Other Holocene	39	49	12	618
Late Pleistocene	20	39	41	443

and include unit weight of 100 lb/ft^3 (1.6 gm/cm^3), a maximum surface acceleration of 0.2 *g* and 10 significant loading cycles for the nearby moderate (M=6.5) earthquake, and a 0.5 *g* maximum surface acceleration and 30 significant loading cycles for the nearby large (M=8) earthquake. The influence of depth to water table was taken into account in the calculation. These data (Table 1) show that saturated clay-free sediments in the youngest unit can be expected to have high susceptibility to liquefaction; similar sediments in the other Holocene unit can be expected to have moderate susceptibility; and saturated clay-free sediments in the late Pleistocene unit generally have moderate or low susceptibility to liquefaction.

Ground Water Depth

One of the primary factors controlling the distribution of liquefiable sediments in the San Fernando Valley is depth to ground water including perched ground water. Liquefaction susceptibility generally decreases with depth of the ground water table for two reasons: (a) The deeper the water table, the greater is the normal effective stress acting on saturated sediments at any given depth. Liquefaction susceptibility decreases with increased normal effective stress. (b) Age, cementation, and compactness of sediments generally increase with depth. Each of these factors also increases resistance to liquefaction. Thus, as depth to the water table increases, and as the saturated sediments become older, more cemented, more compact, and more stressed, the less likely they are to liquefy during an earthquake.

A map showing depth to ground water, including perched ground water, was prepared for part of the San Fernando Valley (Fig. 2). The lines on the map are not contour lines in the usual connotation used by hydrologists, i.e., an equipotential surface. Rather, they enclose areas where our data show that either perched or unconfined ground water has been recently found within the specified intervals of depth. This map was compiled from borehole data and well information supplied by the several agencies and firms acknowledged in this report. Because of sparsity of data in some areas and variations in amounts and elevations of ground water, construction of the map required considerable averaging, generalizing, interpolation, and extrapolation. Where depth lines are not tightly constrained, they are dashed; where they are speculative or positioned by factors other than borehole and well data, they are queried. The following problems are among those that arose in construction of the map. (a) Borings that intersect the water table are sparse in many areas. (b) Water levels in some deep wells may have been higher than the phreatic surface in the surrounding

soil because of artesian pressures at depth. (c) Some measurements, particularly along freeways and certain major storm drains, were recorded as much as 30 years ago, and water levels may have changed in the interim. Where several measurements have been made in one well over a period of years, the average of the measurements taken in the past seven years was used. (d) Seasonal fluctuations in water levels perturb the consistency of the data. (e) Irregular impermeable layers with poorly defined boundaries commonly retain perched water. (f) Errors may have been made in measuring water table levels in some boreholes. These difficulties were accounted for and corrected to the extent possible, but space does not allow enumeration here of these corrections.

With respect to depth to ground water, the following criteria were applied to liquefaction susceptibility: For ground water depths less than 10 ft (3.0 m), maximum possible susceptibility is very high. For water depths between 10 ft (3.0 m) and 30 ft (9.1 m), maximum possible susceptibility is high. For depths between 30 ft (9.1 m) and 50 ft (15.2 m) maximum susceptibility is low. For water depths greater than 50 ft (15.2 m) maximum possible susceptibility is very low. These criteria are based in part on criteria suggested by Youd and Perkins (9).

Map Compilation

The criteria developed in the preceding section and summarized in Table 2 were used to compile a liquefaction susceptibility map for the San Fernando Valley. These criteria were applied to the data compiled on Figs. 1 and 2 to derive the susceptibility map in Fig. 3. In order to show better the detail with which this type of map can be constructed for areas where sufficient data are available, a segment of the susceptibility map is shown at larger scale in Fig. 4. Note that the susceptibility maps presented here represent estimated average climatic conditions. Ground water levels and hence susceptibilities are likely to be higher during wet seasons and lower during extremely dry cycles.

Table 2.--Criteria used in compiling liquefaction susceptibility map

Sedimentary unit	Probable susceptibility of clay-free granular layers		
	Ground water depth, ft(m)		
	<30(9.1)	30(9.1)-50(15.2)	>50(15.2)
Most recent Holocene	High	Low	Very Low
Other Holocene	Moderate	Low	Very Low
Late Pleistocene	Low	Low	Very Low
Late Pliocene and early Pleistocene	Very Low	Very Low	Very Low
Tertiary	Very Low	Very Low	Very Low

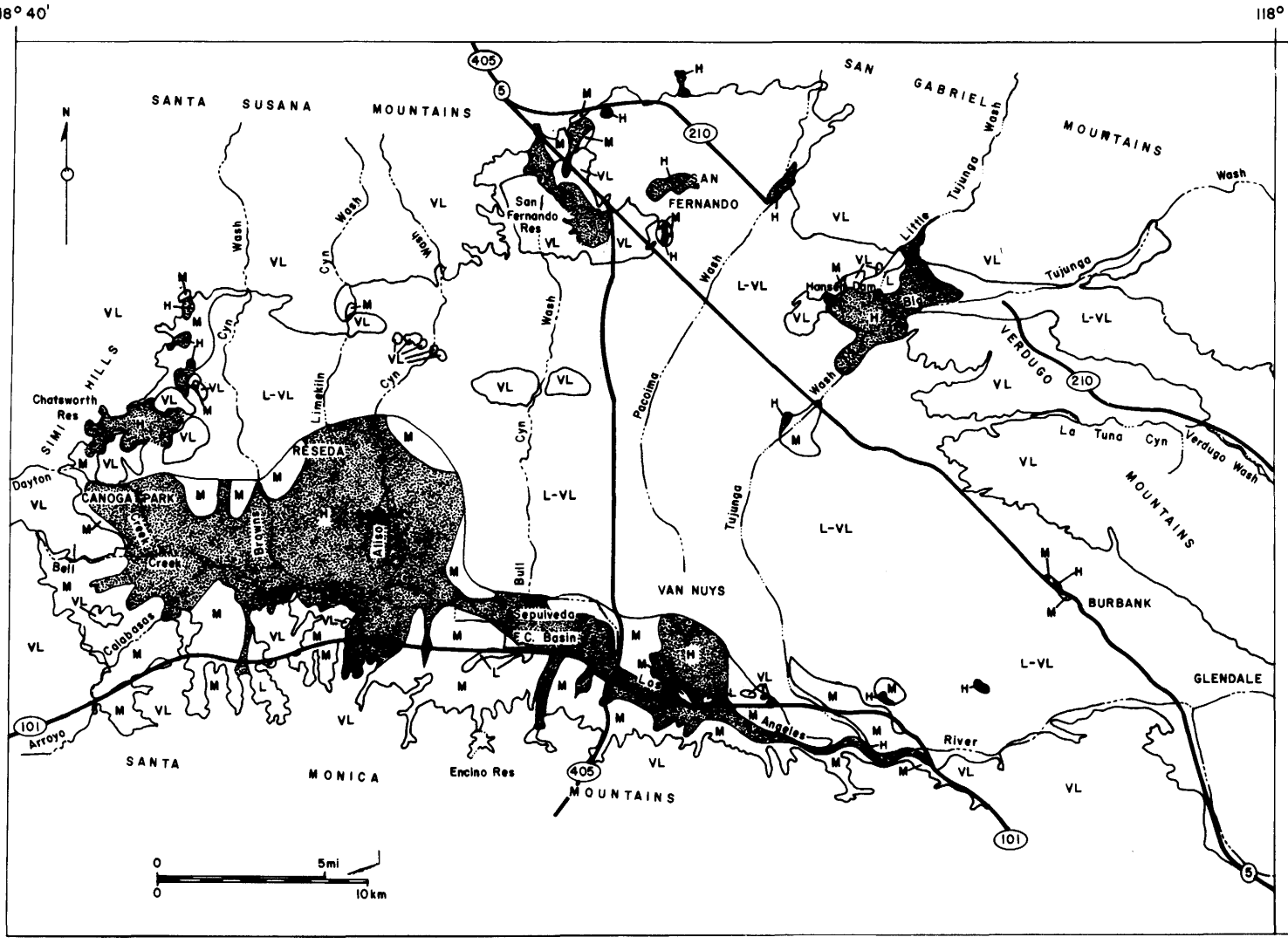

Fig. 3. Zonation map for the San Fernando Valley showing probable susceptibility to liquefaction. Site-specific geotechnical investigations are required to determine susceptibility at a given locality. This map is also a liquefaction potential map with a return period of 46 years for shaking strong enough to cause liquefaction

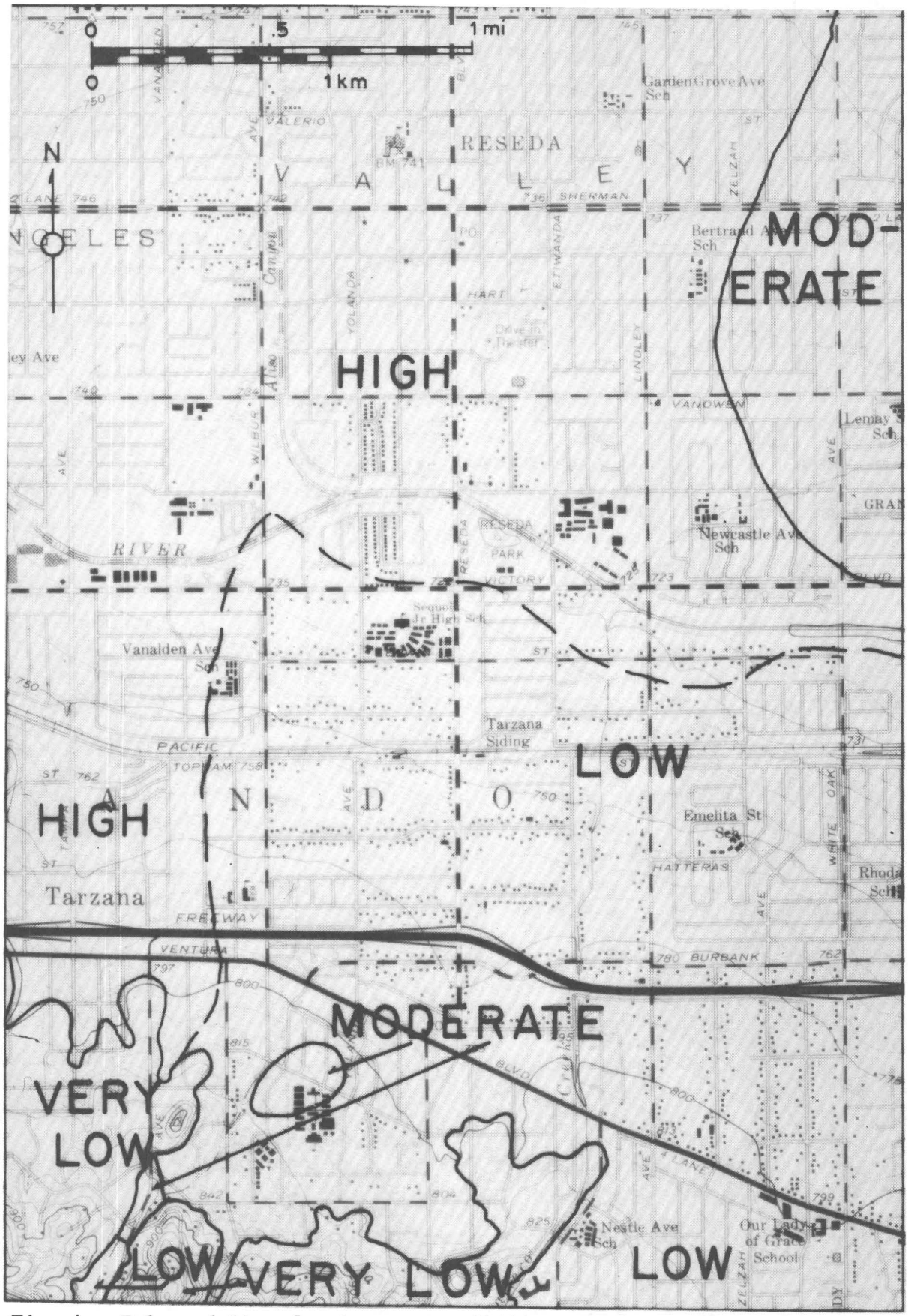

Fig. 4. Enlarged liquefaction susceptibility map for Tarzana area of the San Fernando Valley, California. Susceptibility categories same as Fig. 3.

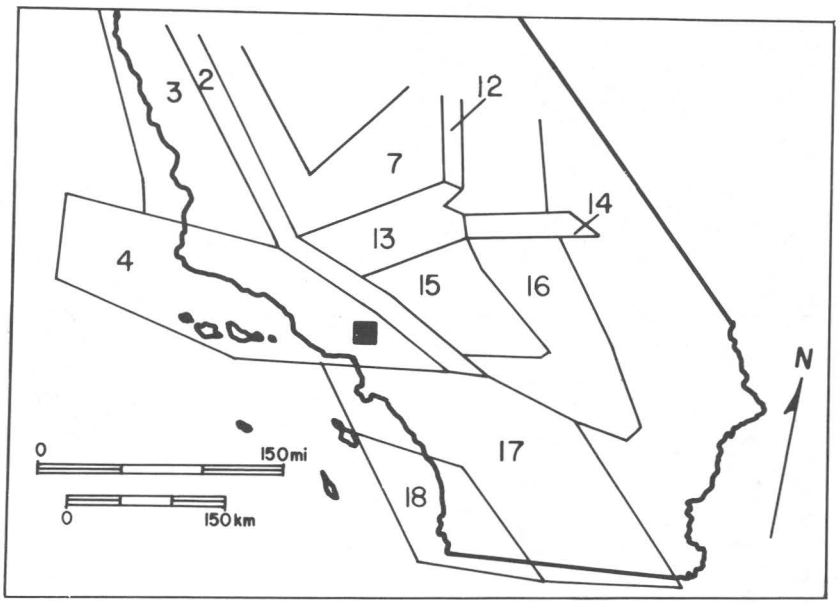

Fig. 5. Seismic source zones in the vicinity of the San Fernando Valley. Only zones 2,4,13, and 17 are significant to liquefaction opportunity in the San Fernando Valley. San Fernando Valley (hachured area) lies in the eastern corner of zone 4. San Andreas fault province corresponds to zone 4.

Table 3.--Normalized seismic parameters for source zones

Zone No.	Number of intensity V's/100 yrs/10^4 km^2 N	b-value for epi-central intensity[2] b_I	Maximum intensity[1] I_o	Maximum magnitude[1] M_c
2	60.6	-.40 up to XI then flat	XII	8.5
3	12.5	-.45	XI	7.9
4	24.2	-.45	XI	7.9
13	129.65	-.45	XI	7.9
14	136.56	-.45	XI	7.9
15	----	-.53	VIII	6.1
16	20.8	-.50	X	7.3
17	70.4	-.45	XI	7.9
18	2.5	-.50	X	7.3

[1]Modified Mercalli Intensity

[2]b-value for magnitude (b_M) = 0.6 b_I

Liquefaction Opportunity Map

A liquefaction opportunity map delineates recurrence intervals for earthquake shaking strong enough to produce liquefaccion in susceptible materials. Information needed to compile an opportunity map includes an estimate of frequencies, magnitudes, and location of expectable future earthquakes and a relation between earthquake source characteristics and the distance from the source to the bound of a zone encompassing sites where liquefaction could be generated. The estimated earthquake sources and frequencies of occurrence in the San Fernando Valley region used in this study (Fig. 5, Table 3) are those previously defined by Algermissen and Perkins (1). The distance relation used is that given by Youd and

Perkins (9). The liquefaction opportunity map plotted on Fig. 6 was derived from these two sets of information. The map shows the return period (inverse annual probability) for liquefaction opportunity from the San Fernando Valley north to the San Andreas fault. The liquefaction opportunity varies only about 20 percent over this area and is effectively constant across the San Fernando Valley; the return period is about 46 years. Figure 7 shows the contribution of the various sources to the annual probability along a meridian section of the map in Figure 6. In general, earthquakes of magnitude less than 6 contribute an insignificant amount to the overall probability of liquefaction. Roughly half of the contribution comes from large-magnitude events occurring locally in the Transverse Ranges province (zone 17, fig. 5) and along the San Andreas fault (zone 2, fig. 5). This contribution is roughly constant across the San Fernando Valley. Large-magnitude events occurring near the Garlock fault to the north are balanced by large-magnitude events occurring south of the Transverse Ranges. As the effect of one region decreases across the San Fernando Valley, the effect of the other region increases.

Liquefaction Potential Map

Superposition of the maps in Figs. 3 and 4 with the map in Fig. 6 yields a liquefaction potential map. In this instance, the return period is constant at 46 years across the area in question, and hence no return period contours appear on the San Fernando Valley area. Thus, for a 46-year return period, the maps in Figs. 3 and 4 show the areas where strong ground shaking is likely to produce liquefaction in sediments with high susceptibility.

SUMMARY AND CONCLUSIONS

A liquefaction potential map has been compiled for the San Fernando Valley, California. The map incorporates assessments of age and type of sedimentary deposits, ground water depth, and expected seismicity into the delineated zones. This map is useful to planners, building officials, engineers, and others responsible for minimizing seismic risk by pointing out areas where potential hazards exist and where further investigation, regulation, zoning, or other measures might be required. The map is not sufficient for evaluation of the actual liquefaction potential at an individual site. Site specific geotechnical investigations are required to make such an assessment.

ACKNOWLEDGMENTS

Appreciation and acknowledgement are given to the following governmental agencies and private firms, who freely provided information for use in this study: U.S. Army Corps of Engineers, California Department of Transportation, California Department of Water Resources, Los Angeles County Flood Control District, Los Angeles County Engineer.

References Cited

(1) Algermissen, S.T., and Perkins, D.M., 1976, A Probabilistic Estimate of Maximum Ground Acceleration in the Contiguous United States; U.S. Geological Survey Open-File Report 76-416.

(2) Holmes, L.C., 1919, Soil Survey of the San Fernando Valley area, Calif., *in* Field Operations of the Bureau of Soils 1915; U.S. Department of Agriculture, Bur. Soils, 17th rept., pl. 63, scale 1:62,500.

(3) Jennings, C.W. and Strand, R.G., 1969, Geologic Map of California, Los Angeles sheet (scale 1:250,000): Calif. Division of Mines and Geology.
(4) Oakeshott, G.B., 1958, Geology and Mineral Deposits of San Fernando Quadrangle, Los Angeles County, Calif: Calif. Division of Mines Bulletin 172, 147 p., 3 pls.
(5) Seed, H.B., and Idriss, I.M., 1971, Simplified Procedure for Evaluating Soil Liquefaction Potential: Journal of the Soil Mechanics and Foundations Division, Amer. Soc. of Civil Engineers, v. 97, no. SM9, p. 1249-1273.
(6) U.S. Department of Agriculture, 1977, Soil Survey of Los Angeles County, Calif. west San Fernando Valley area: an interim, unedited report. 186 p. 5 pl.
(7) Wentworth, C.M. and Yerkes, R.F., Geologic Setting and Activity of Faults in the San Fernando Area, Calif; *in* The San Fernando, Calif. Earthquake of February 9, 1971: U.S. Geological Survey Professional Paper 733, p. 6-16.
(8) Youd, T.L., Nichols, D.R., Helley, E.J., and Lajoie, K.R., 1975, Liquefaction Potential, *in* Studies for Seismic Zonation of the San Francisco Bay Region: U.S. Geological Survey Professional Paper 941-A, p. A68-A74.
(9) Youd, T.L., and Perkins, D.M., 1978, Mapping Liquefaction-Induced Ground Failure Potential: Journal of the Geotechnical Engineering Division, Amer. Soc. of Civil Engineers, v. 104, No. GT4, p. 433-446.

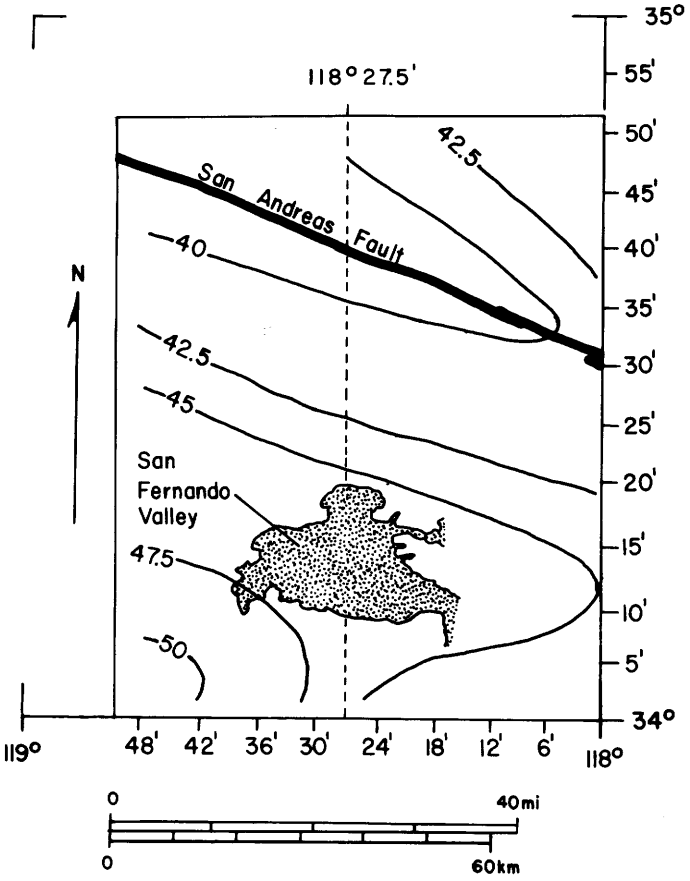

Fig. 6. Return period for liquefaction opportunity in the vicinity of the San Fernando Valley

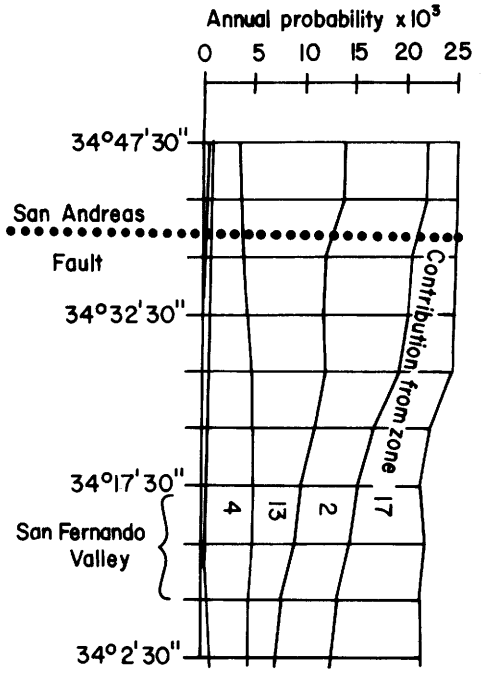

Fig. 7. Contributions to annual probability of liquefaction opportunity for sites along 188° 27.5' meridian. Major contributions to annual probability are due to large magnitude (M>6.4) earthquakes located south of the Transverse Ranges (zone 17), along the San Andreas fault (zone 2), in the vicinity of the Garlock fault (zone 13), and in the vicinity of the Transverse Ranges

PRELIMINARY ASSESSMENT OF SEISMICALLY INDUCED LANDSLIDE SUSCEPTIBILITY

by

D. K. Keefer , G. F. Wieczorek , E. L. Harp and D. H. Tuel

ABSTRACT

Earthquake-induced landslides have taken a large toll in loss of life and property. We are currently engaged in studies aimed at determining which types of landslides are most common during earthquakes and at establishing criteria for mapping susceptibility of slopes to earthquake-induced landsliding. This preliminary summary of our findings deals primarily with the types and abundance of landslides that occurred during 15 historic earthquakes. Preliminary criteria have also been developed for mapping susceptibility to some kinds of landsliding, and these criteria are used herein to prepare an experimental susceptibility map of an area near San Francisco, Calif.

INTRODUCTION

On Sunday afternoon, May 31, 1970, an earthquake of magnitude 7.7 struck Peru. The shock caused a large mass of ice and rock to break away from Mount Huascaran, the highest mountain in the Peruvian Andes. The debris cascaded 600 m down the steep upper slopes of the mountain and landed on the surface of a glacier. It accelerated as it slid across the glacier and poured into the Llanganuco Valley. Below it lay the towns of Yungay and Ranrahirca. Mixed with glacial ice, surface water, and saturated soil, the mass became a huge debris flow and swept down the valley at velocities of 280 to 400 km per hour (28). Eleven kilometers from its source, a relatively small lobe of debris splashed over a ridge 200 to 250 m high and buried the town of Yungay. Almost simultaneously, the main debris lobe crashed into Ranrahirca, devastating it and the small villages around it. Within four minutes the landslide had killed more than 18,000 people (28).

Past Ranrahirca, the debris followed the Llanganuco Valley to its confluence with the Rio Santa. It then turned and flowed down the Santa Valley for more than 50 km, inundating many agricultural fields and causing extensive damage to dwellings, highways, communication networks, and a hydroelectric facility. The Peruvian earthquake was one of the most destructive shocks in recent history, and this single landslide caused approximately 40% of the deaths and a large but undetermined portion of the property damage attributed to that shock (28).

Geologic and historic evidence indicated that Yungay and Ranrahirca were in areas of severe landslide hazard. Eight years earlier, a debris flow not triggered by an earthquake had buried Ranrahirca, killing approximately 4,000 people. In fact, during the 30 years before the earthquake, eight destructive rock fall-avalanches and debris flows had occurred in the Santa Valley (28). None of these landslides were triggered by earthquakes indicating that the landslide hazard is acute there even under non-seismic conditions. According to geologic evidence, many large prehistoric

avalanches and flows also occurred in this area, and Yungay itself was probably built on a flow or avalanche deposit (28). If this evidence had been properly evaluated and acted on before the earthquake, the catastrophes at Yungay and Ranrahirca might have been averted by moving the communities to safer areas.

Many hundreds of thousands of landslides have been triggered by earthquakes, and they have caused enormous losses of life and property. Many landslides occurred in areas where the historic evidence of landslide hazard was not as clear as in the Mount Huascaran area. In fact, many occurred in areas with little or no record of slope instability under nonseismic conditions. We are, therefore, presently studying data from historic earthquakes to determine which types of landslides are most commonly triggered by earthquakes and which geologic environments are most susceptible to seismically triggered slope failure. Our goal is to apply this kind of information to the development of criteria for mapping earthquake-induced landslide susceptibility. Our results are preliminary. This paper presents data on landslides in 15 historic earthquakes and an experimental susceptibility map prepared as a demonstration of how criteria developed in this study can be used.

LANDSLIDE OCCURRENCE DURING HISTORIC EARTHQUAKES

Landslide data have been compiled (Table 1) from 15 historic earthquakes which range in size from the great M 8.6 Kansu, China event of 1920 to the moderate-size M 5.7 Fortuna-Rio Dell, Calif. shock of 1975. We have participated in field investigations following the 1977 San Juan, Argentina, the 1976 Guatemala (11) and the 1975 Fortuna-Rio Dell (18) earthquakes. For the other earthquakes, we have relied almost exclusively on published reports.

Landslide names used in Table 1 conform to those of Varnes (33), which is a revision of Varnes' earlier landslide classification system (32). One major difference in terminology between this report and that of Varnes (33) is in the use of the term "landslide." In this report, all types of slope failures, including falls, avalanches, and flows as well as true slides are considered types of landslides. In Varnes (33), "slope movement" is the general term used to denote all types of movement. In some of the categories in Table 1, two or more types of landslides are lumped together because the published data did not permit more subdivision.

Only landslides that were clearly outlined and that moved far enough to form clearly identifiable deposits were included in Table 1. Thus, sets of cracks or fissures that may have been incipient landslides were not considered. Where more than one type of material or more than one mode of movement were involved in the landslide, it was classified by the predominant material and mode of movement.

Abundances of landslides are grouped into three classes in Table 1. Data on landslide abundances were not always expressed quantitatively in published reports, so in many cases judgments were based on brief accounts of the geographic limits of the regions within which landsliding occurred and our estimates of the number of landslides per unit area in these regions. Geographic coverage of post-earthquake investigations was probably not complete for the 1920 Kansu, 1960 Chile, 1931 Hawke's Bay, or 1968 Inangahua earthquakes, so the information in Table 1 may underestimate the true extent of landsliding for those events. Relative abundance

TABLE 1: LANDSLIDES TRIGGERED BY EARTHQUAKES

LANDSLIDE TYPE[I]	EARTHQUAKE NAME, DATE, AND MAGNITUDE														
	Kansu, China 1920 M 8.6	Alaska 1964 M 8.4	Chile 1960 M 8.4	San Francisco, Calif. 1906 M 8.3	Hawke's Bay, New Zealand 1931 M 7.9	Peru 1970 M 7.7	New Madrid, Mo. 1811 MMI XII	Guatemala 1976 M 7.5	San Juan, Argentina 1977 M 7.4	Hebgen Lake, Mont. 1959 M 7.1	Inangahua, New Zealand 1968 M 7.0	San Fernando, Calif. 1971 M 6.4	Borrego Mountain, Calif. 1968 M 6.4	Managua, Nicaragua 1972 M 6.2	Fortuna-Rio Dell, Calif. 1975 M 5.7
A. LANDSLIDES IN ROCK															
ROCK FALL - AVALANCHES		E	S	M		S				S	S				
SLUMPS AND BLOCK SLIDES			M	E	M	S		S			S	M	S		
FALLS AND SHALLOW, DISINTEGRATING SLIDES		E	M	E	M	E		E	M	E	M	M	S	S	S
B. LANDSLIDES IN UNCONSOLIDATED OR POORLY CONSOLIDATED DEPOSITS (ENGINEERING SOILS)															
FALLS, AVALANCHES, AND SHALLOW, DISINTEGRATING SLIDES	E	M	M	E		E	E	E			S	M	S	S	S
SLUMPS AND BLOCK SLIDES		E	M	E	S	M				S	S	S	S	S	
RE-ACTIVATION OF DORMANT LANDSLIDES		S	S	M		S				S	S	S			
LATERAL SPREADS[II]		E	M	E	M	S	E	S	E			S			
WET FLOWS[II]		E	M	M		S				S	S				
SUB-AQUEOUS LANDSLIDES[II]		E	S					S		S					
C. LANDSLIDES INVOLVING ARTIFICIAL CUTS OR FILLS															
CUT-SLOPE FAILURES		M	M	M	M	M		M	S	S		S	S	S	
LIQUEFACTION-INDUCED LANDSLIDES IN ARTIFICIAL FILLS		S	S	M	S	S					S	S			
LANDSLIDES IN ARTIFICIAL FILLS NOT CAUSED BY LIQUEFACTION			S	S	S	S						S	S	S	

[I] Classifications after Varnes (33).

[II] Liquefaction may be primary or contributing cause of failure.

[III] Small landslides are those judged to contain less than 10,000 m^3 of material.

[IV] Large landslides are those judged to contain more than 10,000 m^3 of material.

Explanation

E - Large number of landslides
> 5,000 small[III] landslides, or
> 100 large[IV] landslides, or
Landslides common over >1000 km^2 area

M - Moderate number of landslides
500 to 5000 small[III] landslides, or
10 to 100 large[IV] landslides, or
Landslides common over 100 to 1000 km^2 area

S - Small number of landslides
< 500 small[III] landslides, or
< 10 large[IV] landslides, or
Landslides common over <100 km^2 area

No symbol - No landslides of this type reported

References:

Kansu, China: 5, 15
Alaska: 19, 31
Chile: 6, 26
San Francisco: 36
Hawke's Bay: 20
Peru: 2, 8, 28
New Madrid: 10
Guatemala: 11, 12
San Juan, Argentina: T. L. Youd, D. K. Keefer, and others, unpub. data
Hebgen Lake: 1, 4, 9, 25, 29, 30
Inangahua: 21, 22, 23, 27
San Fernando: 14, 16, 17, 35
Borrego Mountain: 3
Managua: 7
Fortuna-Rio Dell: 18

categories are defined in Table 1. Because of limitations in the data, numbers used to divide the categories should be regarded as first-order approximations. Classifications based on numbers of landslides rather than on area were applied wherever possible.

The number of landslides triggered by an earthquake correlates strongly with earthquake magnitude. The M 8.4 Alaska earthquake of 1964 probably triggered more landslides than any other seismic event in recent history. In Alaska, landslides were reported from an area of more than 210,000 km^2, which is equivalent in size to half the state of California (19, 31). At the other end of the scale in Table 1, the M 5.7 Fortuna-Rio Dell event of 1975 caused only one large rock fall and a few small debris slides. The Fortuna-Rio Dell earthquake should not be regarded as the lowest magnitude event to cause landsliding. Smaller shocks have triggered landslides, but we have not yet evaluated data from smaller earthquakes.

In Table 2, landslides in the various categories are ranked on the basis of their total abundance in the earthquakes listed in Table 1. The ranking was developed by assigning a numerical value to the abundance classification of each landslide category in each earthquake: E=3, M=2, S=1, No symbol=0. For each category, these numbers were totaled for all 15 earthquakes. The landslide categories were then ranked in order from highest total value through lowest.

TABLE 2: RELATIVE ABUNDANCE OF DIFFERENT TYPES OF LANDSLIDES.

Most Abundant	Falls and shallow, disintegrating slides in rock
	Avalanches, falls, and shallow disintegrating slides in soil
	Lateral spreads
	Cut-slope failures
	Slumps and block slides in soil
	Slumps and block slides in rock
	Wet flows
	Rock fall-avalanches
	Liquefaction-induced landslides in artificial fills[I]
	Re-activation of dormant landslides[I]
	Landslides in artificial fills not due to liquefaction
Least Abundant	Sub-aqueous landslides

The most abundant types of landslides were not necessarily the most damaging. The distribution of landslide damage in past earthquakes is partly due to the location of dwellings or other constructed works in certain landslide source areas or in the paths of certain landslides. However, landslides of several types do appear to have an inherently high potential for causing damage either because they tend to be large, because they tend to move long distances at high velocities, or both. On the basis of data from the 15 earthquakes listed in Table 1, the most hazardous landslides in natural materials are rock fall-avalanches, debris avalanches, wet flows, sub-aqueous landslides, and lateral spreads. Fortunately, some of these types of failures occur in relatively small numbers.

I Identical total numerical value

LANDSLIDE DESCRIPTIONS

Rock fall-avalanches: Rock fall-avalanches are large landslides that travel long distances at high velocities. The Mount Huascaran rock fall-avalanche contained 90 million m^3 of material and flowed more than 60 km at velocities up to 400 km per hour. Nearly all of the rock fall-avalanches listed in Table 1 originated on steep mountain slopes that were hundreds of meters high. Most of these slopes were oversteepened by active fluvial or glacial erosion. The failures occurred in a wide variety of rock types. They were particularly common in closely jointed or deeply weathered rock, many broke loose where planes of weakness dipped out of slopes, and many occurred in unsaturated materials.

Slumps and block slides in rock: Deep-seated slumps and block slides are less common during earthquakes than rock falls and shallow, disintegrating rock slides. They commonly originate on steep slopes, but some continue to move on surprisingly gentle slopes. For example, two block slides triggered by the 1968 Inangahua earthquake moved on shear planes that dipped about 4° (21,22,23). Many slumps and block slides disintegrate into avalanches, but because of their relatively small size and short distance of travel, they generally are not as hazardous as rock fall-avalanches.

Rock falls and shallow, disintegrating rock slides: Landslides of these types are the most abundant slope failures listed in Table 1. It also appears that most shallow rock slides and falls originate on slopes of 35° or steeper (11,30). These landslides are particularly common in rocks that are poorly cemented, closely jointed, or highly weathered. Many slopes where these landslides occur have talus accumulations at their bases below where the earthquake-induced landslides originate (19,30,31).

Falls, avalanches, and shallow, disintegrating slides in soil: On December 16, 1920, a large earthquake shook Kansu Province in China, parts of which were underlain by thick deposits of loess. Loess is a windblown silt held together by a clayey or calcareous binder. Under nonseismic conditions, it is capable of standing in high, nearly vertical slopes. The earthquake apparently disrupted the binder holding the loess particles together. The result was probably the most spectacular and destructive series of earthquake-induced landslides in recent history. Whole villages and towns were buried by huge loess avalanches, and many valleys were filled with debris. These landslides were responsible for a large portion of the 200,000 deaths attributed to the shock (5).

The 1976 Guatemala earthquake also triggered thousands of soil avalanches and slides in a weakly cemented material that forms steep, high slopes under nonseismic conditions (11). There, the susceptible material is a soil derived from volcanic pumice (11). In many other earthquakes, soil avalanches, falls, and shallow, disintegrating slides have occurred in unsaturated, sandy or silty soils with little or no cohesion. The landslides take place most commonly on steep stream banks, ridge flanks, and artificial cuts (3,7,8,10,16,17,19,26,28,31,36).

Slumps and block slides in soil: Deep-seated soil slumps and block slides have also been triggered by many earthquakes listed in Table 1 (3, 16,17,19,20,21,26,28,31,36). They take place in soils derived from many different types of rocks, and they originate on moderate to steep slopes.

Many earthquake-induced slumps and block slides occur in regions where landslide deposits are already abundant (3,16,17,36).

Re-activation of dormant landslides in soil: A surprisingly low number of dormant landslides in soil were re-activated by the earthquakes listed in Table 1. In part, this low number reflects the lack of data on pre-earthquake landslides in many areas. However, the data are remarkably consistent and hold true even for areas such as Guatemala (11), San Fernando (16,17), and Fortuna-Rio Dell (18) where the pre-earthquake landslide distribution was known and where the landslide distribution was re-examined after the shock. It appears that earthquakes do not reactivate large numbers of dormant landslides in soil.

Lateral spreads: Lateral spreads are characterized by coherent blocks of material that move laterally on layers of liquefied sand or silt or of weakened, sensitive clay. The blocks commonly break up along internal fissures, and they may also rotate or subside. The large lateral spread at Turnagain Heights in Anchorage, Alaska was one of the more destructive landslides triggered by the 1964 earthquake (19,24,31). It started at the edge of a steep, flat-topped, coastal bluff, 20 m high, and progressively retrograded back from the face. It caused irreparable damage to 72 houses. The lateral movement took place primarily on a layer of sensitive clay, but liquefaction in sand and silt lenses almost certainly contributed to the failure (19,24,31). Similar, large lateral spreads from steep, high bluffs also took place during the 1811 New Madrid (10) and 1960 Chile earthquakes (26). Lateral spreads also occurred in areas of generally low relief such as river flood plains and deltas during several earthquakes (10,19,20,26,31,35,36).

Many seismically triggered lateral spreads, wet flows, and sub-aqueous landslides (see below) are caused by liquefaction. Techniques of assessing liquefaction susceptibility on a regional basis have been developed by others (37) and are briefly summarized here. Liquefaction commonly develops in saturated, cohesionless sediments such as sands and silts. The liquefaction susceptibility of a deposit is related to its age and depositional environment. River channel deposits, deltaic deposits, and uncompacted fills less than 500 years old have the highest liquefaction susceptibility. Other materials with a significant susceptibility to liquefaction include Holocene flood plain, fan delta, lacustrine, colluvial, dune, loess, and tephra deposits, and several materials deposited in coastal environments (37).

Wet flows: Wet flows are composed chiefly of saturated soils that lose much of their internal cohesion during earthquakes. Flows have been triggered by several earthquakes. Most originated in sandy or silty soils, and many formed where the slope was only a few degrees. Because they can travel long distances at high velocities, they are significant hazards in many areas. Methods of assessing the susceptibility of a soil to liquefaction-induced flow failure are discussed by Youd and Perkins (37).

Sub-aqueous landslides: Sub-aqueous landslides triggered by the 1959 Hebgen Lake (30), 1960 Chile (26), 1964 Alaska (19,31), and 1976 Guatemala (12) earthquakes were complex features involving a combination of slumping, lateral spreading and flow. The most common failure environments were the fronts of deltas or fan deltas, and most sub-aqueous slides were caused, at least partially, by liquefaction. In the Alaska earthquake, massive sub-aqueous slides severely damaged the towns of Valdez,

Whittier, Seward, and Homer (19,31). At least five sub-aqueous landslides in the Valdez area, but not in Valdez proper, had occurred during earthquakes in the preceding 70 years. Largely as a result of the 1964 slide the town was relocated on a non-liquefiable site (19,31). The relatively small number of reported sub-aqueous landslides during earthquakes (Table 2) probably reflects, in part, the difficulty of observing landslides of this type.

Cut-slope failures: Cuts increase landslide susceptibility by locally increasing slope steepness and by disturbing material adjacent to the cuts. Cut-slope failures are widespread during earthquakes (3,7,11, 16,17,19,20,26,28,30,31,36).

Landslides in artificial fills: The most damaging failures in artificial fills have been caused by liquefaction (26,36,37), and these have occurred most frequently in uncompacted saturated sandy fills (37). In addition, much damage to artificial fills has been caused by liquefaction in subjacent materials (19,31). Other landslides not induced by liquefaction have occurred in artificial fills during earthquakes (3,7,16,17,20, 26,28,36). Most failures of this type were small slumps or debris slides. The relatively small number of reported landslides in artificial fills is due, in part, to the fact that artificial fills are much less abundant than natural slopes.

SUMMARY OF LANDSLIDE TYPES AND FAILURE ENVIRONMENTS

Our study has identified several types of landslides that are triggered by earthquakes and some environments in which failures occur. Our preliminary findings are summarized in Table 3. As our study progresses, we anticipate that other environments with high susceptibilities to seismically induced landsliding will be identified and that categories listed in Table 3 will be refined and subdivided for better assessments.

PRELIMINARY MAP OF SEISMICALLY INDUCED LANDSLIDE SUSCEPTIBILITY OF THE LA HONDA AREA

Figure 1 is an experimental susceptibility map of an area near the town of La Honda, in the Santa Cruz Mountains, 40 km south of San Francisco, Calif. The map was prepared to demonstrate how the preliminary criteria summarized in Table 3 can be used to evaluate susceptibility to earthquake-induced landsliding. The preliminary La Honda map (Fig. 1) is subject to revision as our study of landsliding during historic earthquakes progresses. Furthermore, it is a regional map which shows only zones where unfavorable site conditions may exist. Local site conditions, not determined in this study, govern whether specific sites within these zones are actually susceptible to failure. Therefore, it is not intended for use in determining the susceptibility to failure of any given site. Any such site-specific assessment should be carried out by a professional engineering geologist.

Data on the La Honda area came from a detailed engineering geologic field investigation (34), a published map of unconsolidated Quaternary materials (13), and a computer-generated slope map. On the basis of this information and our review of landsliding during historic earthquakes, three types of zones with high susceptibilities to earthquake-induced landslides were identified (Fig. 1). These are areas with slopes greater than 35°, areas underlain by saturated sandy and silty Holocene alluvium,

FIGURE 1: PRELIMINARY SEISMICALLY INDUCED LANDSLIDE SUSCEPTIBILITY MAP OF THE LA HONDA AREA

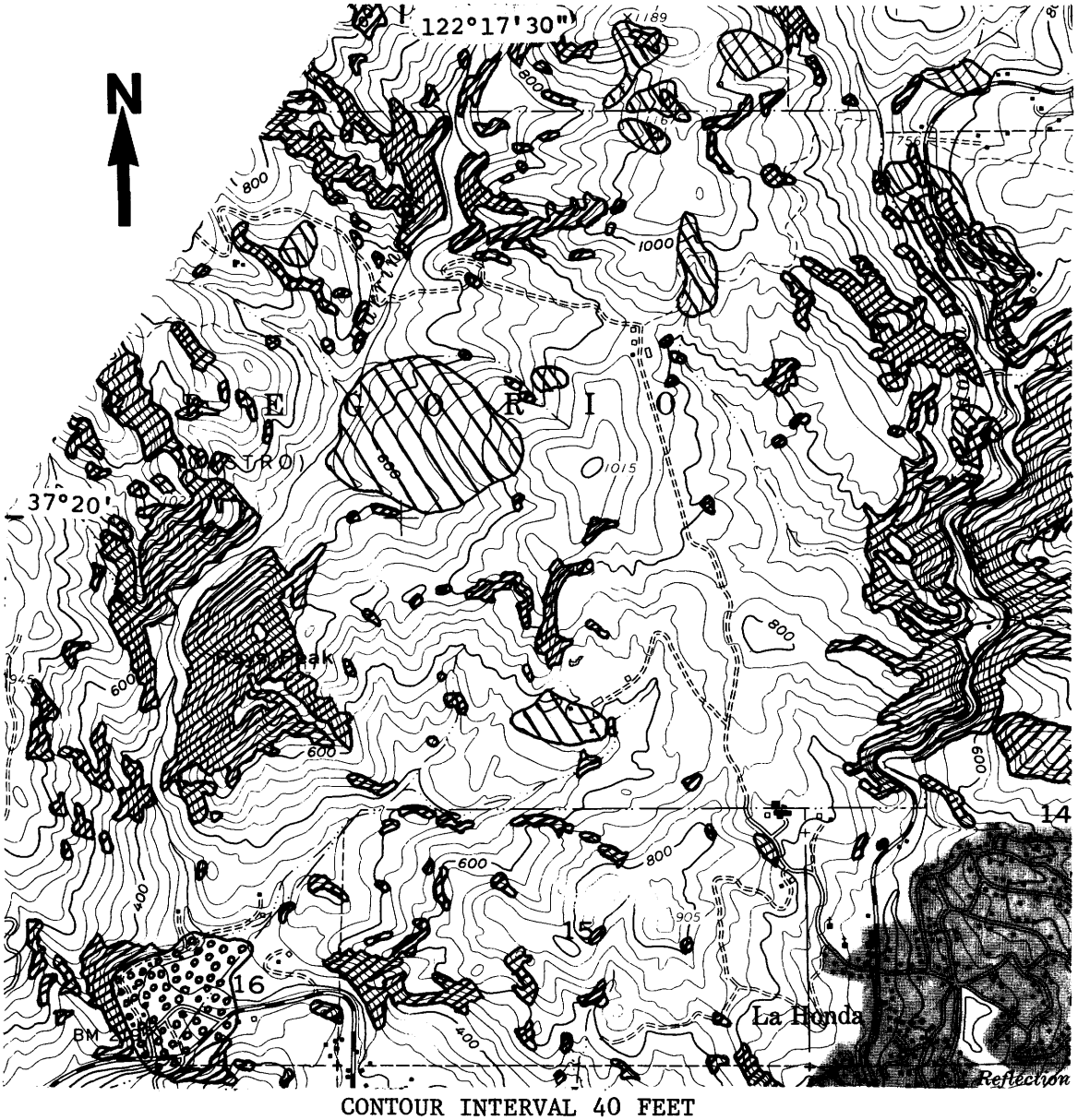

CONTOUR INTERVAL 40 FEET

0 1 KILOMETER

0 1 MILE

ZONES OF HIGH SUSCEPTIBILITY TO SEISMICALLY INDUCED LANDSLIDES

SYMBOL	POSSIBLE LANDSLIDE TYPES	MAPPING CRITERIA
	SOIL AVALANCHES; FALLS, SLUMPS, BLOCK SLIDES AND SHALLOW DISINTEGRATING SLIDES IN SOIL AND/OR ROCK	SLOPES STEEPER THAN 35°
	LATERAL SPREADS AND WET FLOWS	UNDERLAIN BY SATURATED SANDY AND SILTY HOLOCENE ALLUVIUM
	SLUMPS AND BLOCK SLIDES IN SOIL AND/OR ROCK	ACTIVE AND RECENTLY ACTIVE LANDSLIDES

and areas underlain by active and recently active landslides (34). Landslides judged to be dormant (34) are not included in the zones of high susceptibility.

TABLE 3: PRELIMINARY ASSESSMENT OF SEISMICALLY INDUCED LANDSLIDE SUSCEPTIBILITY

LANDSLIDE TYPES	SOME ENVIRONMENTS IN WHICH LANDSLIDES ARE LIKELY TO OCCUR
Rock fall-avalanches	Very steep, very high slopes that are composed chiefly of deeply weathered, closely jointed, or highly sheared rock and that are being oversteepened by active erosion
Slumps and block slides in rock	Moderate to steep slopes in many different types of rock
Rock falls and shallow, disintegrating rock slides	1. Rock slopes steeper than 35° 2. Rock slopes with talus accumulations at their bases 3. Slopes containing weathered, sheared, or closely jointed rock
Falls, avalanches, and shallow, disintegrating slides in soil	1. Steep, high slopes containing certain kinds of weakly cemented materials such as some kinds of loess and some volcanic pumice soils 2. Steep ridge flanks and stream banks containing unsaturated sandy or silty soils with little or no cohesion
Slumps and block slides in soil	Moderate to steep slopes in soils derived from many different types of rocks, particularly in areas with abundant, preexisting landslide deposits
Re-activation of dormant landslides in soil	Only relatively small numbers of dormant landslides are re-activated by earthquakes
Lateral spreads	1. Areas of generally low relief underlain by many different kinds of unconsolidated saturated Holocene sandy or silty materials 2. Steep, high bluffs containing layers of sensitive clay or liquefiable sand or silt as defined in 1. above 3. Uncompacted saturated sandy artificial fills
Wet flows	Steep to very gentle slopes underlain by some kinds of saturated sandy or silty soils

TABLE 3: (con't.)

TYPES (con't.)	ENVIRONMENT (con't.)
Sub-aqueous landslides	Fronts of deltas or fan deltas, particularly in areas underlain by saturated, liquefiable sand or silt
Cut-slope failures	Artificial cuts
Liquefaction-induced landslides in artificial fills	Uncompacted, saturated, sandy fills
Landslides in artificial fills not caused by liquefaction	Many different types of fills

CONCLUSIONS

Predominant types of earthquake-induced landslides and some environments with high susceptibilities to failure have been identified from data about 15 historic earthquakes. Landslides that occurred in greatest numbers in the 15 earthquakes were: falls and shallow, disintegrating slides in rock; falls, avalanches, and shallow, disintegrating slides in soil; lateral spreads; cut-slope failures; slumps and block slides in soil; and slumps and block slides in rock. Many other kinds of earthquake-induced landslides occur relatively infrequently but have high inherent potentials for causing loss of life and property. Landslides that have caused extensive loss of life or property during historic earthquakes include rock fall-avalanches, soil avalanches, lateral spreads, wet flows, sub-aqueous landslides, and liquefaction-induced landslides in artificial fills. Some environments with high susceptibilities to seismically induced landsliding have been identified on a preliminary basis. As our studies progress, it is anticipated that these categories will be refined and that new environments with high susceptibilities will be identified.

REFERENCES

(1) Billings Geological Society, 1960, Earthquake papers: Billings, Montana, Eleventh Annual Field Conference Guidebook, p. 24-85.

(2) Browning, J.M., 1973, Catastrophic rockslide, Mount Huascaran, North-central Peru, May 31, 1970: American Association of Petroleum Geologists Bulletin, v. 57, no. 7, p. 1335-1341.

(3) Castle, R.O., and Youd, T.L., 1972, Engineering geology, *in* The Borrego Mountain earthquake of April 9, 1968: U.S. Geological Survey Professional Paper 787, p. 158-174.

(4) Christiansen, R.L., and Blank, H.R., 1972, Volcanic stratigraphy of the Quaternary rhyolite plateau in Yellowstone National Park: U.S. Geological Survey Professional Paper 729-B, 18p.

(5) Close, U. and McCormick, E., 1922, Where the mountains walked: National Geographic, v. 41, no. 5, p. 445-472.

(6) Duke, C.M., and Leeds, D.J., 1963, Response of soils, foundations, and earth structures: Seismological Society of America Bulletin, v. 53, no. 2, p. 309-357.
(7) Earthquake Engineering Research Institute Conference Proceedings, 1973, Managua, Nicaragua earthquake of December 23, 1972: v. 1, p. 8-264.
(8) Earthquake Engineering Research Institute Earthquake Report Committee, 1970, Peru earthquake of May 31, 1970, preliminary report: Earthquake Engineering Research Institute, 55 p.
(9) Fischer, W.A., 1960, Highlights of Yellowstone geology with an interpretation of the 1959 earthquakes and their effects in Yellowstone National Park: Yellowstone National Park, 62 p.
(10) Fuller, M., 1912, The New Madrid earthquake; U.S. Geological Survey Bulletin 394, 118 p.
(11) Harp, E.L., Wieczorek, G.F., and Wilson, R.C., 1978, Earthquake-induced landslides from the February 4, 1976, Guatemala earthquake and their implications for landslide hazard reduction: International Symposium on the February 4th, 1976 Guatemalan Earthquake and the Reconstruction Process, v. 1.
(12) Hoose, S.N., Wilson, R.C., and Rosenfeld, J.H., 1978, Liquefaction-caused ground failure during the February 4, 1976, Guatemala earthquake: International Symposium on the February 4th, 1976 Guatemalan Earthquake and the Reconstruction Process, v. 2.
(13) Lajoie, K.R., Helley, E.J., Nichols, D.R., and Burke, D.B., 1974, Geologic map of unconsolidated and moderately consolidated deposits of San Mateo County, California: U.S. Geological Survey Miscellaneous Field Studies Map MF-575, Basic Data Contribution 6.
(14) Marachi, N.D., 1973, Dynamic soil problems at the Joseph Jensen Filtration Plant *in* Murphy, L.M., scientific coordinator, San Fernando, California earthquake of February 9, 1971: National Oceanic and Atmospheric Administration, v. 1, part B, p. 815-820.
(15) Meyers, H., and von Hake, C.A., 1976, Earthquake data summary: Boulder, Colorado, National Oceanic and Atmospheric Administration, Environmental Data Service, Key to Geophysical Records Documentation No. 5, 54 p.
(16) Morton, D.M., 1971, Seismically triggered landslides in the area above the San Fernando Valley, *in* The San Fernando, California earthquake of February 9, 1971: U.S. Geological Survey Professional Paper 733, p. 99-104
(17) Morton, D.M., 1975, Seismically triggered landslides in the area above the San Fernando Valley, *in* The San Fernando, California earthquake of February 9, 1971: California Division of Mines and Geology Bulletin 196, p. 145-154
(18) Nason, R., Harp, E.L., La Gresse, H., and Malley, R.P., 1975, Investigations of the 7 June 1975 earthquake at Humbolt County, California, U.S. Geological Survey Open-File Report 75-404, 37 p.
(19) National Academy of Sciences, 1968-73, The great Alaska earthquake of 1964: Washington, D.C., National Academy of Sciences Printing and Publishing Office, v. 1, Geology, and v. 3, Hydrology.
(20) New Zealand Department of Scientific and Industrial Research, 1933, The Hawke's Bay earthquake of 3rd February, 1931: New Zealand Journal of Science and Technology, v. 15, no. 1, p. 1-116.
(21) New Zealand Department of Scientific and Industrial Research, 1968, Preliminary report on the Inangahua earthquake, New Zealand, May, 1968: Research Bulletin 193, 39 p.

(22) New Zealand Society for Earthquake Engineering Bulletin, 1968, The 1968 Inangahua earthquake (conference seminar papers): v. 2, no. 1, 148 p.
(23) New Zealand Society for Earthquake Engineering Bulletin, 1969, Special Inangahua reports: v. 2 , no. 1, 148 p.
(24) Seed, H.B., 1968, Landslides during earthquakes due to soil liquefaction: Journal Soil Mechanics and Foundations Div., American Society of Civil Engineers, v. 94, no. SM 5, p. 1055-1122.
(25) Seismological Society of America Bulletin, 1962, The earthquake at Hebgen Lake, Montana on August 18, 1959 (GCT): v. 52, no. 2, p. 153-273.
(26) Seismological Society of America Bulletin, 1963, Special issue on Chilean earthquakes of May 1960: v. 53, no. 6, p. 1123-1441.
(27) Seismological Society of America Bulletin, 1970, The 1968 Inangahua earthquake: Report of the University of Canterbury Survey team: v. 60, no. 5, p. 1561-1606.
(28) Seismological Society of America Bulletin, 1971, Special issue on Peru earthquake of May 31, 1970: v. 61, no. 3, p. 511-640.
(29) U.S. Coast and Geodetic Survey, 1961, Abstracts of earthquake reports for the Pacific Coast and Western Mountain region, MSA-103, July, August, September, 1959: p. 51-189.
(30) U.S. Geological Survey, 1963, The Hebgen Lake, Montana earthquake of August 17, 1959: U.S. Geological Survey Professional Paper 435, 242p.
(31) U.S. Geological Survey, 1965-1970, The Alaska earthquake, March 27, 1964: U.S. Geological Survey Professional Papers 542-A, 542-B, 542-C, 542-D, 542-E, 542-G, 543-B, 543-E, 543-F, 544-A, 544-B, 544-D, 545-A, 545-C, 545-D.
(32) Varnes, D.J., 1958, Landslide types and processes, *in* Eckel , E.B., ed., Landslides and engineering practice: Highway Research Board Special Report 29, National Academy of Science - National Research Council Publication 554, p. 20-47.
(33) Varnes, D.J., in press, Slope movement types and processes: Chapter 2 *in* Schuster, R.L., and Krizek, R.S., eds., Landslides--analysis and control: Transportation Research Board Special Report 176, National Academy of Sciences.
(34) Wieczorek, G.F., 1978, Landslide susceptibility evaluation in the Santa Cruz Range, San Mateo County, California, Ph.D. thesis, University of California, Berkeley, 278 p.
(35) Youd, T.L., 1971, Landsliding in the vicinity of the Van Norman Lakes *in* the San Fernando, California earthquake of February 9, 1971: U.S. Geological Survey Professional Paper 733, p. 105-109.
(36) Youd, T.L., and Hoose, S.N., 1978, Historic ground failures in northern California triggered by earthquakes: U.S. Geological Survey Professional Paper 993, 177 p.
(37) Youd, T.L., and Perkins, D.M., 1978, Mapping liquefaction-induced ground failure potential: Journal of the Geotechnical Engineering Div., American Society of Civil Engineers, v. 104, no. GT4, p. 433-446.

EARTHQUAKE LOSSES TO BUILDINGS IN THE SAN FRANCISCO BAY AREA

by

S. T. Algermissen and K. V. Steinbrugge[1]

ABSTRACT

Losses in the San Francisco Bay area are simulated for five broad classes of buildings which include the majority of building types found in the area. Losses are expressed in terms of the average percentage of the total actual cash value required to fully repair, in kind, any building in a particular building class. The inventory of dwellings was obtained from census data, and the inventory for buildings other than dwellings is derived from land-use classification in the San Francisco Bay area supplemented by minimal field work. Long-term annual losses for the various building classes range from 0.1 to 1.6 percent. For a large earthquake on the San Andreas fault, the range in percent loss is about 5.0 to 25 percent, depending on the building class. The 1970 value of dwellings in the nine-county Bay area was $30.289 billion. Annual average losses to dwellings is estimated at $271 per dwelling. The average loss per dwelling as a result of a large earthquake on the San Andreas fault would be about $1,355; the total loss (1970), about $1.5 billion.

INTRODUCTION

The primary economic losses to buildings as a result of earthquakes depend on three principal factors: (1) the spatial distribution of the various kinds of buildings exposed to ground shaking and geological hazards (landslides, liquefaction, surface faulting, etc.); (2) the spatial distribution of earthquake shaking and geological hazards associated with an earthquake; and (3) the susceptibility of each building class to loss. The purpose of this study is to present a methodology for the estimation of losses to buildings other than dwellings to complement earlier studies of single-family dwellings and to provide a general technique for the estimation of (a) total losses from single large earthquakes and (b) average losses resulting from earthquakes over a period of time. The nine-county San Francisco Bay area (fig. 1) is used to test the methodology for the calculation of losses resulting from earthquakes. The losses computed are expressed in terms of percent loss by class of construction. The percent loss is defined here to mean the average percentage of the total actual cash value required to fully repair, in kind, any building of a particular class represented by a particular degree of Modified Mercalli Intensity Scale. Only losses associated with ground shaking are estimated.

---

[1] Manager, Earthquake Department, Insurance Services Office, San Francisco, California.

METHODOLOGY

Losses to buildings other than one- to four-family dwellings have been calculated as follows:

(1) The spatial distribution of buildings throughout the nine-county area is approximated by class of construction for each U.S. Census Tract in the study area.

(2) Relationships are developed between percent loss (as previously defined) and the various degrees of the Modified Mercalli (MM) Intensity Scale--the measure of ground shaking used in this study.

(3) MM intensities for each census tract are determined for (a) individual earthquakes of interest and (b) ensembles of earthquakes.

(4) The results from (1), (2), and (3) are used to calculate the loss to each class of construction that can be attributed to the occurrence of a particular earthquake or series of earthquakes.

For example, the percent loss to buildings in, say, class C, due to a particular earthquake, is

$$\sum_i [P(C)_i][L_C(I)_i] \qquad (1)$$

where:

$P(C)_i$ = percent of the buildings of class C in the nine-county area that are located in census tract (i)

$L_C(I)_i$ = percent loss to buildings of class C when shaken at MM intensity I in census tract (i).

The summation is made over the census tracts of interest.

Methods for the estimation of earthquake losses to dwellings in California were developed in earlier studies (references 1, 2, 3, 4), and so no detailed description of the methods will be given here.

BUILDING CLASSIFICATION

An abridged description of the building classification used in this earthquake-loss simulation study is shown in table 1. These classifications are similar to those used by the majority of the property-casualty insurance companies in the United States and have the advantage of over 50 years experience, including testing after earthquakes.

Table 1.--Building classification used in this study

Notation used in loss tables 3 and 4	Brief description of subclasses of five broad building classes
1A	Wood-frame and frame-stucco dwellings.
1B	Wood-frame and frame-stucco buildings not qualifying under 1A (usually large-area nonhabitational units); (not considered in this study).
2A	One story, all metal; floor area less than 20,000 feet^2.
2B	All metal buildings not considered under 2A.
3LA	Steel frame, superior damage-control features; less than four stories.
3LB	Steel frame; ordinary damage-control features; less than four stories.
3LC	Steel frame; intermediate damage-control features (between 3LA and 3LB); less than four stories.
3LD	Floors and roofs not concrete; less than four stories.
3HA, 3HB, 3HC, 3HD	Descriptions are the same as for 3LA, 3LB, 3LC, and 3LD except that buildings have four or more stories.
4LA	Reinforced concrete; superior damage-control features; less than four stories.
4LB	Reinforced concrete; ordinary damage-control features; less than four stories.
4LC	Reinforced concrete; intermediate damage-control features (between 4LA and 4LB); less than four stories.
4LD	Precast reinforced concrete, lift slab, less than four stories.
4LE	Floors and roofs not concrete, less than four stories.
4HA, 4HB, 4HC, 4HD, 4HE	Descriptions are the same as for 4LA, 4LB, 4LC, 4LD, and 4LE except that buildings have four or more stories.
5A	Dwellings, not over two stories in height, constructed of (a) poured-in-place reinforced concrete, with roofs and second floors of wood frame or (b) adequately reinforced brick or hollow-concrete-block masonry, with roofs and floors of wood (not considered in this study).
5B	One-story buildings having superior earthquake damage-control features, including exterior walls of (a) poured-in-place reinforced concrete, and (or) (b) precast reinforced concrete, and (or) (c) reinforced brick masonry or reinforced-concrete brick masonry, and (or) (d) reinforced hollow-concrete-block masonry. Roofs and supported floors are of wood or metal-diaphragm assemblies. Interior bearing walls are of wood frame or any one, or a combination, of the aforementioned wall materials.
5C	One-story buildings having construction materials listed for Class 5B, but with ordinary earthquake damage-control features.
5D	Buildings having reinforced concrete load-bearing walls and floors and roofs of wood, but not qualifying for Class 4E; and buildings of any height having Class 5B materials of construction, including wall reinforcement; also included are buildings with roofs and supported floors of reinforced concrete (precast or otherwise) not qualifying for Class 4.
5E	Buildings having unreinforced solid-unit masonry of unreinforced brick, unreinforced concrete brick, unreinforced stone, or unreinforced concrete, where the loads are carried in whole or in part by the walls and partitions. Interior partitions may be wood frame or any of the aforementioned materials. Roofs and floors may be of any material. Not qualifying are buildings having nonreinforced load walls of hollow tile or other hollow-unit-masonry, adobe, or cavity construction.
5F	Buildings having load-carrying walls of hollow tile or other hollow-unit-masonry construction, adobe, and cavity-wall construction, and any building not covered by any other class (not considered in this study).

BUILDING INVENTORY

The inventory was developed in the following manner:

(1) A direct correlation was assumed to exist between specific building classes and land-use designations. For example, large-area buildings that constitute subclass 2B, all-metal structures, are usually aircraft hangars, steel plants, major manufacturing facilities, or large warehouses, and, accordingly, are situated in land-use areas primarily zoned for industrial purposes. This assumption makes possible the determination of the geographic distribution of building classes throughout the study area. Modification of this assumption for any one building class or subclass was made on the basis of field sampling and personal knowledge.

(2) All building classes and building values were assumed to be uniformly distributed within the designated mapped zones. An equal distribution of building value is reasonably consistent with policy assumed in zoning ordinances formulated by the respective county planning commissions and regional agencies. This assumption was modified when field sampling and personal knowledge of the authors indicated that it gave obviously incorrect results.

(3) Nonconforming uses are not included in the geographic distribution of building classes. In addition, small isolated pockets of semicommercial developments in suburban areas are not considered. In comparison to the major commercial areas tabulated, the values of these semicommercial developments are relatively insignificant. Insofar as possible, their values are included in the nearest major commercial area and are accounted for by a factor related to population distribution based on the 1970 census. In any event, visual surveys indicate that, except for the all metal gasoline service stations located in these random pockets, the majority of these structures are wood-frame buildings.

(4) Land-use data obtained from the "Atlas of Urban and Regional Change" (5) were plotted on the "Census Tract Outline Map" (6), and the land-use designations were converted to the appropriate building class. Data compatibility with the respective land-use maps provided by the various county planning commissions was confirmed by cross-checking data sources. Mapped results were partially verified through data collected from the detailed city and street maps available for urban centers located in the San Francisco Bay area.

(5) Final mapping results were checked using visual field surveys of critical areas.

(6) Special service areas found in the San Francisco Bay area, such as San Francisco Presidio, Port of San Francisco, Hamilton Air Force Base, Moffett Naval Air Field, U.S. Naval Magazines at Port Chicago and Concord, Oakland Army Base, Oakland Naval Supply Center, Nimitz Field Naval Air Station in Alameda, San Quentin Penitentiary, and Mare Island, among others, were not included in the mapping of building classes.

(7) The area within each census tract having a particular land-use code (equated to building class) was measured. The area of each building class in each census tract was then summed to determine the total area of a particular building class in the nine counties considered in this study. The percentage of any building class in any census tract is then:

$$\frac{\text{Area of the particular building class in the census tract}}{\text{Total area of that building class in the nine-county area}} \times 100$$

A more complete discussion of the development of the building inventory, together with examples, may be found in (7).

GROUND SHAKING - LOSS RELATIONSHIPS

The estimation of losses resulting from earthquakes requires that relationships be known or developed between the intensity of ground shaking and the degree of damage to structures by class of construction (fig. 2). The measure of the intensity of ground shaking used in this study is the Modified Mercalli Intensity Scale (8). Limitations of the scale have been discussed in several papers (for example, 9, 10).

Development of the loss-intensity relationships used in this study entailed three steps: (1) examination of loss for a number of earthquakes; (2) analysis of existing building cost data; and (3) integration of (1) and (2), using engineering judgment based on actual earthquake experience, into loss-intensity relationships. Because of the large number of classes of construction and the many construction components included in nondwelling classes, the present attempt to develop loss-intensity relationships must be considered as preliminary.

The most useful published sources of loss data are found in the studies of the most recent earthquakes, although data extending back to the 1906 San Francisco shock still have substantial value. A review of several publications showed that the damage data in the publications are not usually compatible. Further, a more detailed review of all major sources shows that data are far from complete for all intensities for all building classes. It then follows that interpolation and judgment must be used with the published record of actual losses to produce loss values.

Analysis of existing building cost data has shown that the variations in the cost percentages among construction components for any particular building class permit only very approximate loss estimates when applying loss averages to any particular building.

The development of loss-intensity relationships, then, requires the integration of actual earthquake loss with current cost data. It also requires the interpretation of earthquake loss data and their relation to each class of construction in terms of the Modified Mercalli Intensity Scale. Actual earthquake losses must be analyzed with relation to isoseismal maps that have been prepared for recent earthquakes. It is

important to note that this step effectively amounts to a more definitive description of losses at each intensity level than exist in the original MM Intensity Scale. In this sense, development and loss-intensity relationships for the various construction classes represents a further definition or refinement of the MM scale based on an analysis of loss experience and cost. At the present time we believe that MM intensity maps, together with the loss-intensity relationships developed using relevant experienced judgment, are the best bases for this kind of study. Indeed it is the only basis for which extensive data are available.

For damage-analysis purposes, the lower intensity limit of the Modified Mercalli Intensity Scale is the threshold of damage, which varies with the kind of building as well as with the kind of ground motion but is generally VI or VII. The threshold normally includes "imaginary" damage, which may decrease the actual lower limit by one intensity unit. By "imaginary" damage we mean damage that the owner/occupant believes occurred during the shock, but which was actually in existence before the earthquake. On the other hand, the upper intensity limit is determined by the intensity at which ground-vibration effects to buildings are overshadowed by geologic effects, such as landsliding, faulting, and failures of structurally poor ground. This upper limit is normally given as MM intensity IX in insurance practice. This limit of IX is somewhat arbitrary since vibrational effects on buildings will increase somewhat with increasing intensity, but becomes overshadowed by building damage resulting from geological effects.

Percent loss-MM intensity relationships are, in general, not linear. The general, qualitative characteristics of loss-intensity curves for various building classes have been discussed elsewhere (2, 7); the preliminary nature of this study precluded the determination of the detailed shape of the intensity-loss curves. As usable approximations, linear relationships were developed. In figure 2, percent losses from 0 to 10 have been estimated to the nearest 1 percent. Percent losses above 10 percent are estimated to the nearest 5 percent.

ESTIMATION OF GROUND SHAKING

MM intensities were assigned to all census tracts for all earthquakes of interest. Two techniques were used to assign intensities to census tracts. For earthquakes having maximum epicentral intensities from VI to VIII, average isoseismal maps were used. For earthquakes having maximum intensities greater than VIII, isoseismal maps were constructed using data from special studies (11, 12).

Average isoseismal maps (for earthquakes VI $< I_o <$ VIII) were constructed in the following manner:

(1) The average area shaken at each intensity level was determined for each earthquake in the San Francisco Bay area for which an isoseismal map was available. The same general approach was used in an earlier study of single-family dwellings (3, 4), and all of the intensity data used in that study, together with additional new material, was used to construct average isoseismal maps.

(2) Isoseismal patterns were considered to be elongated in the direction of faulting. This holds true in the San Francisco Bay area because earthquakes are shallow (< 15 km) and strike-slip faulting predominates, at least in the larger earthquakes that are of most interest to this study.

(3) Using $M=1+2/3\ I_o$, where I_o is the maximum MM intensity and M is magnitude, and $\log L=-0.39+0.34\ M$, where L is fault rupture length (3) in kilometers, the shapes of average isoseismal maps were constructed using

$$A_I=2W_IL+\pi W^2{}_I, \qquad \text{(see fig. 3)}$$

where A_I=area enclosed by the intensity I isoseismal plus higher intensities

and

W_I=width of zone bounded by the intensity I isoseismal plus higher intensities.

(4) The orientation of the isoseismals (the strike of L in fig. 3) for any particular historical earthquake was taken to be the same as the strikes of faults in the San Francisco Bay area that are known to have been active near the earthquake epicenter during or since Quaternary time (13). Earthquakes that could not be associated with specific faults were assumed to have circular isoseismals. Table 2 gives the values of W (fig. 3) and L for elongated isoseismals and the radius R for circular isoseismals for all intensities associated with earthquakes of maximum intensities VI through VIII.

Table 2.--Parameters for construction of average isoseismals for $VI \leq I_o \leq VIII$

Maximum intensity I_o and associated intensities I	Fault length L (km)	Width[1] W (km)	Radius[2] R (km)
VIII:	58	1.65	8.00
VII	--	5.90	15.55
VI	--	17.54	30.90
VII:	35	3.17	8.92
VI	--	9.98	17.84
VI	20	3.95	8.18

[1]The width (W) and radius (R) are the maximum distances for each intensity.

[2]The radius (R) is for the circular isoseismals, which are assigned to earthquakes not associated with specific faults.

(5) The isoseismals constructed for earthquakes having $VI \leq I_o \leq VIII$ average the effects on surficial materials over broad areas. Consequently, the intensity of shaking at individual sites may differ considerably from on the average intensity map. The effect of site amplification was, to some extent, taken into account by dividing the surficial geology throughout the area into three units. Incremental intensities were assigned to these three units and added to or subtracted from the average intensities. The units and incremental intensities are bay mud (+1.0); alluvium (0); and bedrock (-1.0). These units are defined in more detail and discussed by Borcherdt et al., (12). The incremental intensities assigned here differ slightly from, but are in general agreement with, those suggested in (12).

LOSS CALCULATIONS

Losses were calculated for each class of construction using earthquakes that occurred during the following time intervals: 1800-1974 (175 years); 1800-1899 (100 years); 1900-1974 (75 years); and 1907-1974 (68 years). The losses are expressed as the average annual percent loss to buildings of each construction class in the nine-county San Francisco Bay area. The inventory, exclusive of wood-frame dwellings (Class 1A), is updated to 1973. Class 1A inventory is based on 1970 United States census data. The results are shown in table 3. Losses for two large earthquakes of interest in the Bay area--one, a maximum intensity X on the San Andreas fault, and the other, a maximum intensity IX on the Hayward fault--are shown in table 4.

DISCUSSION OF RESULTS

The four samples of historical seismicity data shown in table 3 indicate that, in general, the largest losses are associated with the 100-year period 1800-1899. This is a consequence of the three large earthquakes that occurred during the period: in 1838 on the San Andreas fault, and in 1836 and 1868 on the Hayward fault. In addition, the percent losses to buildings are considered constant (at the intensity IX level) for intensities above IX. Actual losses increase for intensities greater than IX, but the losses are increasingly caused by geologic effects that have not been considered in this report. The earthquakes of 1836, 1838, and 1868 are believed not to have been as large as the 1906 earthquake, but they would be about as effective in causing vibration damage. It is interesting to note also that, even though the earthquake history of the San Francisco Bay area is probably not complete for damaging shocks for the 1800-1899 period, the losses are generally the highest of any time interval considered. Best long-term average loss estimates are probably obtained from the losses simulated using either the 175-year seismicity sample (1800-1974), the 100-year sample (1800-1899), or the 75-year sample (1900-1974) even though the average losses computed using these three seismicity samples are all low, but for different reasons: The time spans that include 19th century data are incomplete, whereas the 1900-1975 sample contains only one large shock (1906). Data for the 68-year period, 1907-1974, are reasonably complete for damaging shocks, but yield useful average losses only if one believes that large damaging earthquakes will not occur in the Bay area during some period of interest in the future.

The losses shown in table 4, simulated for a maximum MM intensity X earthquake on the San Andreas fault and a maximum intensity IX earthquake on the Hayward fault, seem to indicate that the percent losses for the two earthquakes would be very similar from the point of view of vibration damage. Nearly equal losses result partly from the flat shape of the intensity-loss curves for intensities above IX and partly from the geometry of the Bay area and the high concentration of buildings in the east Bay area. Dollar loss estimates are available only for one- to four-family dwellings, the value of the dwellings being obtained from census data as previously reported (1, 2, 3, 4). There were approximately 1.1175 million one- to four-family dwellings in the nine-county study area having a replacement cost value of $30.3 billion and an average value of $27,100 in 1970. A conservative long-term annual average loss (based on table 3) might be 1 percent of the replacement cost value or about $271. Average total losses to dwellings as a result of a large earthquake would be about 5 percent of value, or $1.51 billion, or an average loss per dwelling of $1,360.

Table 3.--Estimated average annual percent losses in the nine-county San Francisco Bay area, based on the historical seismicity during four time intervals

Building Subclass	175 years (1800-1974)	100 years (1800-1899)	75 years (1900-1974)	68 years (1907-1974)
1/ 1A	0.702	0.663	0.755	0.692
2A	0.131	0.153	0.102	0.043
2B	0.160	0.201	0.106	0.028
3LA	0.166	0.198	0.123	0.032
3LB	0.822	0.820	0.826	0.652
3LC	0.208	0.248	0.154	0.040
3LD	0.822	0.820	0.826	0.652
3HA	0.260	0.357	0.132	0.008
3HB	0.539	0.705	0.317	0.098
3HC	0.325	0.446	0.165	0.010
3HD	0.539	0.705	0.317	0.098
4LA	0.208	0.248	0.154	0.040
4LB	1.175	1.171	1.180	0.931
4LC	0.291	0.347	0.215	0.056
4LD	1.410	1.406	1.416	1.117
4LE	1.292	1.288	1.298	1.024
4HA	0.325	0.446	0.165	0.010
4HB	0.769	1.007	0.453	0.139
4HC	0.539	0.705	0.317	0.098
4HD	0.923	1.208	0.543	0.167
4HE	0.846	1.108	0.498	0.153
5B	0.208	0.248	0.154	0.040
5C	0.822	0.820	0.826	0.652
5D	1.057	1.054	1.062	0.838
5E	1.521	1.589	1.430	1.083

1/ Class 1A inventory is based on 1970 census data.

Table 4.--Estimated percent losses for two large earthquakes in the nine-county San Francisco Bay area

Building Subclass	Percent losses for MM intensity X on the San Andreas fault	Percent losses for MM intensity IX on the Hayward fault
1A	5.04	4.03
2A	4.17	3.38
3LA	6.59	5.15
3LB	13.07	11.47
3LC	8.24	6.44
3LD	13.07	11.47
3HA	9.34	9.42
3HB	16.73	16.82
3HC	11.67	11.78
3HD	16.73	16.82
4LA	8.24	6.44
4LB	18.68	16.30
4LC	13.07	11.47
4LD	22.47	19.56
4LE	20.54	20.65
4HA	11.67	11.78
4HB	23.89	24.04
4HC	16.73	16.82
4HD	28.67	28.84
4HE	26.28	26.44
5B	8.24	6.44
5C	13.07	11.47
5D	16.81	14.74
5E	25.41	22.51

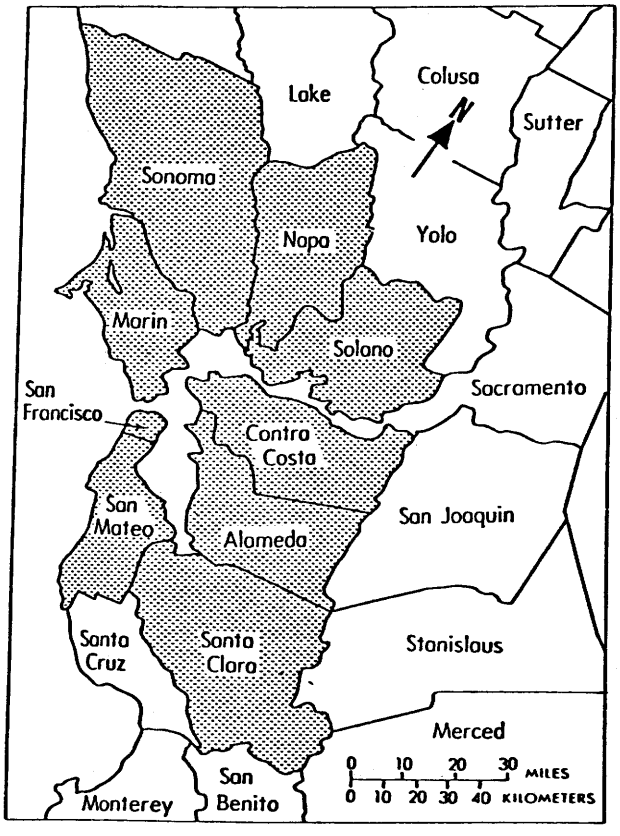

Figure 1.--Location map of northern California showing the nine-county area studies in this report.

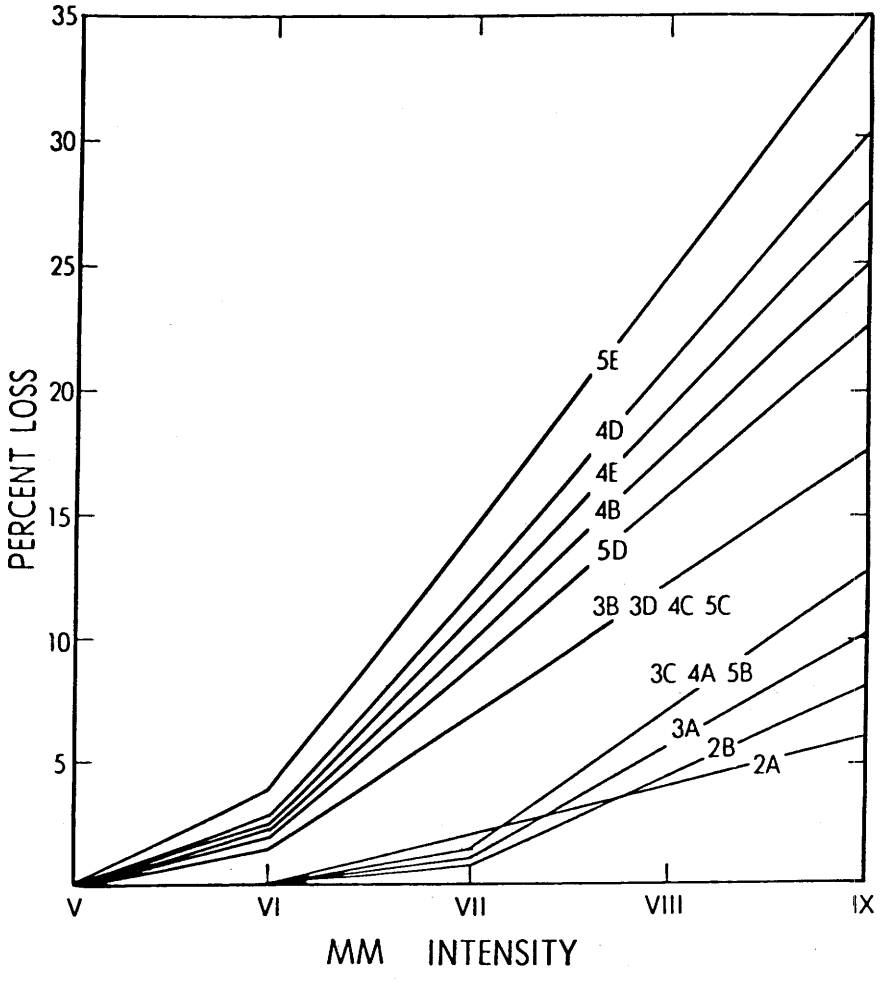

Figure 2.--Modified Mercalli intensity--loss relationship (by class of construction) used in this study. Descriptions of the various classes may be found in table 1. High-(H) and low-(L)rise subclasses of class 3 and class 4 have been combined.

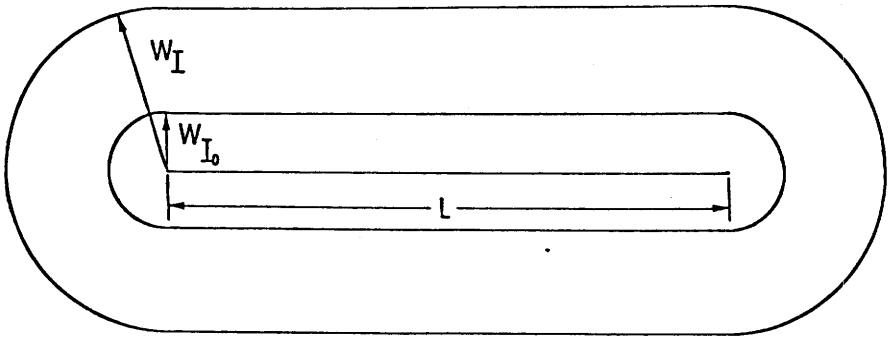

Figure 3.--Schematic showing the construction of average isoseismal maps (see text for discussion).

REFERENCES

1. U.S. Coast and Geodetic Survey, 1969, Summary and recommendations, in Studies in seismicity and earthquake damage statistics, 142 p.

2. Steinbrugge, K. V., McClure, F. E., and Snow, A. J., 1969, Appendix A, in Studies in seismicity and earthquake damage statistics: U.S. Coast and Geodetic Survey, 142 p.

3. Algermissen, S. T., Stepp, J. C., Rinehart, W. A., and Arnold, E. P., 1969, Appendix B, in Studies in seismicity and earthquake damage statistics: U.S. Coast and Geodetic Survey, 68 p.

4. Rinehart, W. A., Algermissen, S. T., and Gibbons, Mary, 1976, Estimation of earthquake losses in single-family dwellings: U.S. Geological Survey Open-File Report 76-156, 57 p., plus appendices.

5. U.S. Geological Survey, 1973, Atlas of Urban and Regional Changes, San Francisco Bay area: U.S. Geological Survey Open-File Report, 44 maps, 1:62,500.

6. Western Economic Research Company, 1973, Census Tract Outline Map of the Bay Area and Vicinity: Sherman Oaks, Calif., Scale 1:125,000.

7. Algermissen, S. T., Steinbrugge, K. V., and Lagorio, H. J., 1978, Estimation of earthquake losses to buildings (except single-family dwellings): U.S. Geological Survey Open-File Report 78-441, 146 p., plus appendices.

8. Wood, H. O., and Neumann, Frank, 1931, Modified Mercalli Scale of 1931: Seismological Society of America Bulletin, v. 21, p. 277-283.

9. Voight, D. S., and Byerly, P., 1949, The intensity of earthquakes as rated from questionnaires: Seismological Society of America Bulletin, v. 39, p. 21-26.

10. Richter, C. F., 1958, Elementary seismology: San Francisco, Calif., W. H. Freeman & Co., 768 p.

11. Algermissen, S. T. (principal investigator), Rinehart, W. A., Dewey, J. W., Steinbrugge, K. V. (principal consultant), Lagorio, H. J., Degenkolb, H. J., Cluff, L. S., McClure, F. E., Scott, Stanely, and Gordon, R. F., 1972, A study of earthquake losses in the San Francisco Bay area--A report prepared for the Office of Emergency Preparedness: U.S. Department of Commerce, National Oceanic and Atmospheric Administration, Environmental Research Laboratories, 220 p.

12. Borcherdt, R. D., Joyner, W. B., Warrick, R. E., and Gibbs, J. F., 1975, Response of local geologic units to ground shaking, in Studies for seismic zonation of the San Francisco Bay area: U.S. Geological Survey Professional Paper 941-A, p. A52-A67.

13. Wesson, R. L., Helley, E. J., Lajoie, K. R., and Wentworth, C. M., 1975, Faults and future earthquakes: U.S. Geological Survey Professional Paper 941-A, p. A5-A30.

EXAMPLES OF SEISMIC ZONATION IN THE SAN FRANCISCO BAY REGION

by

W. J. Kockelman and E. E. Brabb

ABSTRACT

Six examples of seismic zonation at various scales by cities and counties in the San Francisco Bay region show that scientific information can be used effectively in avoiding earthquake hazards and mitigating damage. The zonation method involves postulating an earthquake, grouping geologic materials with similar physical properties, predicting the geologic effects of an earthquake, and combining the geologic effects on a map. The method has been used by the Cities of Mountain View, Novato, and San Francisco and the Counties of Marin, Santa Clara, and San Mateo to develop zones which were used as a basis for their general plans, seismic safety plans, development policies or ordinances.

INTRODUCTION

The proceedings of the International Conference on Microzonation for Safer Construction Research and Application, Seattle, 1972 included papers on the state of the art, various techniques, and a preliminary analysis of zonation methods. The papers lack uniform definition of "seismic zones," lack consensus on the scale and detail of seismic zone maps, and reveal the need for an unambiguous zonation method (10).

Three events have encouraged communities to attempt seismic zonation: passage of the Alquist-Priolo Act by the California Legislature requiring special studies in zones encompassing potentially and recently active faults (5), preparation and adoption of seismic safety plan elements by cities and counties as required by California statue (4), and further development of a seismic zonation method (2). The method has four steps: postulating an earthquake of a given size and location; grouping geologic materials with similar physical properties; predicting effects of the postulated earthquake for each geologic unit by type of hazard or failure, namely surface rupture, ground shaking, flooding, liquefaction potential, and landsliding; and combining geologic effects by zones on a map (1).

The following six examples of seismic zonation by cities and counties in the San Francisco Bay region illustrate applications of the method.

INVESTIGATION ZONES

Three "investigation zones" are derived and mapped at a scale of

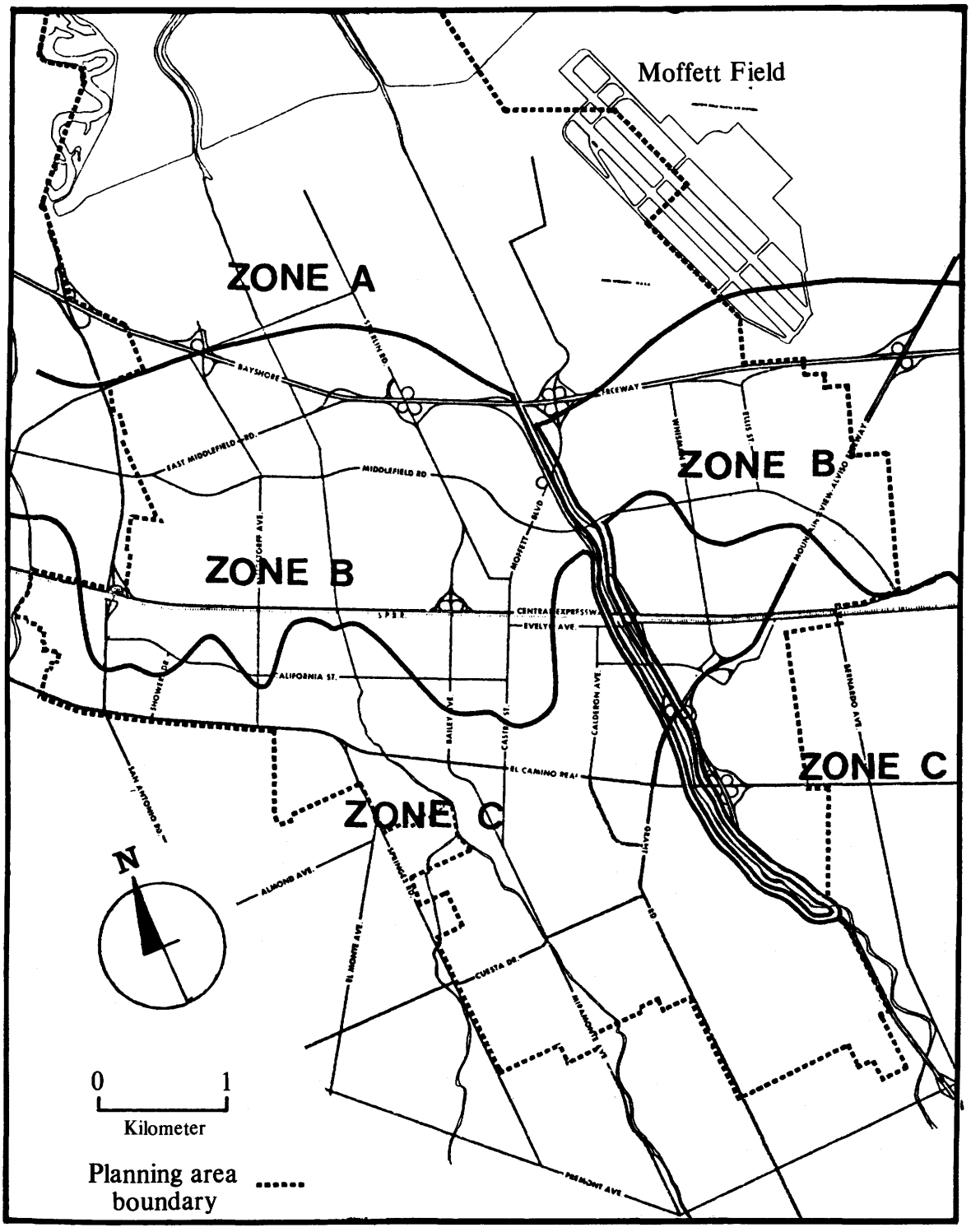

Figure 1.--City of Mountain View "investigation zones." The boundaries of the zones separate areas with different geologic properties. Zone A, for example, is underlain by water-saturated bay mud with a moderate to high liquefaction potential whereas zone B contains seasonally saturated alluvial fan deposits that may liquefy only when the water table is high (6, 20). Different development policies have been adopted for each of the zones (8).

1:48,000 (fig. 1) by the City of Mountain View Planning Department from its review of various earth-science information. Ground shaking and ground failure are considered the primary earthquake problems (8).

An earthquake on either the San Andreas or Hayward fault systems is assumed (7). Design earthquakes of magnitudes 8.0 and 6.5 may be implied from the Department's use of potential liquefaction data (6, 20).

Each "investigation zone" contains geologic units with similar physical properties. Zone A is underlain mostly by water-saturated bay mud. Zone B is underlain by weakly consolidated mud, silt and sand that are seasonally saturated. Zone C is underlain by somewhat coarser grained alluvium that is generally well drained and unsaturated (8, 9).

Geologic effects are predicted for each group of geologic units having similar properties. For example, "Moderate to substantial settlement and/or differential settlement may occur" in zone A, "Deep liquefaction and significant settlement ... is possible" in zone B, and "Neither significant settlement nor ground failure is likely to be experienced" in zone C (8).

With the aid of the zone map (fig. 1), areas of "relative seismic concern," such as those where loss of life, property damage and economic dislocation may occur, are delineated on the City's existing "General Plan Map." Land uses are subdivided into categories by importance, such as hospitals and fire stations that must provide emergency services after an earthquake; by occupancy, such as schools and other buildings that contain large numbers of people; and by type of construction, such as single-family dwellings. Development policies, such as "open space and low intensity uses shall be encouraged for sites most susceptible to earthquake damage," and "Uses should be limited to those where risk of loss of life, property damage, and social and economic dislocations are acceptable if liquefaction or settlement takes place," are specified for each land use group in each zone (8).

The zones, areas of "relative seismic concern," and land-use development policies have been incorporated into the City's Safety Element and adopted by the City Council as part of its general plan (8).

BUILDING DAMAGE LEVELS

Four levels of building damage aggregated on a block basis are estimated and mapped at a scale of 1:48,000 (fig. 2) for the San Francisco City Planning Department (3, 14).

A repetition of the 1906 earthquake (magnitude 8.3) originating on the San Andreas fault is assumed. Earthquakes with smaller magnitudes are also considered (3).

Soil and rock types are combined on the basis of similar engineering properties, and their susceptibility to earthquake failure is discussed (3). Their properties are considered in estimating the types of potential ground motion such as peak ground acceleration, spectral response acceleration, and predominant periods for deep or soft soil deposits (14).

City Assessor's data on construction type, year built, number of

stories, floor area, and use of each building along with earthquake history were considered to obtain average damage factors for each block. The factors were then weighted to obtain the four levels of estimated building damage shown in figure 2 (14).

Hazards such as seiches, tsunamis, landslides, and dam failures are considered and mapped but are not generally used in developing the four levels of damage. These hazards are to be treated as "additional hazards;" for example, a building with a "slight" damage rating (fig. 2) that is apt to slide down a hill with a landslide should have its rating changed to "severe" (3).

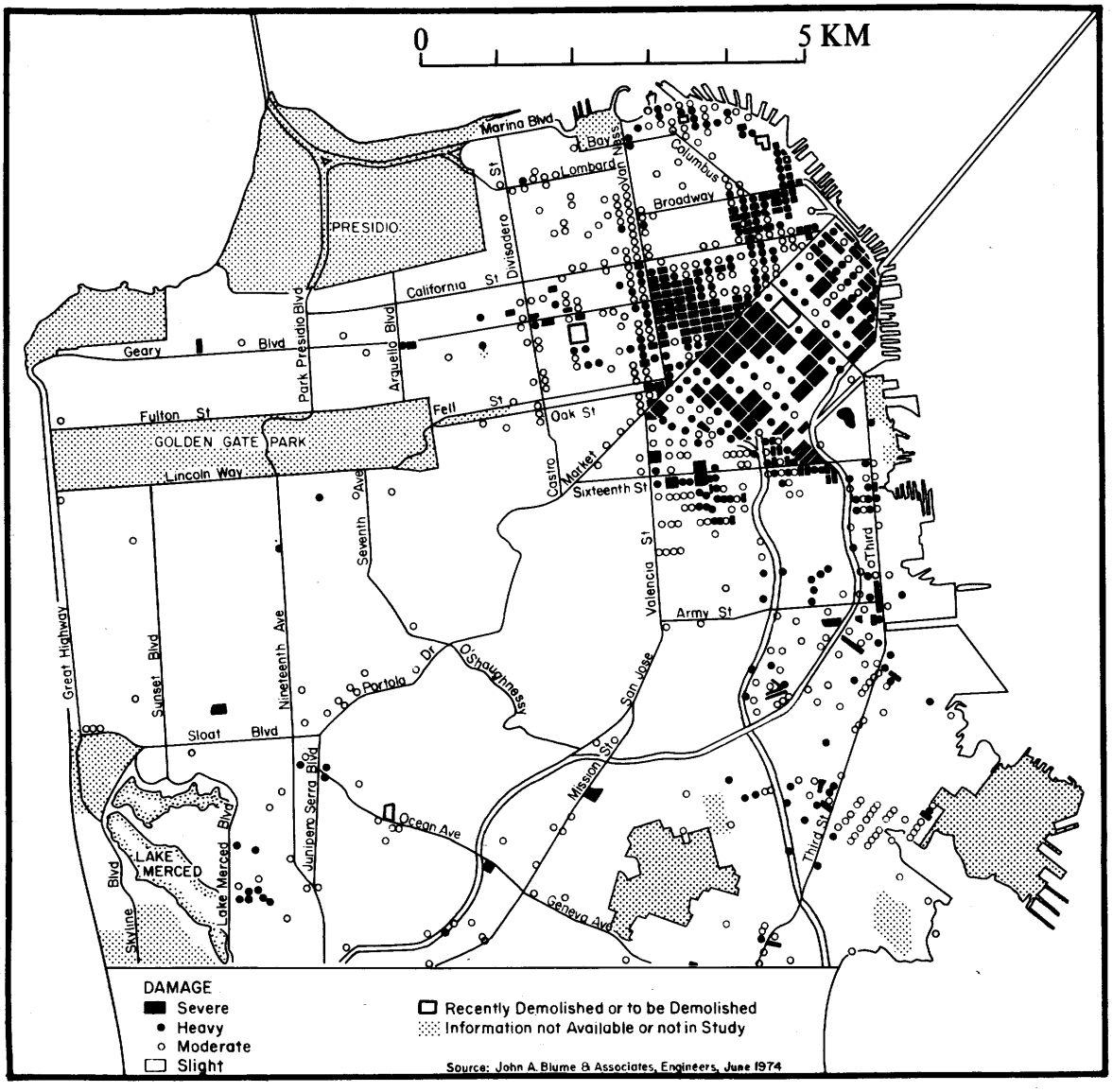

Figure 2.--Estimated building damage for a severe earthquake in the San Francisco area. Abatement of hazards associated with these buildings is recommended in San Francisco's Community Safety Plan (14).

Policies related to building damage levels such as "Initiate orderly abatement of hazards from existing buildings and structures" and "Abate existing hazards in all critical community facilities" are recommended (14).

The building damage levels, "additional hazards" and policies have been incorporated into the City's Community Safety Plan and adopted by the Board of Supervisors as part of the City's comprehensive plan (14).

EARTHQUAKE RISK ZONES

Five "earthquake risk" zones are developed and mapped at a scale of 1:12,000 (fig. 3) for the Novato area by the California Division of Mines and Geology in cooperation with the County of Marin and the City of Novato (13). Ground shaking, surface rupture, ground failure, and landslides are considered as having the highest potential for damage, whereas tsunamis are considered not to be significant potential hazards (12, 13). An earthquake of approximately magnitude 8 with an epicenter in the northern San Francisco Bay area is postulated (13).

Geologic materials are grouped into five zones on the basis of similar physical properties; for example, "firm, relatively unweathered bedrock" in zone A, "relatively shallow compacted alluvium and colluvium" in zone B, "deep upslope landslide deposits" in zone D, and "bay mud" in zone E. In addition, a symbol is placed over the trace of the potentially active Burdell Mountain fault (13).

Some geologic effects of the postulated earthquake are predicted for each zone; for example, "subject to relatively high frequency vibrations" in zone A, "may be threatened by landsliding" in zone B, and "rapid differential settlement" in zone E. In addition, each zone is rated from probable low to probable high damage. The geologic materials, geologic effects, and damage ratings are combined and mapped by zone on figure 3 (13).

Recommendations related to the risk zones, such as "large public structures ... not be located on any demonstrated fault trace," "residential developments on fill may not be a fitting use" in zone E, and "Engineering geology reports, based on detailed geological mapping, [should] be required" in zone D, are made (13).

The "earthquake risk" zones and recommendations have been considered by the City of Novato and the County of Marin and used as a basis for their seismic safety plan elements.

SEISMIC SAFETY ZONES

Three "seismic safety zones" are developed and mapped at a scale of 1:62,500 (fig. 4) by the Santa Clara County Planning Department with assistance or contributions from the California Division of Mines and Geology, private consultants, and members of the U.S. Geological Survey (18). Dam failures, tectonic creep, dike failures, tsunamis, seiches, landslides, ground-shaking and surface ruptures were considered and the potentially hazardous ones were combined in zones on a "relative seismic stability" map (18). This map also includes nonseismic geologic hazards, such as landslides triggered by rainfall. The original map is printed in

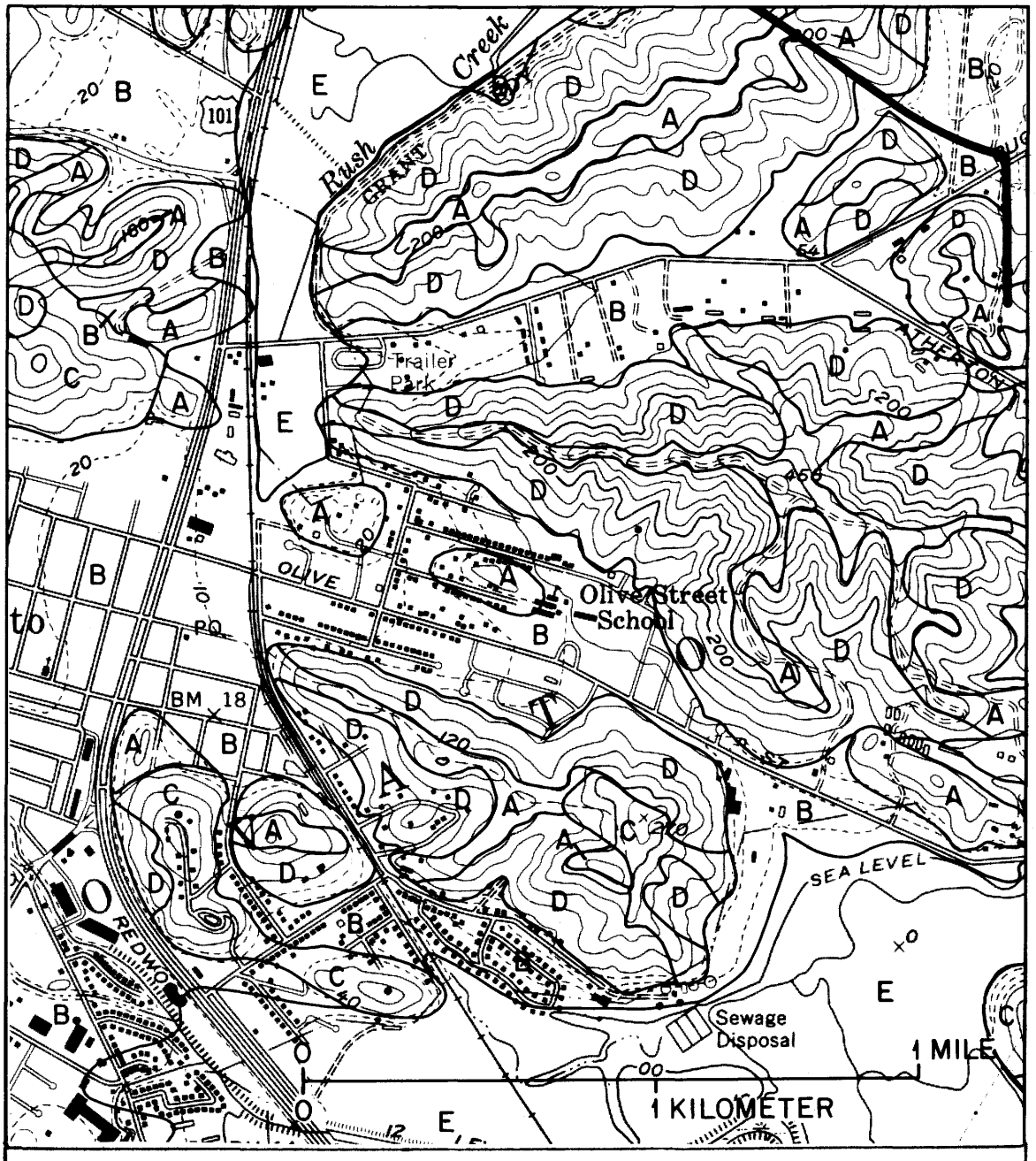

A	Areas of probable low damage. These areas are underlain by firm, relatively unweathered bedrock that crops out at the surface or is covered by only thin layers of soil or colluvium.
B	Areas of probable low to moderate damage. These areas are underlain by relatively shallow, compacted alluvium and colluvium on flat or gently sloping surfaces.
C	Areas of probable low to moderate damage. These areas are underlain by sheared bedrock.
D	Areas of potentially high damage. These areas are underlain by landslide deposits and by thick deposits of colluvium or deeply weathered bedrock on steep slopes.
E	Areas of probable high damage. These areas are underlain by bay mud ranging in thickness from a few feet to more than 100 feet.
▬	Fault

Figure 3.--Earthquake risk zones in the Novato area, Marin County, California (13).

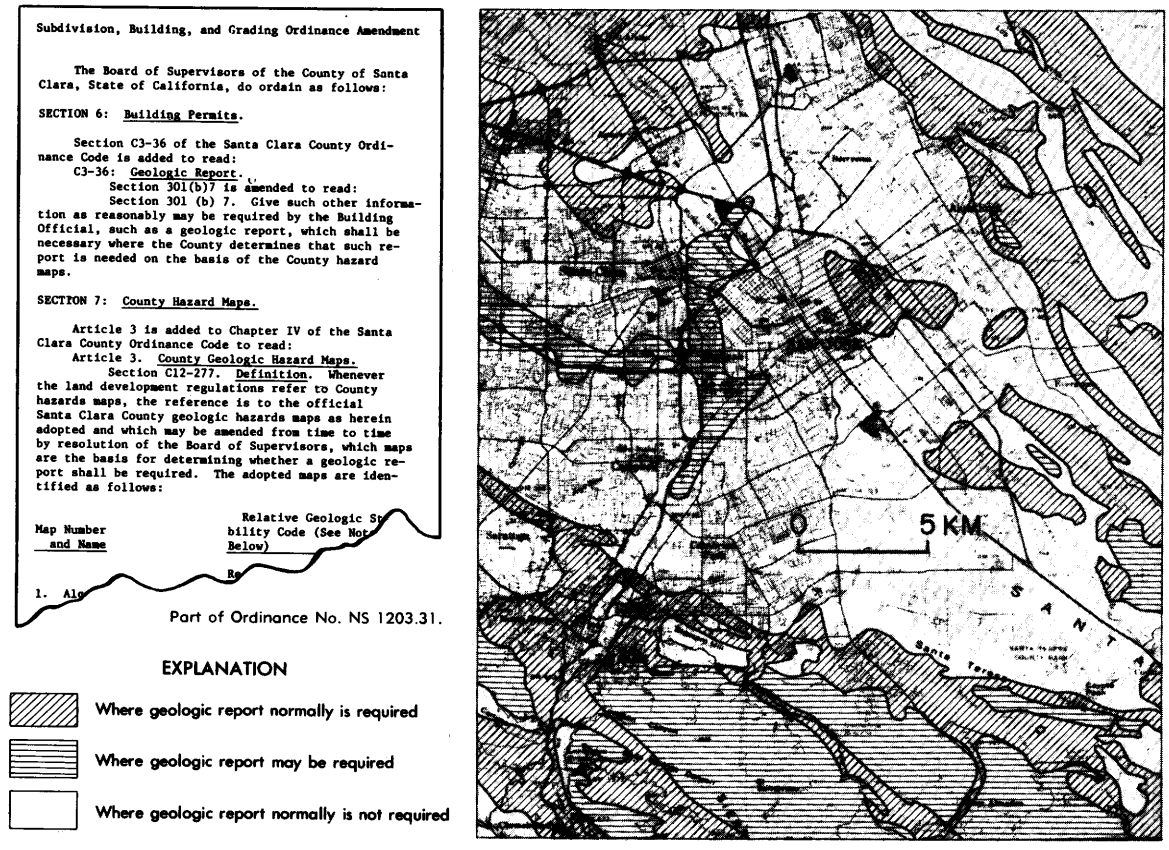

Figure 4.--Part of the official seismic stability map for Santa Clara County (18). Scale 1:250,000.

stoplight colors--red, yellow, and green--to make the information more easily understood by the general public.

A recurrence of the 1906 earthquake (magnitude 8.3) along the San Andreas fault zone in the San Francisco Bay area may be implied from the Department's discussion of the various seismic hazards (18).

Geologic units are grouped on the basis of similar physical properties, and the geologic effects are predicted for each group. For example, fine-grained water-saturated sand or silt within 6 meters of the ground surface would be considered to have a high potential for liquefaction and would normally require geologic investigation before any development is approved. The same materials within 6 to 15 meters of the surface are considered to have a moderate potential for liquefaction and might require a geologic investigation. In most cases, the county geologist decides whether and what level of geologic investigation is required.

Maps of other county plan elements, such as utility, transportation, community facilities, and urban development, are compared with the zone map to indicate their relation to the seismic safety zones (18). Recommendations to minimize the possible loss of life and property are made for each

county plan element. For example, "Emergency operations center structures should be evaluated for seismic vulnerability and should be designed and constructed to assure the continuity of vital services following a damaging earthquake," and "Proposed transportation routes, facilities and structures should be evaluated for potential vulnerability and built only if problems can be sufficiently mitigated" (18).

The three zones and recommendations are included in the County's Seismic Safety Plan which was unanimously adopted by the County Planning Commission and Board of Supervisors. In addition, the seismic safety zones have been adopted by the Board of Supervisors as the County's official geologic hazard maps. The County Ordinance Code has been amended so as to require site investigations and geologic reports based on the official geologic hazards map. Four sections of the code are affected: major subdivisions, minor land divisions, building sites, and grading. The amendment provides for site investigations and geologic reports so as to discourage development on, or adjacent to, known potentially hazardous areas. The reports are to be prepared by an engineering geologist registered in the State, be submitted to the County for approval, and specify the remedial measures that will make a safe development (17).

GEOTECHNICAL HAZARD SYNTHESIS

Thirteen geologic materials and seven geologic hazards are compiled, combined, and mapped at a scale of 1:24,000 (fig. 5) by the San Mateo County Planning Department and its consultant. Primary consideration is given to the extent and location of faults and to liquefaction potential; however, landslides, dam failure, and tsunamis are also considered and mapped. Seiches are considered but not mapped (11).

A magnitude 7.5-8.3 earthquake on the San Andreas fault is assumed for ground shaking. For fault displacement, a maximum expected magnitude 8.25 earthquake for the San Andreas fault and magnitude 7.0 for the Seal Cove-Gregorio fault are used (11).

Geologic materials are grouped on the basis of similar physical properties, for example, "younger estuarine mud and artifical fill" as no. 1, "beach and dune sand" as no. 4 "colluvium" as no. 5, and various "bedrock" hardnesses as nos. 6-13 (11).

Earthquake stability is predicted for each geologic material--"poor, fair, or good" depending upon geologic structure, slope angle and landslide and soil creep potential. Earthquake intensity is predicted for each geologic material unit--"strong, very strong, violent, very violent, and weak" depending upon the distance from the San Andreas fault (11).

The geotechnical hazard synthesis is part of the County's Seismic and Safety Elements of the General Plan. These elements include recommended policies and implementation programs regarding existing land use, future land use and development, zoning and division of land, and critical-use structures that are directly related to the geotechnical hazard synthesis maps; for example, "Determine the level of acceptable risk which can be borne, utilizing the ... Maps," and "Integrate geotechnical hazard data ... into zoning and subdivision ordinances" (16). The elements, including the geotechnical hazard synthesis maps and recommended policies and implementa-

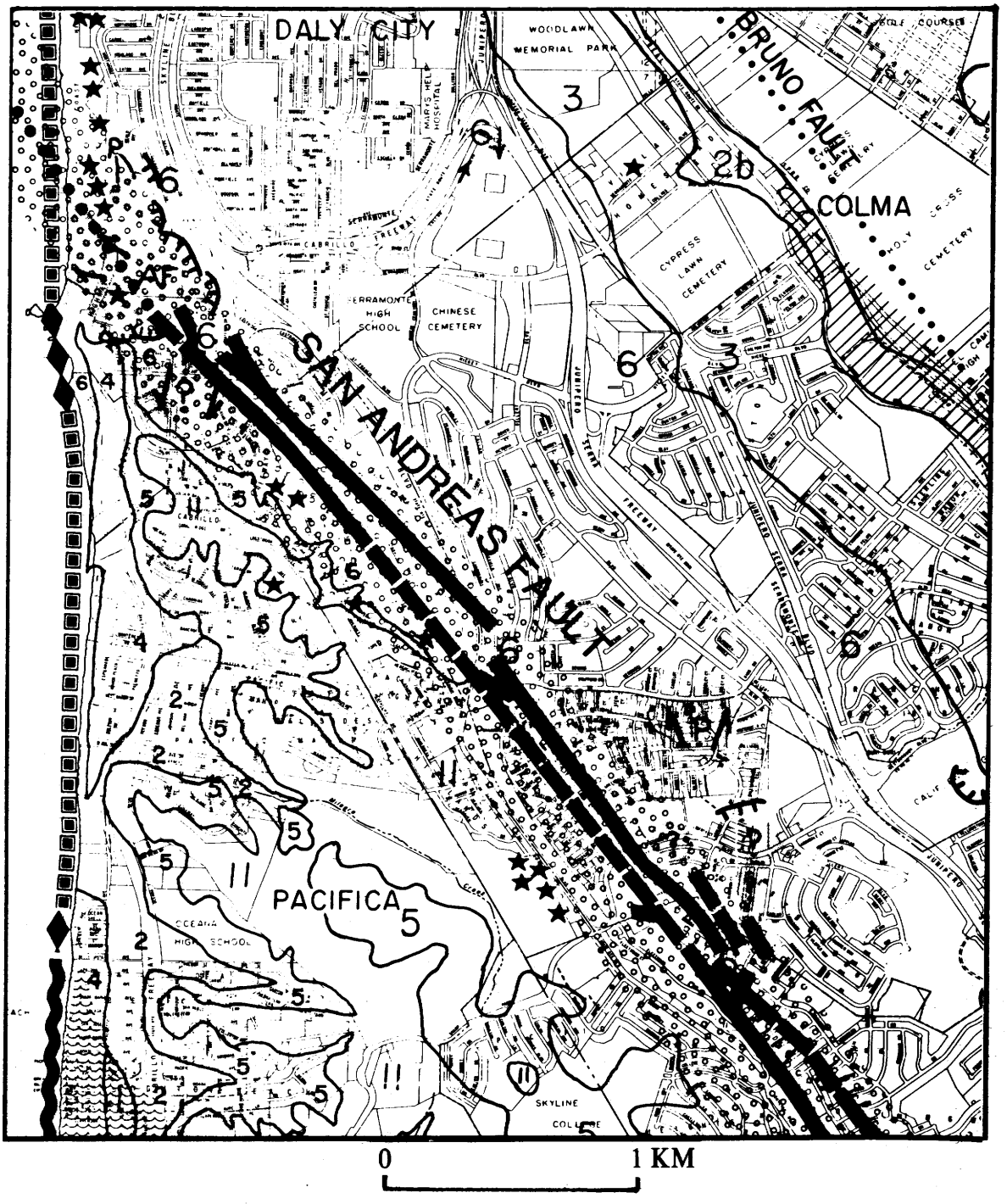

Figure 5.--Part of the geotechnical hazard synthesis map for San Mateo County (11), scale 1:24,000. The explanation for this map is complex, combining information on geologic processes, such as faulting, landsliding, coastal erosion, and liquefaction, with information on geologic materials, shown by numbers on the map. The material units are further subdivided by both seismic and engineering characteristics. For example, areas designated "2b" are underlain by alluvial fan deposits ranging in coarseness from silt to gravel, have poor to fair slope stability, moderate liquefaction potential, good to fair stability in terms of the intensity of ground shaking during a 7.5-8.3 M earthquake, and have good foundation properties.

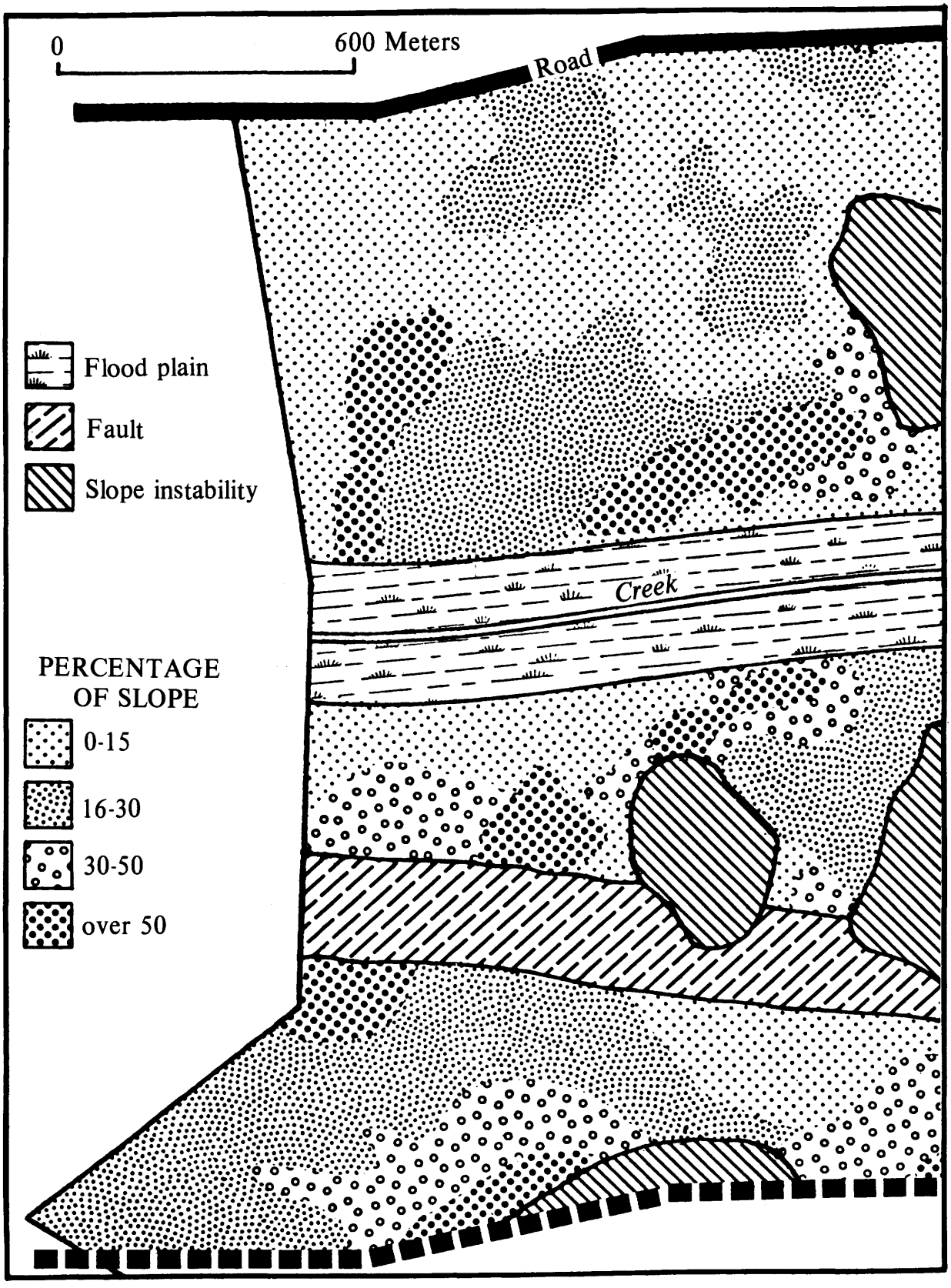

Figure 6.--Hypothetical property in San Mateo County with seismic and geologic constraints. Dwelling units in the fault zone and on landslides are limited to one per 16 hectares (40 acres). Similar low dwelling-unit densities are required along flood plains and on steep slopes (19).

tion programs, have been adopted by the County Board of Supervisors (16).

RESOURCE MANAGEMENT ZONING DISTRICT

Eleven land categories are derived and mapped at various scales by the San Mateo County Planning Department. Seven of the categories (fig. 6) were considered serious seismic or geologic constraints to development (19).

A 7.5-8.3 magnitude earthquake on the San Andreas fault is implied from the seismic hazard information used by the Department (19).

The seismic and geologic constraints are grouped on the basis of similar physical properties--faults, slopes, flood plains, and slope instability. Geologic effects are predicted for two categories; "potential surface deformation due to fault movement," and high, moderate, and low "susceptibility of slopes to failure landslides" (19).

The Department recommended that the permitted density of residential development proposed in each category be reduced to minimize risk exposure and to carry out the objectives and policies of the County's open-space and conservation plans (19).

The Board of Supervisors adopted an ordinance creating a resource management zoning district (15). In addition to the principal uses permitted in the district, the maximum number of dwelling units is limited by special density regulations. The regulations are applied to each application for a zoning permit through the use of a density matrix worksheet (15, 19). For example, 100 hectares (250 acres) of the hypothetical property shown on figure 6 would lie in the fault and slope instability zones where the number of dwellings would be only one per 16 hectares (40 acres).

CONCLUSION

The seismic zonation method can be applied by cities and counties to avoid earthquake hazards, to reduce loss of life, and to mitigate damage. The examples help clarify the definition, scale, and detail of "seismic zones" and provide a workable method for presenting earthquake effects in a form usable by scientists, engineers, land-use planners, decisionmakers, and other citizens.

REFERENCES CITED

(1) Borcherdt, R. D., Brabb, E. E., Joyner, W. B., Helley, E. J., Lajoie, K. R., Page, R. A., Wesson, R. L., and Youd, T. L., 1975, Predicted geologic effect of a postulated earthquake in Borcherdt, R. D., ed., Studies for seismic zonation of the San Francisco Bay region: U.S. Geological Survey Professional Paper 941-A, p. 88-94.

(2) Borcherdt, R. D., ed., 1975, Studies for seismic zonation of the San Francisco Bay region: U.S. Geological Survey Professional Paper 941-A, 102 p.

(3) Blume, John A. and Associates, 1974, San Francisco seismic safety investigation: San Francisco, CA, 124 p.

(4) California Legislature, Amendment to the local planning chapter,

1972: California Government Code, sec. 65302 (f), West's annot. Codes.

(5) _____Alquist Priolo special studies zones act, 1975: California Public Resources Code, secs. 2621 et seq., West's annot. Codes.

(6) City of Mountain View Planning Department, 1974, Safety element: Earth science data interpretive report, Background report I, Mountain View, CA, 31 p.

(7) _____1975, Relative concern zones, structural hazards, critical facilities and fire hazards: Background report II, Mountain View, CA, 47 p.

(8) _____1975, Safety element of the general plan: Resolution no. 10392, Amend. No. 16, adopted February 24, 1975, Mountain View, CA, 14 p.

(9) Helley, E. J., and Brabb, E. E., 1971, Geologic map of late Cenozoic deposits, Santa Clara County, California: U.S. Geological Survey Miscellaneous Field Studies Map MF-335.

(10) International Conference on Microzonation for Safer Construction Research and Application, Seattle, 1972: Proceedings, Seattle, WA, Vols. I and II, 987 p.

(11) Leighton & Associates and San Mateo County Planning Department, 1976, Geotechnical hazard synthesis map: Redwood City, CA, 7 sheets.

(12) Rice, Salem J., 1973, Geology and geologic hazards of the Novato area: California Division of Mines and Geology, 47 p.

(13) _____1975, Geology for planning - Novato area: California Division of Mines and Geology, 56 p., 6 pls.

(14) San Francisco Department of City Planning, 1974, Community safety plan - A proposal for citizen review: 68 p.

(15) San Mateo County Board of Supervisors, 1973, Ordinance No. 2229, adding a Resource Management District and regulations to the county zoning ordinance: Adopted December 20, 1973, 24 p.

(16) San Mateo County Planning Department, 1976, Seismic and safety elements of the general plan: Redwood City, CA, Vol. I, 57 p., Vol. II, 141 p.

(17) Santa Clara County Board of Supervisors, 1974, Ordinance No. NS 1203.31, amending the subdivision, building, and grading ordinances, and adding geologic hazard maps to the County Ordinance Code: Adopted November 6, 1974, 11 p.

(18) Santa Clara County Planning Department, 1975, Seismic safety plan, An element of the general plan: San Jose, CA, 119 p.

(19) Woolfe, Donald A., 1973, San Mateo County Planning Depart, Adoption of the resource conservation area density matrix and policy statement: Memorandum dated September 21, 1973, 32 p.

(20) Youd,T. L., Nichols, D. R., Helley, E. J., and LaJoie, K. R., 1975, Liquefaction potential in Borcherdt, R. D., ed., Studies for seismic zonation of the San Francisco Bay region: U.S. Geological Survey Professional Paper 941-A, p. 68-74.

THE USE OF EARTHQUAKE AND RELATED INFORMATION IN REGIONAL PLANNING--WHAT WE'VE DONE AND WHERE WE'RE GOING

by

Jeanne B. Perkins[1]

ABSTRACT

ABAG has used several techniques for combining earth science maps. These techniques include land capability analysis and various methods of calculating maximum earthquake intensity and cumulative economic risk due to earthquake damage. The resulting maps and data are more easily used in ABAG's planning programs, including:

- o providing data on characteristics of large vacant industrial sites and potential seaports
- o locating areas deserving further study for use as potential disposal sites for hazardous wastes
- o assessing the impacts of alternative future land use alternatives
- o reviewing regionally-significant development proposals on a continuing basis
- o providing information to city and county staff

ABAG's earthquake program plans to refine the existing earthquake maps by experimenting with the ways in which other relationships among geology, faults, topography, earthquake recurrence intervals and damage affect these maps. ABAG also expects to relate these maps more systematically to various land development patterns.

INTRODUCTION

ABAG is a regional comprehensive planning agency that is owned and operated by the local governments of the San Francisco Bay Area. It was established in 1961 to meet regional problems through the cooperative action of its member cities and counties.

The Bay Area is one of the most seismically active areas in the United States. The effects of earthquakes also usually cross city and county boundaries. Consequently, earthquake preparedness is a major regional concern.

SOME TECHNIQUES FOR COMBINING MAPS

Because it is difficult for planners and elected officials to deal directly with the reams of social, environmental, and economic information available concerning any given area or issue, ways of consolidating

[1]Regional Planner, Association of Bay Area Governments, Berkeley, California

earth science data to slant that information to each application become valuable. Two techniques for combining earthquake and other earth science maps that ABAG staff have found useful are described below.

Maximum Earthquake Intensity and Cumulative Economic Risk

An earthquake intensity map groups together a variety of different causes of earthquake damage; although shaking is the dominant cause of damage, other factors such as liquefaction, landsliding, fault rupture, and changes in ground level can also contribute to intensity. Figure 1 is an example of a maximum earthquake intensity map for the San Francisco Bay Area based on the techniques developed by Borcherdt, et al. (1). This map is not the only maximum intensity map that can be developed; altering the way that intensity is related to distance from a fault can produce a different map. This type of map can be used with information on existing buildings to forecast locations of maximum damage for use in planning emergency response measures and for designating areas of critical concern.

A cumulative economic risk map can relate the expected damage to particular types of buildings over time. Such maps rely on intensity information as well as information on the amount of damage that can be expected for each intensity and general type of building and information on how often a particular earthquake is likely to occur. Figures 2A - D are examples of risk maps. They indicate the total expected percent damage due to earthquakes resulting from any of the major active faults in part of the Bay Area for any given area for two types of small buildings: wood-frame (Figures 2A and C) and other types (Figures 2B and D). Risk maps may be used in evaluating the relative costs due to earthquakes for new buildings in various locations throughout the region and for designating areas where special precautions may be needed. However, the intensity-cost information is not a sufficient basis for engineering decisions at a specific site, for these require specific knowledge of the process causing damage. The graphic appearance of a risk map is very dependent on how often earthquakes are assumed to occur on each fault. Figures 2A and B use a different set of recurrence intervals than Figures 2C and D.

Land Capability Analysis

Any microzonation map, though a representation of the earthquake problem, cannot by itself represent the problems due to all geologic constraints, let alone all environmental, social or economic constraints. By relating each geologic problem to some common denominator, such as cost or lives lost, one can effectively compare the geologic concerns or can add these concerns together, using traditional or computerized map overlaying techniques. Figure 3 is an example of such a map, based on cost information for residential development in Santa Clara County.

FIGURE 1

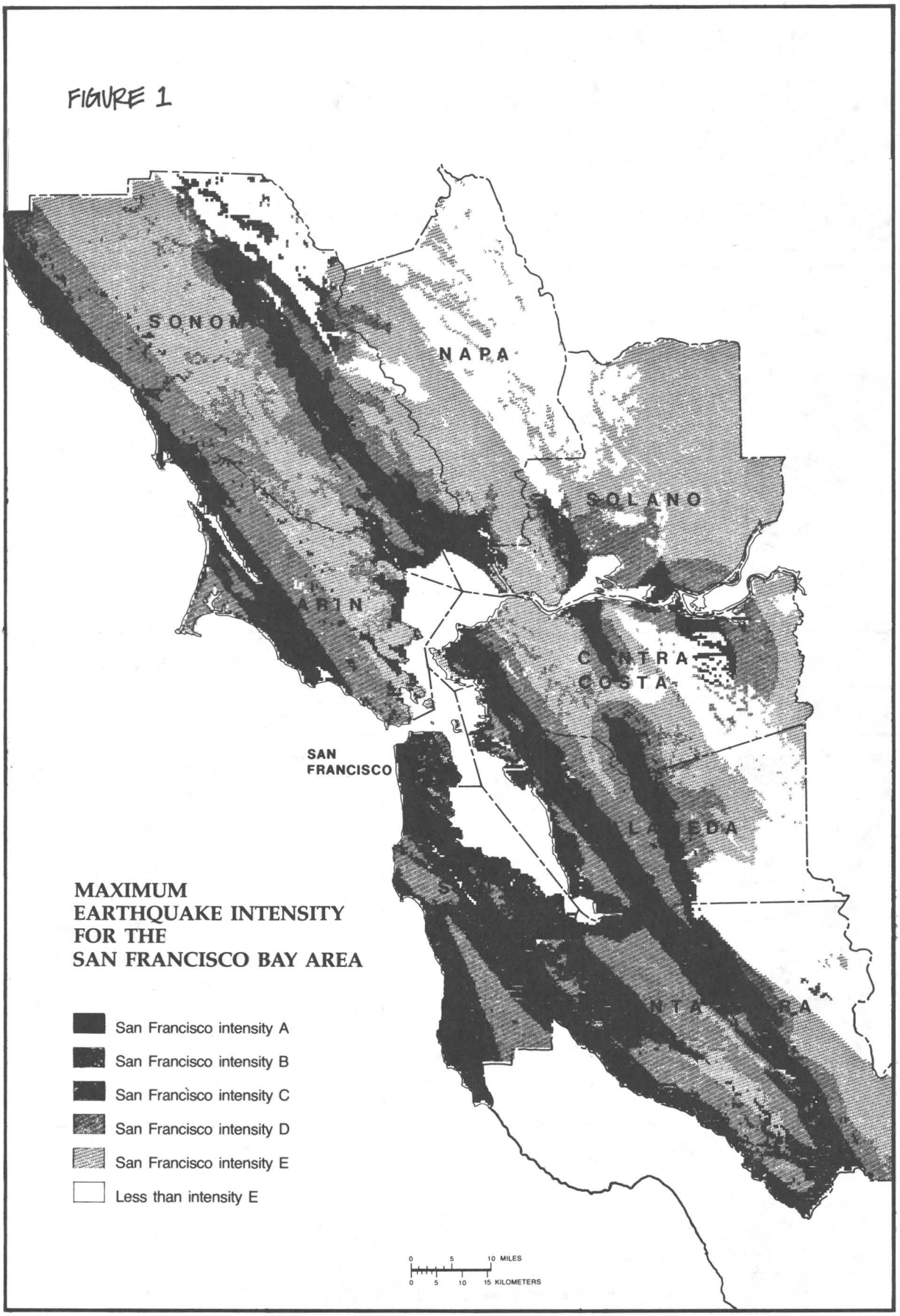
SONOMA
NAPA
SOLANO
MARIN
CONTRA COSTA
SAN FRANCISCO
ALAMEDA
SANTA CLARA
MAXIMUM EARTHQUAKE INTENSITY FOR THE SAN FRANCISCO BAY AREA
San Francisco intensity A
San Francisco intensity B
San Francisco intensity C
San Francisco intensity D
San Francisco intensity E
Less than intensity E
0 5 10 MILES
0 5 10 15 KILOMETERS

FIGURE 2:

SAMPLE CUMULATIVE ECONOMIC RISK MAPS FOR EARTHQUAKE DAMAGE

SMALL WOOD-FRAME BUILDINGS

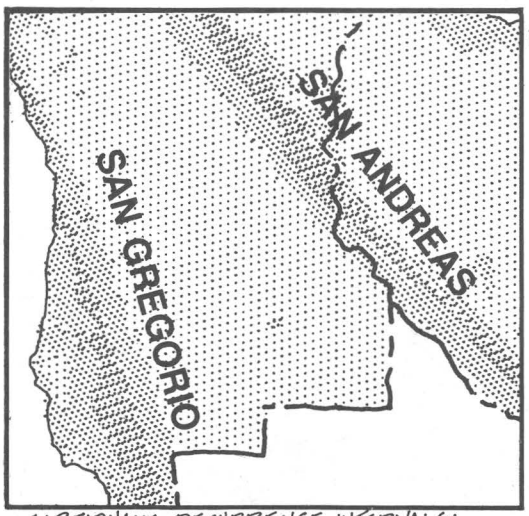

FIGURE A

EARTHQUAKE RECURRENCE INTERVALS:
SAN ANDREAS: 100 YRS. SAN GREGORIO: 100YRS.

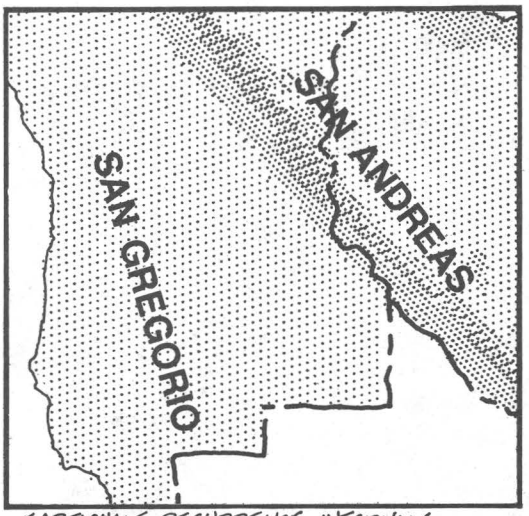

FIGURE C

EARTHQUAKE RECURRENCE INTERVALS:
SAN ANDREAS: 100 YRS. SAN GREGORIO: 1000 YRS.

OTHER SMALL BUILDINGS

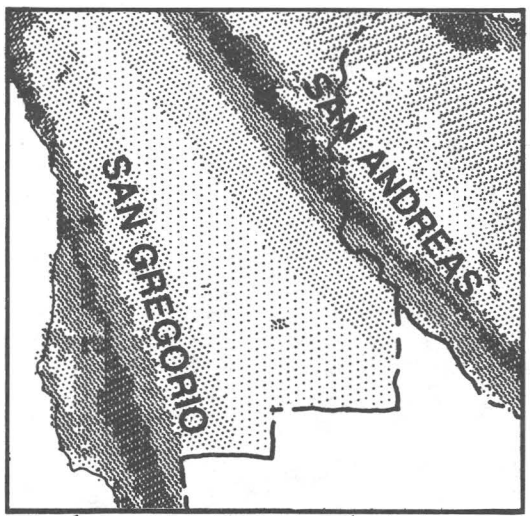

FIGURE B

EARTHQUAKE RECURRENCE INTERVALS:
SAN ANDREAS: 100 YRS. SAN GREGORIO: 100 YRS.

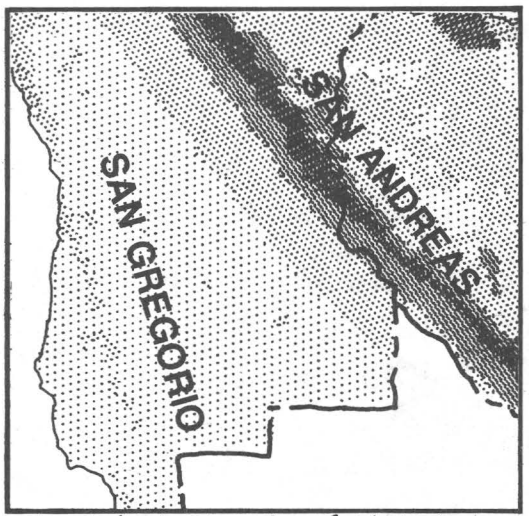

FIGURE D

EARTHQUAKE RECURRENCE INTERVALS:
SAN ANDREAS: 100 YRS. SAN GREGORIO: 1000 YRS.

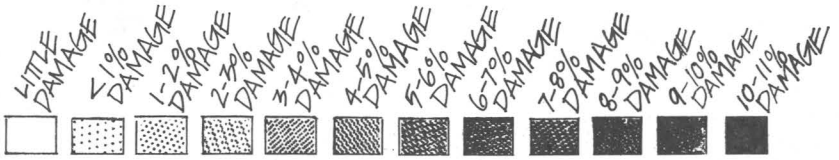

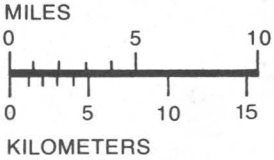

FIGURE 3

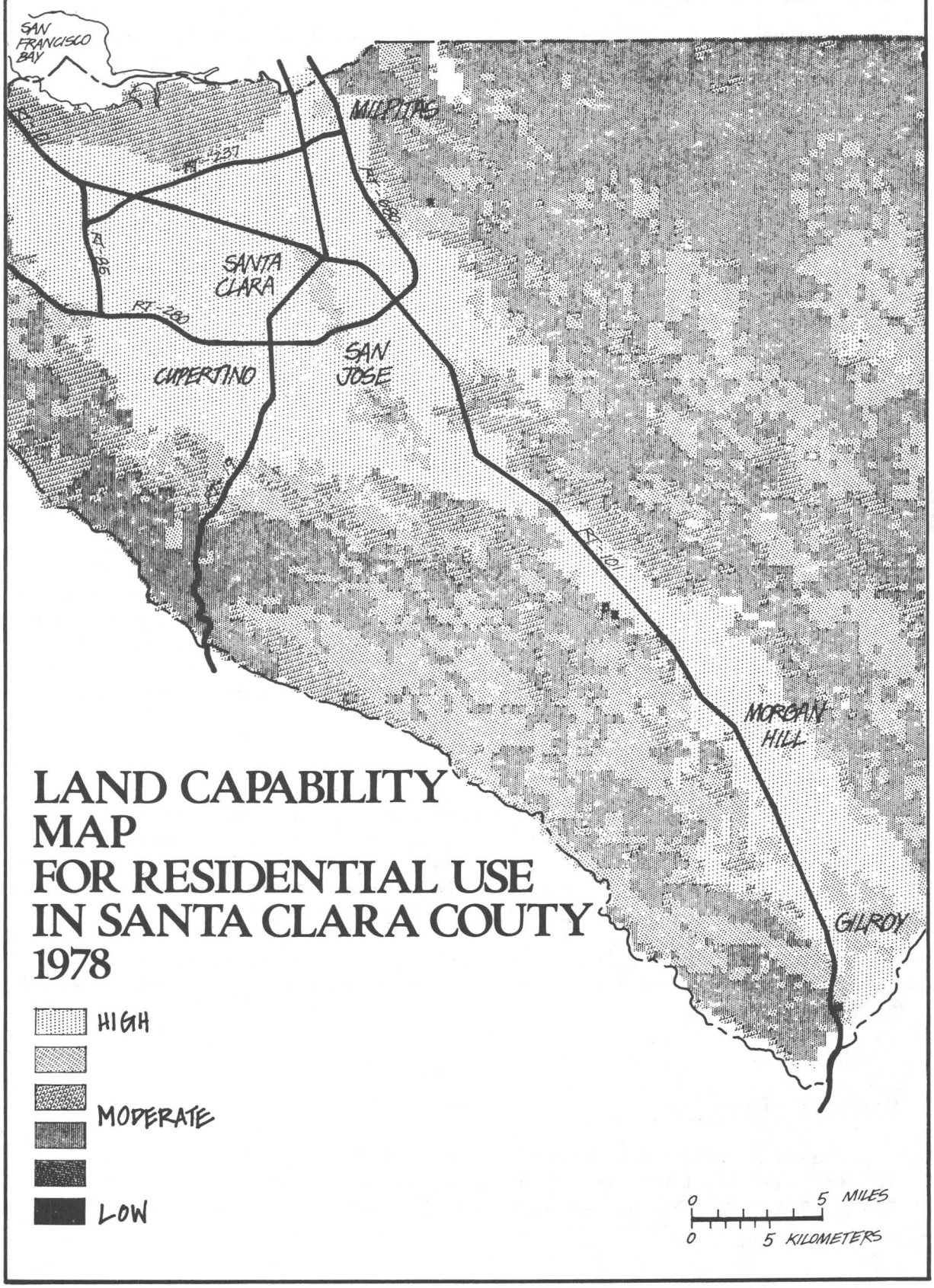

LAND CAPABILITY MAP FOR RESIDENTIAL USE IN SANTA CLARA COUTY 1978

SAMPLE USES

Solid Waste Planning

The earthquake intensity map and other geologic and hydrologic maps were used with map-related criteria to screen the Bay Area to find those general areas that warranted further study for use as disposal sites for hazardous waste.

After additional screening using other social and environmental criteria, ABAG staff discovered that only four of the nine Bay Area counties had areas worthy of additional study.

Special Facilities

The problem of overlaying maps may be avoided by simply providing a listing of the level of concern (high, moderate or low) for environmental safety issues in the form of a computer display. If land capability information is also available, a general indicator of overall concern for environmental safety also can be included. Separate displays have been prepared for approximately 450 vacant industrial sites and 173 proposed seaport sites in the Bay Area.

Assessment of Development Patterns

As part of assessing the environmental impacts of planning programs, it is important to know the relationship of geologic hazards to alternative land use or development patterns. Earthquake intensity and related information has been used in assessing the implications of policies that encourage more dense central city growth as opposed to less compact development in suburban and rural areas in the region. It has also been used in assessing development patterns intended to reduce commute distances for Santa Clara County.

Implementing Regional Policies

As the designated areawide clearinghouse, ABAG reviews local plans and projects that propose to use Federal and State funds. One of the review criteria used is the completeness of the description of geologic and seismic hazards affecting the site. Microzonation maps and information on other geologic hazards is used in the reviews.

In addition, ABAG assists cities and counties in obtaining earthquake information and incorporating that information into their programs as time permits.

FUTURE PLANS

Updating Information

Because earthquake microzonation is such a dynamic field, it is essential that all maps can be easily updated. All of the basic information, including geology and land use, the modeling techniques, and the

products, including maps and displays, are integrated in ABAG's computerized Bay Area Spatial Information System (BASIS). Thus, as better information on correlations between geologic materials and earthquake intensity or on recurrence intervals becomes available, the interpretive maps and the related information will be modified easily. The system also allows cities and counties to modify the maps for their own uses. Maps can be produced at non-standard scales, such as 1:60,000 for Santa Clara County. Requests can be fulfilled to group peat soils with Bay mud, rather than with alluvium, for generating a maximum intensity map for Contra Costa County.

Future Applications

Several interesting projects using earthquake and related information should be completed by December 1979. The displays for special facilities will be expanded to include existing and proposed airports and solid waste disposal sites. The work on assessment of development patterns should be dramatically improved when detailed information on current and projected land use is placed in BASIS. Such information also will be extremely valuable for planning emergency services. A more formal program will be instituted for ensuring that cities and counties more actively use the earthquake map information.

BIBLIOGRAPHY

1. Borcherdt, R.D., Gibbs, J.F., and Lajoie, K.R., 1975, Maps Showing Maximum Earthquake Intensity Predicted for Large Earthquakes on the San Andreas and Hayward Faults, Southern San Francisco Bay Region, California, U.S. Geological Survey Miscellaneous Field Studies Map MF-709.